Investigation of Nonlinear Vibrations of Nuclear Fuel Rods with Non-Classical Boundary Conditions

Giulio Franchini

Master of Engineering

Department of Mechanical Engineering

McGill University
Montréal, Québec
2020-04-02

A thesis submitted to McGill University in partial fulfilment of the requirement of the degree of Master of Engineering

© Giulio Franchini 2020

Contents

Acknowledgements	4
Abstract	5
Abrégé	6
Chapter 1 Introduction	7
Chapter 2 Nonlinear Vibrations of a Nuclear Fuel Rod Supported by Spacer	9
Abstract	9
2. Experimental setup	13
2.1. System under test	13
2.2. Instrumentation and data acquisition	20
3. Experimental results	24
3.1. Empty rod in air	24
3.2. Rod with freely moving pellets in air	29
3.3. Rod with fixed pellets in air	32
3.4. Empty rod in water	34
3.5. Rod with freely moving pellets in water	37
3.6. Rod with fixed pellets in water	39
4. Damping identification	41
4.1. Identification process	41
4.2. Results and discussion	43
5. Conclusions	46
Acknowledgements	48
References	49
Chapter3 Nonlinear Vibrations of a 3x3 Reduced Scale PWR Fuel Assembly Supported by Spacer	
Abstract	54
1. Introduction	55
Vibrations of fuel bundles in PWRs	57
Identification of damping	60
Single DOF model for forced vibrations of fuel bundles around the fundamental frequency	60
2. Experimental setup for the fuel assembly	61
2.1. Experiments in air and quiescent water	61
2.2. Experiments in axially flowing water	69
2. Experimental results	74

33 91
91
91
92
92
98
99
00
)5
)5
06
07
10
15
16
22
22
22
25

Acknowledgements

First of all I thank Professor Marco Amabili for welcoming me into his laboratory and introducing me to the exciting world of vibrations.

Dutiful is the thanks to the two post docs Dr. Giovanni Ferrari and Dr. Prabakaran Balasubramanian who have shown great skills of patience and teaching, as well as technicians Mathieu Beauchesne and Lydia Dyda.

Of course I would like to thank Framatome Canada Ltd. and the Natural Sciences and Engineering Research Council of Canada for the technical and financial support of this project.

Abstract

Any thermal circuit that uses a liquid as an energy transport system is subjected to fluid-structure iteration between the coolant and the heat exchanger. In power plants for energy production, such as nuclear reactors, this iteration can generate unwanted vibrations of significant amplitude that must be investigated for safety and life prediction. Nuclear fuel assemblies of Pressurized Water Reactors (PWR) must be able to withstand external excitations ranging from large amplitude seismic motions of the reactor to flow-induced vibrations from the surrounding coolant water. The present study is an experimental work that investigates the nonlinear vibrations of nuclear fuel rods supported by spacer grids: this is a type of support giving nonlinear boundary conditions. The experiments consist of measuring the vibration response of different rod configurations - single rod with and without tungsten pellets, which simulate uranium pellets, and a 3x3 fuel bundle made by a cluster of rods - under a step-sine harmonic excitation at different force levels and in the frequency neighborhood of the fundamental mode of vibration. If the excitation is large enough, the response of the rod displays nonlinear phenomena such as the shift of the resonant frequency and a one-to-one internal resonance. The research investigates the response of the system in air, in quiescent water and in axial water flow. The latter was achieved inside a water tunnel. Results of a specifically designed test show that spacer grids give a bilinear hysteretic behavior to the system dynamics. This is important for a future development of advanced nonlinear numerical models of nuclear fuel assemblies.

Abrégé

Tout circuit thermique qui utilise un liquide comme système de transport d'énergie est soumis à une itération de structure fluide entre le liquide de refroidissement et l'échangeur de chaleur. Dans les centrales électriques pour la production d'énergie, telles que les réacteurs nucléaires, cette itération peut générer des vibrations indésirables d'amplitude significative qui doivent être étudiées pour la sécurité et la prévision de la vie. Les assemblages de combustible nucléaire des réacteurs à eau pressurisée (REP) doivent être capables de résister à des excitations externes allant des mouvements sismiques de grande amplitude du réacteur aux vibrations induites par l'écoulement de l'eau de refroidissement environnante.La présente étude est un travail expérimental qui étudie les vibrations non linéaires des crayons de combustible nucléaire supportés par des grilles d'espacement: il s'agit d'un type de support donnant des conditions aux limites non linéaires. Les expériences consistent à mesurer la réponse vibratoire de différentes configurations de tiges - une seule tige avec et sans pastilles de tungstène, qui simulent des pastilles d'uranium, et un faisceau de combustible 3x3 fabriqué par un groupe de tiges - sous une excitation harmonique pas à pas à différents niveaux de force et dans le voisinage fréquentiel du mode fondamental de vibration. Si l'excitation est suffisamment importante, la réponse de la tige affiche des phénomènes non linéaires tels que le décalage de la fréquence de résonance et une résonance interne un à un. La recherche étudie la réponse du système dans l'air, dans l'eau de repos et dans l'écoulement axial de l'eau. Ce dernier a été réalisé à l'intérieur d'un tunnel d'eau. Les résultats d'un test spécialement conçu montrent que les grilles d'espacement donnent un comportement hystérétique bilinéaire à la dynamique du système. Ceci est important pour un développement futur de modèles numériques non linéaires avancés d'assemblages de combustible nucléaire.

Chapter 1 Introduction

In this manuscript-based thesis for articles we will see the work done in the vibration and hydrodynamics laboratory during my path as a master student. The work consists of three articles published or submitted on non-linear vibrations of mechanical components suitable for the production of energy through nuclear fission technology. In particular, we investigated the dynamic behavior of fuel rods of Pressurized water reactor (PWR) in relation to the Spacer Grids designed by Framatome. In this thesis you will find results of various configurations according to the most effective technologies present in McGill laboratories. Dynamic understanding of these components is of fundamental importance for the operational safety of nuclear reactors.

Before explaining the content of the chapters of this thesis, it is useful for the reader to contextualize the study area, the needs and the purpose of this research.

This primary circuit consists of a pressure vessel, which contains the core formed by fuel elements inside which the control bars slide. The neutron moderator is water, which also acts as a cooling fluid. The water, by subtracting energy by conduction from the hot core, pushed by a recirculation pump, interacts with the group of fuel rods producing vibrations. These fuel rods are long slender tubes (about 4m length and 1cm in diameter) held together by the spacer grids. Therefore, the iteration that arises between fluid and structure is that of a body traversed axially by the fluid which, given its speed and pressure, is capable of producing vibrations harmful in the long run to the structure in use. In the following thesis the contribution given by the spacer grids produced by Framatome and kindly granted to our laboratory will be sought.

A vibrational study of the mechanical components in use makes the engineering design complete, especially in terms of safety and life prediction. For the amplitude of the vibrations and for the reactions introduced by the spacer grids, it is necessary to collect information of this system with original experiments we have made.

In the first article, *Nonlinear vibrations of a nuclear fuel rod supported by spacer grids* (Nuclear Engineering and Design , Volume 361, May 2020,

https://doi.org/10.1016/j.nucengdes.2019.110503), you will find the study of a single bar mounted between two spacer grids. The dynamic behavior around the first fundamental frequency of the system is investigated in different configurations. Results characterize the dynamics of the empty rod or of the rod with pellets inside, free or axially constrained. Experiments are repeated both in air and with the rod immersed in water.

Understanding the results of a simple system has allowed us to evolve the complexity of our experiments and to produce interesting results for a second publication: *Nonlinear vibrations of a* 3x3 reduced scale PWR fuel assembly supported by spacer (Nuclear Engineering and Design, Volume 364, August 2020, https://doi.org/10.1016/j.nucengdes.2020.110674). In this second publication, there are results obtained for a more complex configuration of the system, that is for a cluster of fuel rods. We carried out the study in quiescent water and in axial flow conditions, testing the system inside a water tunnel at McGill laboratories, with different flowrates.

The third and final article is *Nonlinear vibrations of beams with bilinear hysteresis at supports: Interpretation of experimental results* (submitted for journal publication). In this chapter, attention is on the boundary conditions of the systems studied in the two previous articles. Targeted experiments revealed a strongly bilinear behavior of the spacer grids which led to the development of a numerical model. The model proved to be optimal for the description of the dynamic behavior both in the time domain and in the frequency domain. There is a clear link in the study developed the three scientific articles. The degree of complexity of the responses that we measured allows to characterize the complex nonlinear dynamics of these components for the nuclear industry.

Chapter 2

Nonlinear Vibrations of a Nuclear Fuel Rod Supported by Spacer

Giovanni Ferrari^a, Giulio Franchini^a, Prabakaran Balasubramanian^a, Francesco Giovanniello^a, Stanislas Le Guisquet^a, Kostas Karazis^b, Marco Amabili^a

AMcGill University, Dept. of Mechanical Engineering, Macdonald Engineering Bldg., 817 Sherbrooke St. W, Montreal H3A 0C3, Quebec, Canada

BFramatome Inc., 3315 Old Forest Rd., Lynchburg, 24501 VA, USA

Running headline: Non-linear vibrations of a nuclear fuel rod supported by spacer grids

Keywords: PWR fuel rods, Nonlinear vibrations, Fluid-structure interaction, Damping identification, Spacer grids

Abstract

The internal components of Pressurized Water Reactors (PWRs), particularly nuclear fuel assemblies, must be able to withstand Flow Induced Vibrations (FIV) during operating conditions and during extreme accident conditions, such as earthquakes. Nuclear fuel assemblies are composed of long slender tubes, filled with uranium pellets that are bundled together by periodic support provided by the spacer grids. Spacer grids are square structures used to increase thermal mixing in the core and provide support to the fuel rods and guide tubes allowing for the installation and removal of nuclear fuel rods. Nevertheless, spacer grids constitute a nonlinear flexible boundary condition experiencing friction forces and impacts complicating the dynamics of the fuel rod-spacer grid system. In order to improve safety margins in the design of nuclear fuel assemblies, it is of great interest to understand the nonlinear behavior at the interface of the spacer grids with the fuel rods, investigating the complexity due to the nonlinear evolution of the system stiffness and damping properties. In particular, the effect of the constant evolution of the vibration

amplitude as a function of the change of the excitation forces on the dynamics of the fuel rod response is still undetermined. Experiments were carried out in quiescent water and in air to understand the nonlinear vibration response of a single zirconium fuel rod supported by spacer grids. The vibration response under a step-sine harmonic excitation at different force amplitude levels in the frequency neighborhood of the fundamental mode was measured. The response of the rod displayed nonlinear phenomena such as the shift of the resonant frequencies, multiple solutions with some instabilities (jumps) and hysteresis, and a weak one-to-one internal resonance. Tests were performed on an empty rod and on a rod filled with tungsten pellets representative of nuclear fuel. The pellets were let free to move and were subsequently blocked axially to reproduce the effect of the beginning-of-life constraint in operational nuclear plants. The experimental data were processed by means of a simplified identification procedure to extract the damping parameters of the vibrating system. The equivalent viscous damping is found to increase and to be a function of the level of excitation and of the peak vibration amplitude.

1. Introduction

Clusters of arrays of cylindrical elements subjected to external fluid flow, with both axial and cross flow components, are common in power generation (Chen, 1985, Païdoussis, 2006; Weaver et.al., 2000). Fluid-structure interaction is minimized by design, when possible, to avoid large amplitude instabilities.

The cores of Pressurized Water Reactors (PWRs) are constituted of arrays of fuel rods, which are slender zirconium alloy tubes containing pellets of fissionable material. Spacer grids are used to bundle large numbers of fuel rods in structured arrays forming fuel assemblies, which are prone to reaching large-amplitude vibrations due to fluid-structure interaction (Bhattacharya, 2013; Dragunov *et al.*, 2013; Païdoussis, 2006), potentially leading to catastrophic consequences. The tubes in PWRs and in steam generators are subjected to external parallel flow and, therefore, to random vibrations induced by flow noise; flutter and divergence instability may also appear, if the design of the exchangers does not properly take fluid-structure interaction into account (Kaneko *et al.*, 2013). While empirical formulations are readily available in the nuclear industry for the design of fuel bundles subjected to axial flow, a number of details pertaining the physical mechanisms of instability remain unknown.

Choi *et al.* (2004) investigated numerically and experimentally fuel rods immersed in quiescent fluid and supported by spacer grids. Several papers available in literature investigated the flow-induced vibrations of fuel bundles numerically (Au-Yang and Burgess, 2007; Chen, 1975; De Santis & Shams, 2017; Hofstede *et al.*, 2017; Kang *et al.*, 2001; Kim and Kim, 2005; Liu *et al.*, 2012; Liu *et al.*, 2017; Païdoussis and Curling, 1985; Sandström, 1987; Simoneau *et al.*, 2011) as well as experimentally (De Pauw *et al.*, 2015).

Uranium pellets are normally compressed axially inside fuel rods by means of a spring-operated system. Modeling the effects of pellets on the dynamics of the fuel rod is difficult; the pellet effects are currently addressed with the introduction of dry friction and impact modeling. However, Park et al. (2009) related the stability of the system with the change in the natural frequency of the rod accounting for the presence of pellets. In Ferrari et al. (2018), it is clearly shown that there is significant correlation between damping and rod vibration amplitude. Similarly, in the present study the effect of pellets is not modeled mathematically but observed through its consequences on the experimental results.

Spacer grids (SGs) are employed in nuclear reactors to keep nuclear fuel rods (as well as guide and instrumentation tubes) safe at the correct relative position, while allowing for fuel rod thermal expansion and the removal of rods when necessary. Spacer grids rely on elastic and rigid contact points and surfaces to keep the rods in position by means of preload and friction. In presence of large vibrations of the rods, fretting may occur at the contact surface with the spacer grids, leading to potential fuel leaking (Bakosi et al., 2013; Hu et al., 2016; Kim, 2010). Moreover, spacer grids have an important influence on the fluid flow along the nuclear fuel bundle (Rehme and Trippe, 1980). Consequently, the design of spacer grids, which is outside of the scope of this article, is discussed in detail in the relevant literature. The effect of spacer grids on the dynamics of rods is investigated by means of the finite element (FE) method by Choi et al. (2004). However, to the knowledge of the authors, no study in the literature investigates in detail the effects of spacer grids on nonlinear large-amplitude vibrations. Spring-and-dimple SG feature a continuous contact between the elastic element and the fuel rod; moreover, for sufficiently large amplitudes of vibrations, their designs allow for (i) gaps at the interface between the rod and spacer grid, and impacts with the dimples, and (ii) friction at the dimples and at the spring interfaces resulting from axial vibration. Consequently, the spring characteristic for spacer grids is strongly nonlinear (Schettino, 2017). Lastly, the importance of Coulomb friction increases with the age of the spacer

grid because of the decrease in the force exerted by the springs due to creep (Campbell and Chen, 2017).

The complex task of identifying the parameters governing the nonlinear vibrations of fuel rods was tackled by several authors in the literature (Adams et al., 1998; Adhikari and Woodhouse, 2001a, 2001b; Bennett et al., 1997). Among the nonlinear parameters, damping and its evolution for structures undergoing large amplitude vibrations are objects of abundant speculation. The trend of damping for fuel assemblies in flowing water was studied with respect to the first eigenfrequency by Viallet and Kestens (2003), with respect to fluid velocity by Connors et al. (1982), with respect to multi-span tube instabilities by Hassan (2011) and with respect to response nonlinearity by Brenneman and Shah (2000), Collard et al. (2004), Fardeau et al. (1997). Vandiver (2012) introduced a dimensionless damping parameter for the flow-induced vibrations of cylinders. The nonlinear elastic parameters and the equivalent modal viscous damping for several simple continuous structures were identified by the same research group in the following studies (Alijani et al., 2016; Amabili et al., 2016; Amabili & Carra, 2012; Delannoy et al., 2015; Delannoy et al., 2016). Finally, the concept and the tools developed for reference structures were employed on fixed-fixed nuclear fuel rods by Ferrari et al. (2018). The response of the fuel rod for the case with fixed nuclear fuel rod boundary conditions has exhibited: (i) nonlinear hardening behavior; (ii) an important one-to-one internal resonance due to the axial symmetry; and, (iii) a nonlinear increase of the equivalent modal damping related to the amplitude of vibration. In that study the presence of one-to-one internal resonances - the interaction of two modes of vibration with the same natural frequency - was investigated. A single degree-of-freedom modified Duffing oscillator (Amabili, 2008) can be used to describe the large-amplitude vibrations of single fuel rods excited by a harmonic force around the fundamental resonant frequency. The oscillator is capable to reproduce several phenomena encountered in experiments, such as hysteresis, jumps in vibration amplitude and other instabilities leading to chaotic responses. An additional degree-of-freedom can be added to take into account the one-to-one internal resonance due to the axial symmetry and to describe the energy transfer between the main vibration mode directly excited (driven mode) and the non-linearly coupled orthogonal mode with the same shape (companion mode).

In the present study, forced small-amplitude and large-amplitude vibration experiments were performed on zirconium alloy fuel rods provided by Framatome. Subsequently, damping was estimated through an identification method applied to a simplified single degree-of-freedom model. While previous studies by the same research group focused on fixed-fixed boundary conditions, here the actual constraints found in Framatome PWR bundles were applied. The constraints at the rod ends were provided by zirconium spacer grids with springs and dimples. As in Ferrari *et al.* (2018), single fuel rods were tested both in air and in quiescent water. Flowing fluid conditions and clusters of tubes are not included in this investigation (they will be included in subsequent studies). It was recently shown that damping in the large-amplitude vibration regime can be described more effectively by nonlinear damping models (Amabili 2018b; Amabili 2018c; Amabili 2019; Balasubramanian *et al.* 2017 and Balasubramanian *et al.*, 2018). However, in the present study a modal viscous damping ratio was preferred for simplicity. Consequently, it became necessary to adjust the damping value according to the vibration amplitude to match the experiments, which were conducted at several levels of harmonic force excitation. An increase of the equivalent viscous damping constitutes an obvious advantage in the view of increased safety and reduced vibrations.

2. Experimental setup

2.1. System under test

Two zirconium spacer grids identical to those employed in PWRs by Framatome were employed in this study. Each spacer grid is composed of 17x17 cells allowing the passage of 264 fuel rods and 25 tubes (24 guide tubes and 1 instrumentation tube). Specifically, fuel rods are supported by springs and dimples present in the spacer grids, as it can be seen in the cross section in Fig. 1. The spring preload/force acting on the fuel rods keeps them in position.

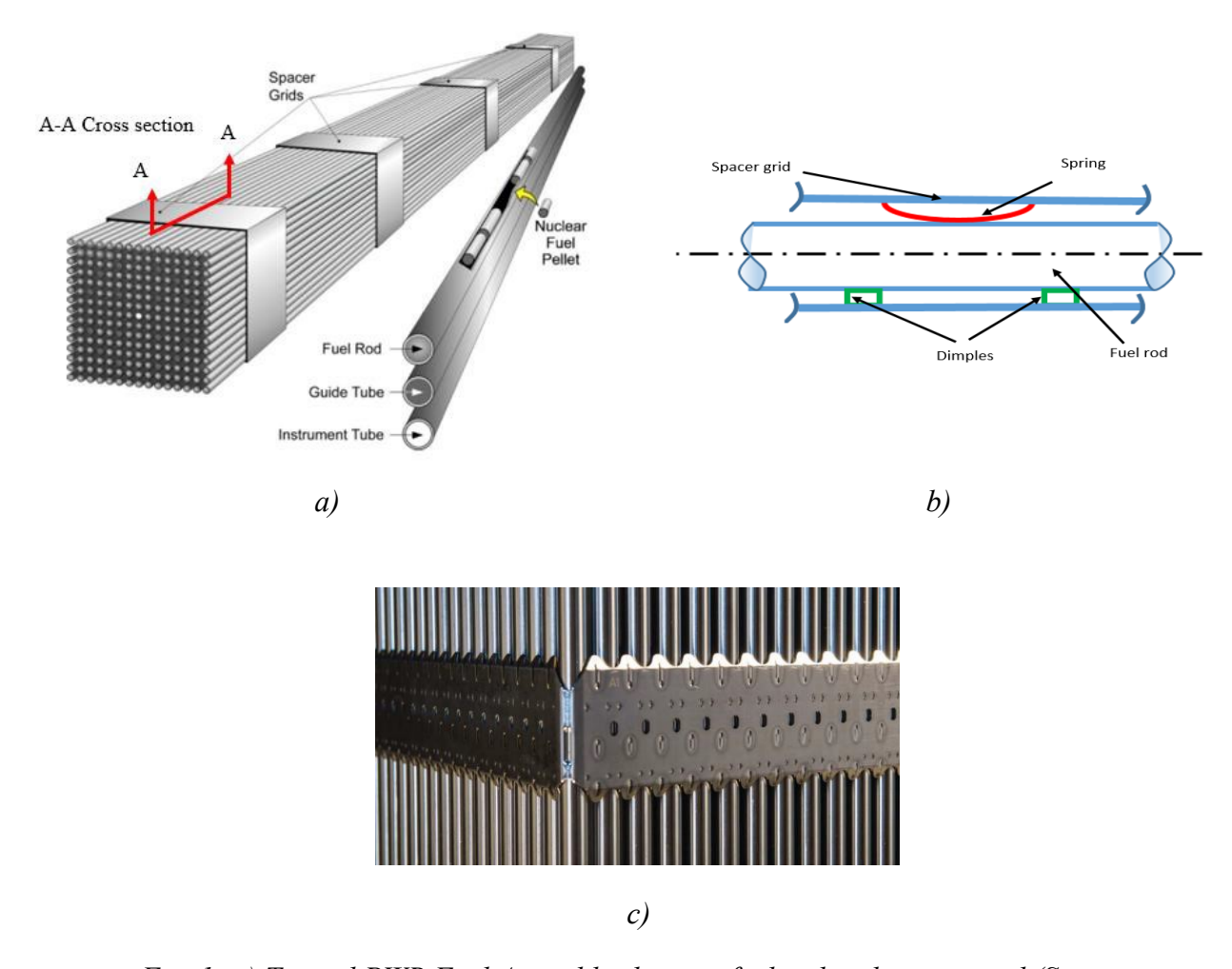


Fig. 1: a) Typical PWR Fuel Assembly showing fuel rod and spacer grid (Source: energy.gov); b) [A-A Cross section] Boundary condition of fuel rod with spacer grid; c) Photograph of fuel rods installed through a spacer grid.

In the experimental apparatus the spacer grids were kept parallel at a distance of 900 mm by means of four 3/4" threaded steel rods. The threaded rods were anchored to an acrylic frame (which is also the water tank wall) by means of bolts (see

Fig. 2). Great care was taken so that the spacer grids were not affected by compression or traction/torsional forces due to the bolts connecting the system to the acrylic frame. As the central cell of both spacer grids was intended to lodge one special guide tube during nuclear operations, an immediately adjacent fuel rod cell was employed to allow the passage of the rod under test. The rod was kept in a horizontal configuration; gravity in fact is not expected to play a significant role on the dynamics of the rod because of its light weight.

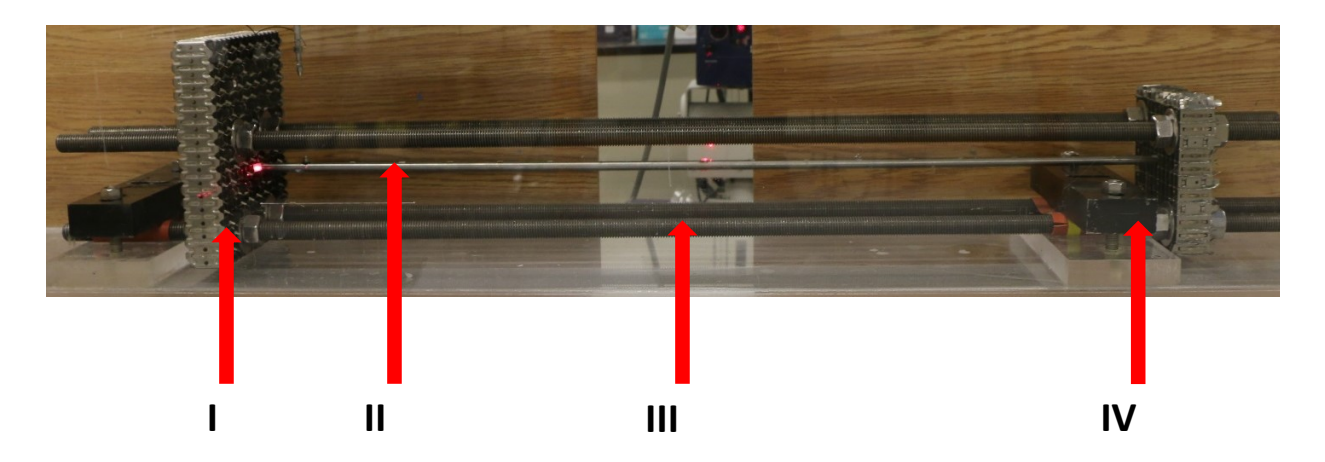


Fig. 2: Vibrating system complete with boundary conditions: I) Spacer Grid; II) Vibrating zirconium alloy rod; III) Structural spacers; IV) Clamps.

Framatome Canada Ltd. provided hollow zirconium rods identical to the ones used in the cores of their PWRs, but shorter in length (Fig. 3). The overall length of the rods under test is in fact 988 mm and the length left free to vibrate is 900 mm. The difference in length between the tested rod and the typical length of a span between two spacer grids found in PWRs is not expected to alter qualitatively the dynamics of the system. The material properties of the zirconium alloy are displayed in Table 1. The external and internal diameter of the rods are 9.50 mm and 8.28 mm respectively; however, one end of each rod is flared, to allow the insertion into the spacer grids, while the other presents a clamping diameter. The two machined ends of the fuel rods protrude beyond the springs and the dimples of the spacer grids. As such, they play no role in boundary conditions.

 Table 1

 Material properties of a zirconium-alloy rod

Density (kg.m³)	Young's modulus (GPa)	Poisson's ratio
6450	95	0.37

(a)

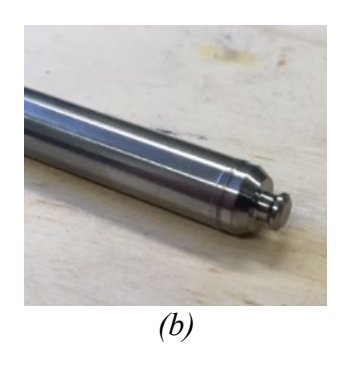




Fig. 3: Zirconium fuel rod under test, (a); clamping end (b); insertion end (c).

To characterize the preload forces exerted by the spacer grids on the fuel rods, dedicated static tests were performed. One rod, identical in diameter to the fuel rods, was installed on one spacer grid. A force parallel to the middle plane of the spacer grid was applied and measured, respectively, by a Brüel & Kjær electrodynamic exciter, model 4824, and an Interface force transducer, model WMC-100, at 81.5 mm from the middle plane of the spacer grid as shown in Fig. 4. The amplitude of the force was varied slowly in both directions around the equilibrium position (the fuel rod is originally positioned perpendicular to the spacer grid). As a result, it was possible to plot the rotational stiffness of the constraint under a torque applied on the fuel rod. Since the spacer grid features elastic slots for fuel rods and rigid slots for guide tubes, it was considered likely that the apparent stiffness of different cells in the spacer grid would change. Because of this, the test was repeated in two different cells, one adjacent to the location of the guide tube and one further away from the GT location. The results shown in Fig. 5 indicate that the equivalent rotational spring is strongly nonlinear. The loading cycles, moreover, have a wide hysteresis loop. The overall stiffness of the cell closer to the guide tube is higher, while its hysteresis is lower. Since all materials are expected to behave elastically during the test, the likely cause of the hysteresis is the presence of friction. It is noted here that two sets of spring and dimples are present, one acting in the direction of the force and one in the perpendicular direction. The latter does not oppose the rotation with elastic force but introduces friction during the rotation as it remains in contact with the rod. The former does not constitute an obvious source of friction during the rotation, but may introduce friction if, for large displacements, an axial sliding of the rod inside the cell happens. The loops are closed by rectilinear segments joined by sharp corners. The portions at higher

stiffness, such as those after the inversion of the load direction, can be justified by the initial absence of sliding (static friction). As soon as sliding starts, the apparent stiffness of the spring decreases suddenly (dynamic friction). Another cause of the changes in the slope of the loading curves is the change in the support given by the dimples. In fact, for a portion of the loading the fuel rod is supported by two dimples in the main loading direction. According to the direction and to the amplitude of the force, one dimple loses contact and all the load is transferred to the remaining dimple. A detailed investigation of the elastic and anelastic constraint given by the spacer grids is left to future experimental studies.

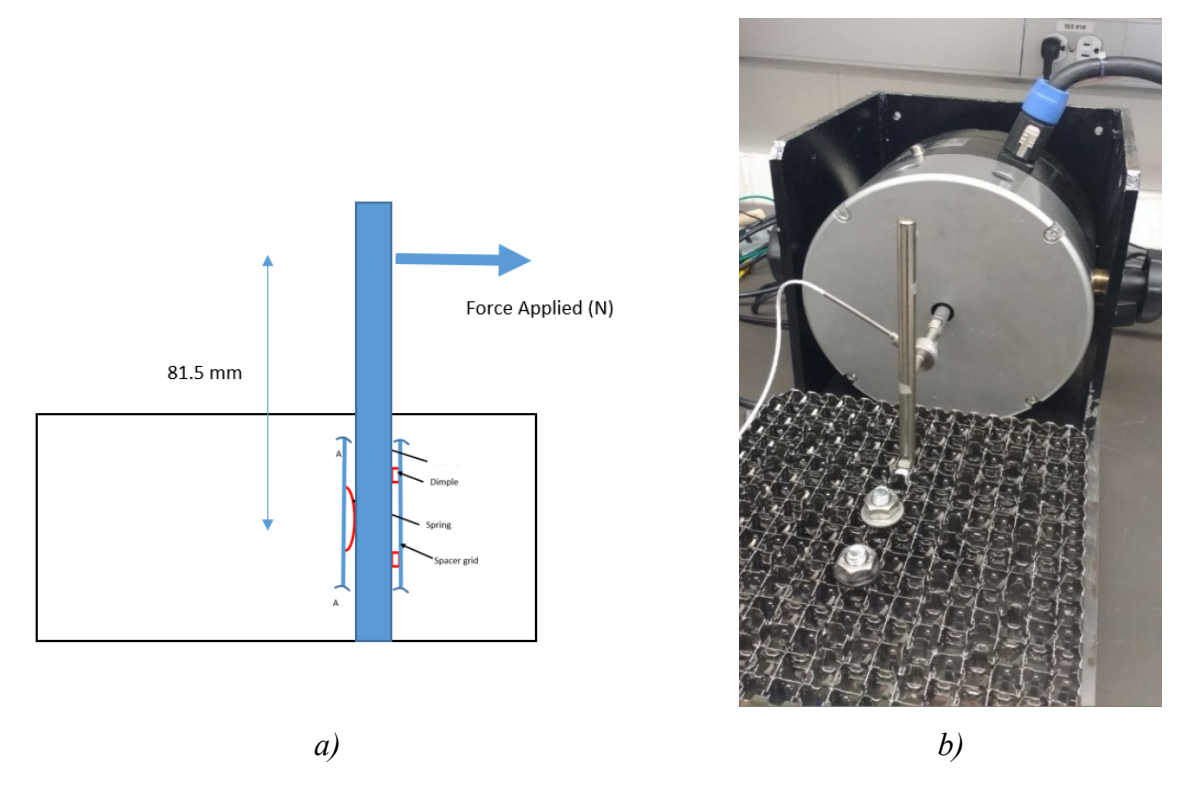


Fig. 4: Measurement of the spacer grid – fuel rod spring characteristic: a), schematics; b), photograph of the experiment.

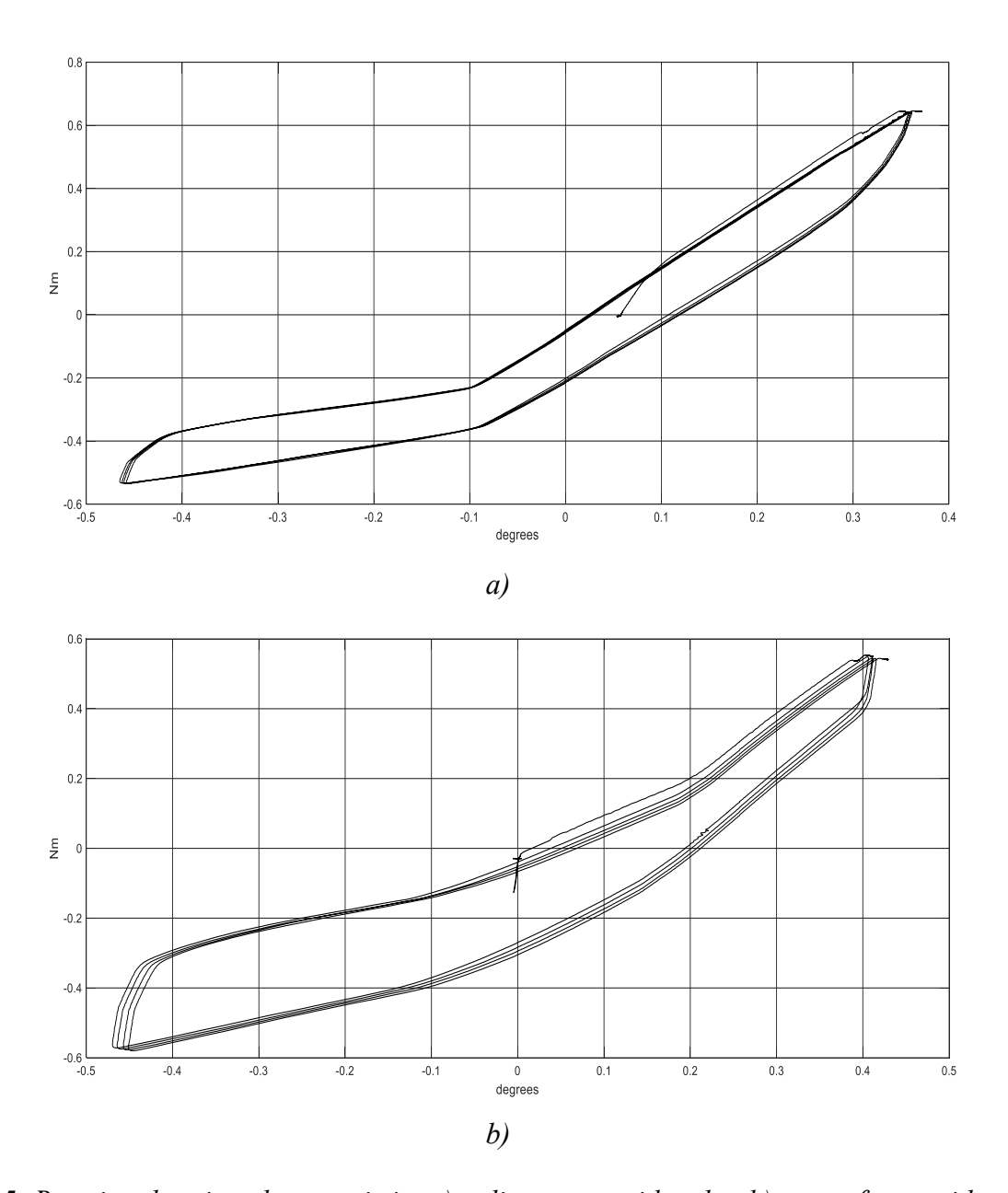


Fig. 5: Rotational spring characteristic: a), adjacent to guide tube; b), away from guide tube.

Framatome provided both empty rods and rods containing cylindrical tungsten carbide pellets, identical in dimension and density to the fissile pellets present in the rods of PWR cores. The fuel rods become 5.80 times heavier than in the empty configuration with the addition of the pellets. Both empty rods and rods filled with tungsten pellets were tested in the present study. The diameter and the overall axial length of tungsten pellets are slightly smaller than the clearance present inside the fuel rods. This axial and radial play is present also for real fissile pellets and constitutes a necessary precaution against the strong thermal dilation occurring during the plant operation. In

PWRs, a spring is employed to keep the pellets packed axially while allowing thermal expansion; in this study, a threaded device was provided to recreate a similar axial compression (Fig. 6). This device recovers the axial gap while the radial one remains unchanged; however, the friction between the packed pellets may oppose the radial motion as well. To study the effect of the motion of the pellets, the rods were tested in two configurations: i) letting the pellets move freely; and, ii) recovering the axial gap through the threaded device.

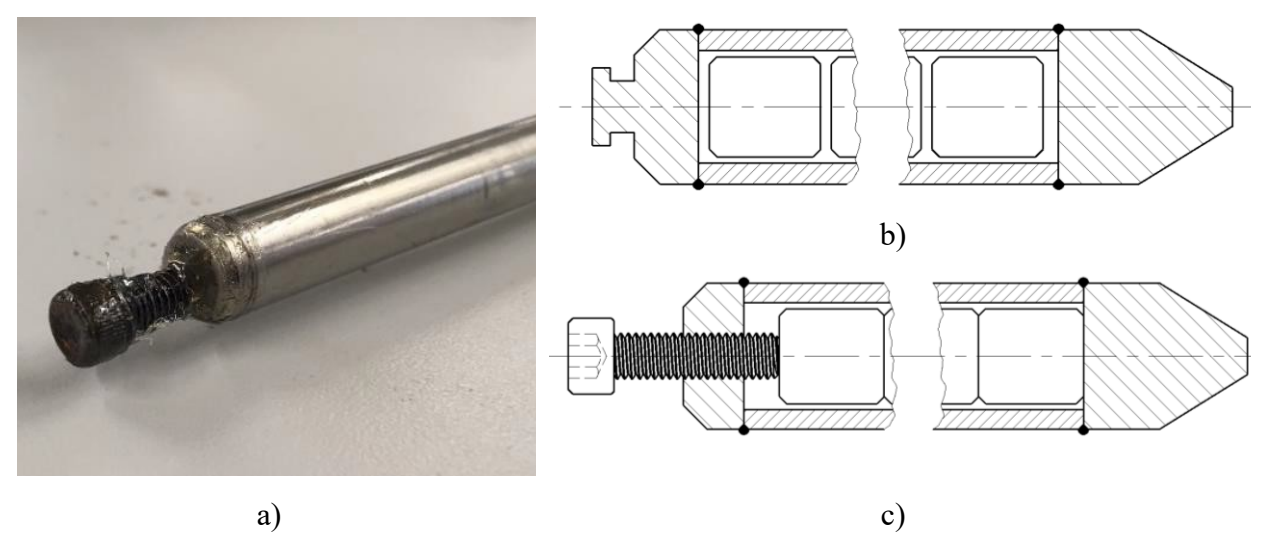


Fig. 6: a) Threaded device used to pack fuel pellets axially;
b) schematic of the fuel rods as provided by Framatome (free pellets);
c) schematic of the fuel rods with threaded device packing the pellets axially (fixed pellets).
Schematics not in scale.

The system was installed inside a clear acrylic tank which has the following dimensions: 1524 mm long, 300 mm wide, and 300 mm deep. The tank allows the performance of experiments both in air and in quiescent water. The dimensions of the tank are much larger than the diameter of the fuel rods, therefore the volume of water contained in the tank can be considered as infinitely extended around the vibrating system. Consequently, no fluid-structure interaction is expected, besides the virtual mass effect of the liquid displaced by the rods during vibration. Since the rods are parallel to the ground and the tank is open on the top, a free surface is available for the access of the instrumentation necessary for the excitation. No sloshing was detected on the free surface, even during the most severe vibrations of the fuel rods. A distance of 100 mm between the axis of the rod under test and the free water surface was kept during tests.

2.2. Instrumentation and data acquisition

The rod under test was subjected to forced excitation. The forced vibration excitation consists of one point force exerted in the vertical direction by an electrodynamic exciter (Brüel & Kjær model 4810) and measured in real time by a force transducer (Brüel & Kjær model 8203). The excitation is applied at a distance of 50.8 mm measured from the face of one of the two spacer grids directed towards the center of the tank. This distance was chosen according to the following criteria: i) it does not coincide with any node of the transversal normal modes of the fuel rod expected in the low frequency range, thus the excitation can have an effect on these modes during modal analysis; ii) it is far enough from the constraints to give enough energy to the fundamental vibration mode, object of nonlinear analysis, expected to have no nodes; iii) it is far enough from the center of the rod, which is the likely antinode of the fundamental mode. If the excitation force was applied at the antinode, its projection on the modal shape and the consequent energy transfer would be too large, resulting in a strong interaction of the motion of the shaker and of the structure. Subsequently, this would result in a poor control of the forcing amplitude. The forced vibration excitation system is shown in Fig. 7. Between the electrodynamic exciter and the rod a harmonic steel wire (stinger) is interposed, as per common practice in modal testing. The stinger, because of its high bending flexibility, does not allow the application of loads perpendicular to the axis of the exciter and of bending moments. However, its extremely small bending stiffness may increase marginally the apparent stiffness for the vibrations perpendicular to the axis of the exciter.

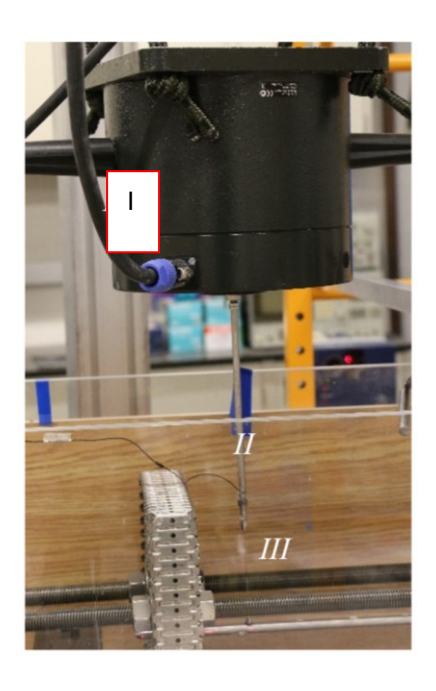
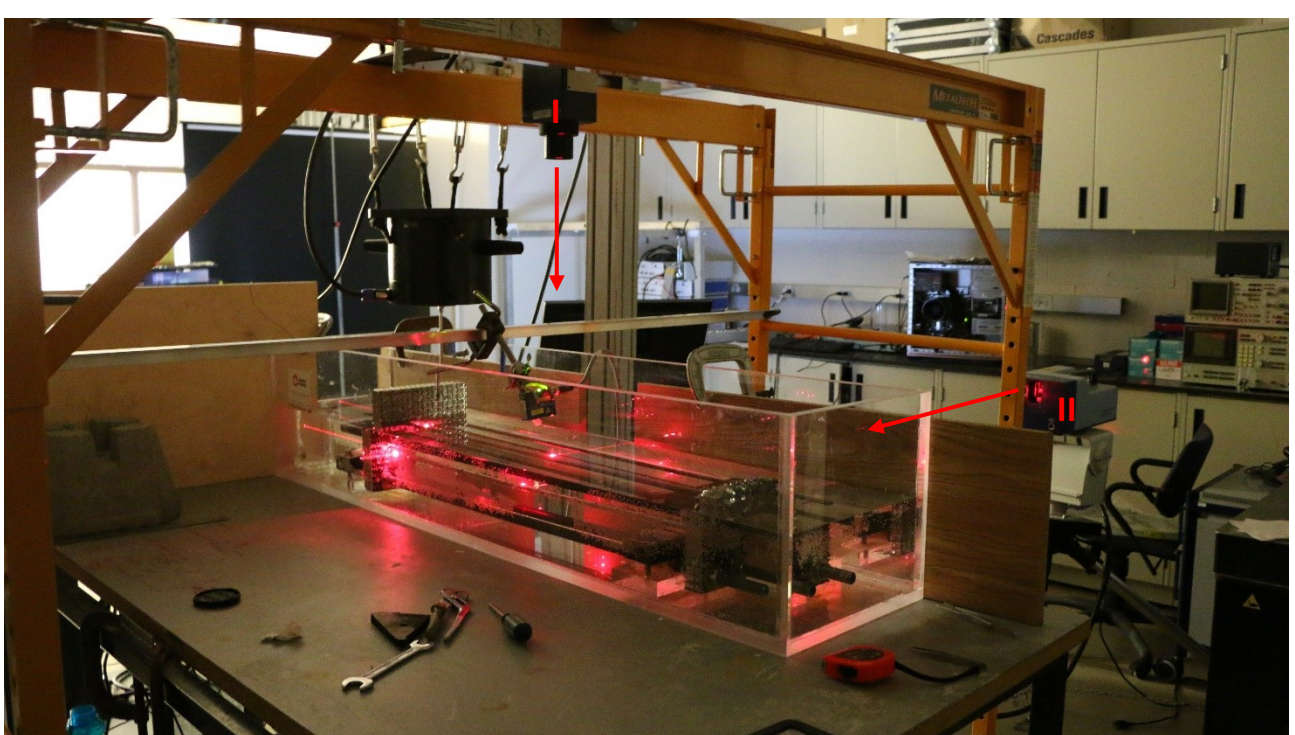
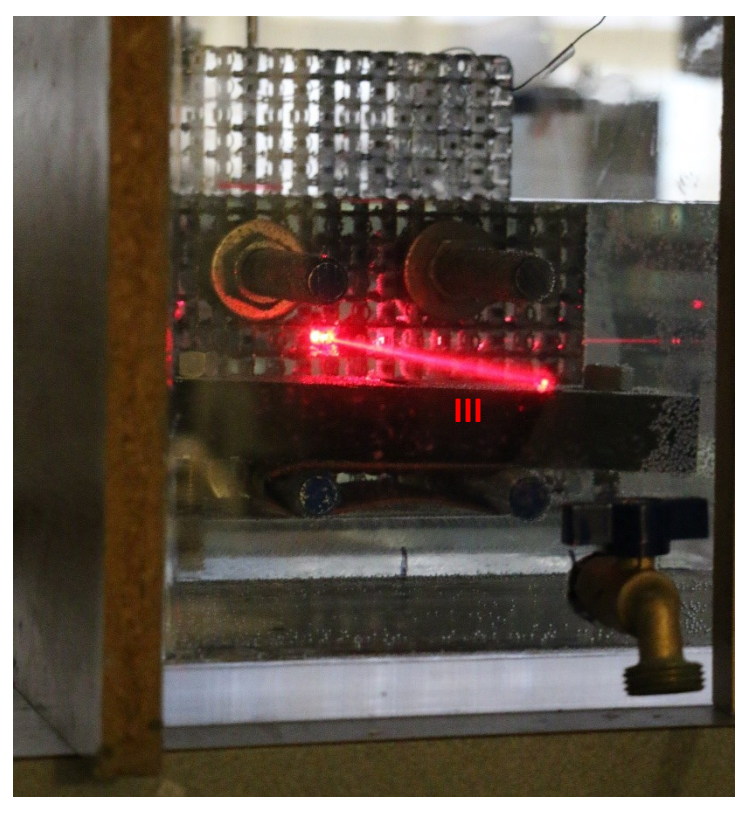


Fig. 7: Excitation system complete with force transducer: I) electrodynamic exciter; II) force transducer; III) stinger.

A no-contact vibration measurement system based on laser Doppler vibrometry was employed to measure the motion of the rods even through surrounding water and clear acrylic walls. Laser heads by Polytec (Single point laser head model OFV-505 and Scanning laser head model PSV-400) were employed with velocity and displacement decoders (velocity measurements were employed for modal analysis and displacement measurements for nonlinear testing). One OFV-505 head was employed to measure the vertical vibration of the beam, parallel to the direction of excitation, in order to perform modal analysis and reconstruct mode shapes. The laser head was in fact aimed manually and in a sequential fashion to each one of a set of points discretizing the surface of the fuel rod under test. Pseudo-random broadband excitation was applied at each aiming point to obtain the Frequency Response Function of the point with a frequency resolution equal to 0.193 Hz. The FRF was calculated according to the H1 estimate averaging five responses and five excitations. Subsequently, the PolyMAX algorithm by Siemens LMS was employed to reconstruct the sum FRF of the structure and the normal modes of vibration and to estimate the modal parameters. Additional laser heads were also used to measure the horizontal (PSV-400) and the axial (OFV-505) vibration of the rod during large-amplitude vibration. Because of the axial symmetry of the fuel rods, normal modes are expected to appear in perpendicular couples sharing the same frequencies. Normal modes perpendicular to the direction of the excitation may appear

because of nonlinear coupling terms becoming relevant for large excitation amplitudes (one-toone internal resonance between the directly driven mode and the companion mode, as discussed by Amabili et al. (2016)). This justifies the presence of a laser directed horizontally (perpendicular to the direction of excitation). Axial vibration was also measured because, in presence of largeamplitude vibrations and boundary conditions allowing axial slip, a transversal displacement can correspond to important axial motions. The low-frequency vibration modes of the beam are expected to be transversal (flexural) in nature and parallel to the direction of the excitation. Since the first vibration mode of a beam is expected to have its maximum transversal displacement at one half of the length of the rod, the horizontal and vertical laser heads were aimed correspondingly. For the symmetric character of the first vibration mode, instead, the maximum axial displacement is expected to happen at the two ends of the rod. The vibrating system is perfectly symmetrical with respect to a plane perpendicular to the fuel rod under test, parallel to the two spacer grids and located at a distance of 450 mm from each spacer grids (where 450 mm is one half of the free length of the fuel rods). In particular, the boundary conditions are perfectly symmetric with respect to this plane. Therefore, if existent, the axial slips at the two spacer grids are expected to be equal and opposite. Correspondingly, the laser measuring the axial displacement was aimed at one end of the rod. The setup of the laser measurement system is shown in Fig. 8.





b)

Fig. 8: a) Transversal measurement,

I): scanning laser head by Polytec (horizontal velocity and displacement);

II): single point laser head by Polytec (vertical velocity and displacement);

b) Axial measurement,

III): detail of the laser beam from the single point laser head by Polytec

III): detail of the laser beam from the single point laser head by Polytec (axial velocity and displacement) hitting one end of the test rod.

Nonlinear frequency-amplitude and frequency-phase curves were obtained through a stepped-sine technique based on the Siemens LMS TEST LAB testing system. A sinusoidal excitation was chosen because it provides large energies at specific frequencies; the frequency of the sine varies slowly by frequency steps of 0.05 Hz so that a neighborhood of the resonance of interest is investigated. At each frequency step, the initial 40 time periods are discarded to make sure that any transient has decayed, then 10 periods are recorded and, based on the latter, the frequency spectrum is calculated. The variation must be monotonic since nonlinear systems features hysteresis and instabilities; tests conducted by increasing the frequency will be named UP tests and tests conducted by decreasing the frequency will be named DOWN tests in the following

sections. A closed-loop feedback control was employed so that the amplitude of the excitation remained within a 0.5% tolerance from the constant target value. Uncertainty regarding the force excitation value is in fact the largest source of inaccuracy during vibration tests; the use of laser Doppler sensors is preferred since they provide excellent measurement accuracy.

3. Experimental results

As anticipated, the rods were tested for: 1) empty configuration; 2) filled with pellets; and 3) filled with pellets packed axially, both in (a) air, and (b) in still water, for a total of 6 configurations. For each of the following six sub-sections, corresponding to the six experimental configurations described previously, the modal analysis will be presented first. It was verified that the modal shapes remain the same for all the tests and it was chosen for conciseness to present the frequency response function (FRF) and the normal modes for the first case only. The frequency-amplitude diagrams that describe nonlinear vibrations are then presented separately for the three directions of the measurements.

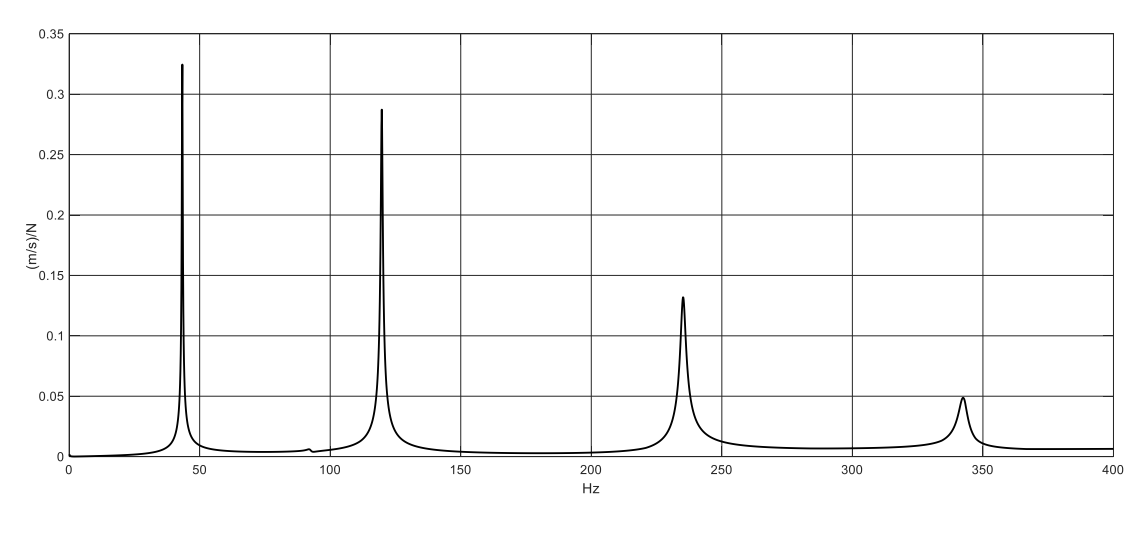
As shown in Ferrari *et al.* (2018), a hardening behavior is expected for fixed-fixed nuclear fuel rods. The following cases, however, will be softening in nature (the frequency decreases with the forcing amplitude). The decrease in the stiffness of the system for increasing forcing and vibration amplitudes has not been explained physically so far. For softening systems, the maximum vibration is typically reached by DOWN curves. However, for such damped systems a negligible hysteresis (difference between DOWN and UP curves) was measured.

3.1. Empty rod in air

In the frequency range 0-400 Hz, the empty rod presents four vibration modes for which the number of longitudinal flexural waves equals the order of the mode. This correspondence was noticed for all the cases under study; therefore, the normal modes and the Frequency Response Function will be presented for the empty rod exclusively. It was noticed that, as the mode number and the number of longitudinal half-waves increase, the motion at the boundary conditions (the springs of the spacer grids) increases as well. This may suggest that i) the vibration of the spring constitutes an important part of the modal shape and ii) the spacer grids allow an important rotation

and/or an important displacement. However, it must also be noticed that the measurement cannot be carried out at the exact location of the boundary conditions (the points of contact between springs, dimples and fuel rods) but at a finite distance from them (basically, at the plane that constitute the surface of the spacer grids). It can be noted anyway that mode IV presents significant rattling at the constraints, which could justify higher damping values. Indeed, a higher modal damping was measured for mode IV, not only for the empty rod in air, but in most experimental cases treated in the following sections as well. While the determination of the exact shape of the normal modes of vibration is outside the scope of this investigation, it was also verified that the first four vibration modes and the external excitation share the same plane. The modal damping values obtained from modal analysis are shown in Fig. 9 and listed in

Table 2. Modal damping in this case increases with mode number; this contradicts some results found in the relevant literature (*e.g.*, (De Pauw et al., 2015)), where the fundamental vibration mode presents the largest damping. However, in the following cases in air and in water, various trends of modal damping and mode order are observed and presented. A proper discussion on the relationship between mode number and modal damping in PWR cores should take into account fluid flow, which is not included in this experimental study. Moreover, the authors have encountered several examples of systems where modal damping does not decrease with mode order (*e.g.*, (Alijani et al., 2016)).



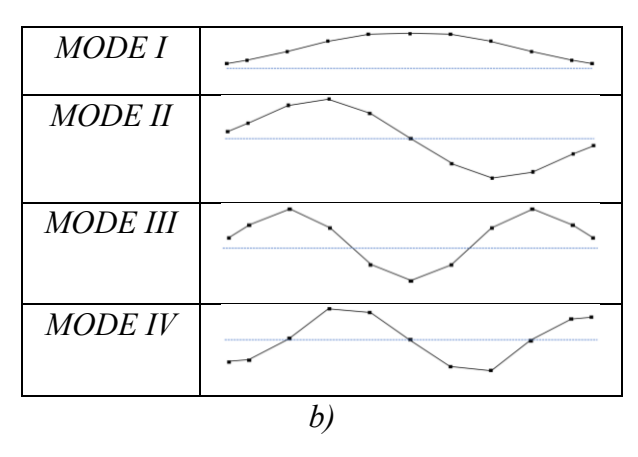


Fig. 9: FRF (a) and normal modes (b) of the empty rod.

Table 2Modal parameters of the empty rod in air

Nada	No. half	Frequency	Damping
Mode	waves	(Hz)	(%)
I	1	44	0.37
П	2	120	0.31
Ш	3	236	0.45
IV	4	343	0.51

The rod reaches a vibration amplitude approximately 3 times larger than its thickness during stepped sine tests. The nonlinear character of the vibration is manifested by the nonlinear jumps present in the amplitude chart for some excitation levels shown in Fig. 10. Such jumps are present even for relatively low force amplitudes. The trend of the nonlinear jumps is clearly softening, since the peak vibration frequency shifts towards lower values for larger forces. The companion mode has a resonant peak at a slightly higher frequency than the driven mode (Fig. 11). This can be justified by geometric imperfections (not measured) and by the sag of the rod under its own weight (amounting to a maximum value of approximately 2 mm at the middle of the length). It can be conjectured that, because of the sag due to weight, the nonlinear spring elements in the spacer grids are in a preloaded state that results in a reduced stiffness in the vertical direction.

The results in Fig. 11 also feature the influence of the driven mode as an additional peak. The interaction between the two modes is evident for forces larger than 0.5 N. For a more detailed treatment of the internal resonance in axisymmetric structures, the reader is referred to Amabili *et al.* (2016). No traveling wave is present since the companion mode remains in amplitude much smaller than the driven mode. However, the horizontal vibration is given by a vibration mode and not by simple measurement noise or poor measurement alignment, because of the following reasons: i) the horizontal vibration has a clearly distinct peak amplitude; ii) the relative phase between the vertical and the horizontal vibration is approximately 90 degrees, which is typical for one-to-one internal resonances due to axial symmetry (Fig. 13). Since the phase charts do not give any additional relevant information, they will be omitted in the subsequent experimental cases. Lastly, the axial mode, shown in Fig. 12, is comparable to the companion mode in amplitude, but it is influenced mostly by the shape of the driven mode.

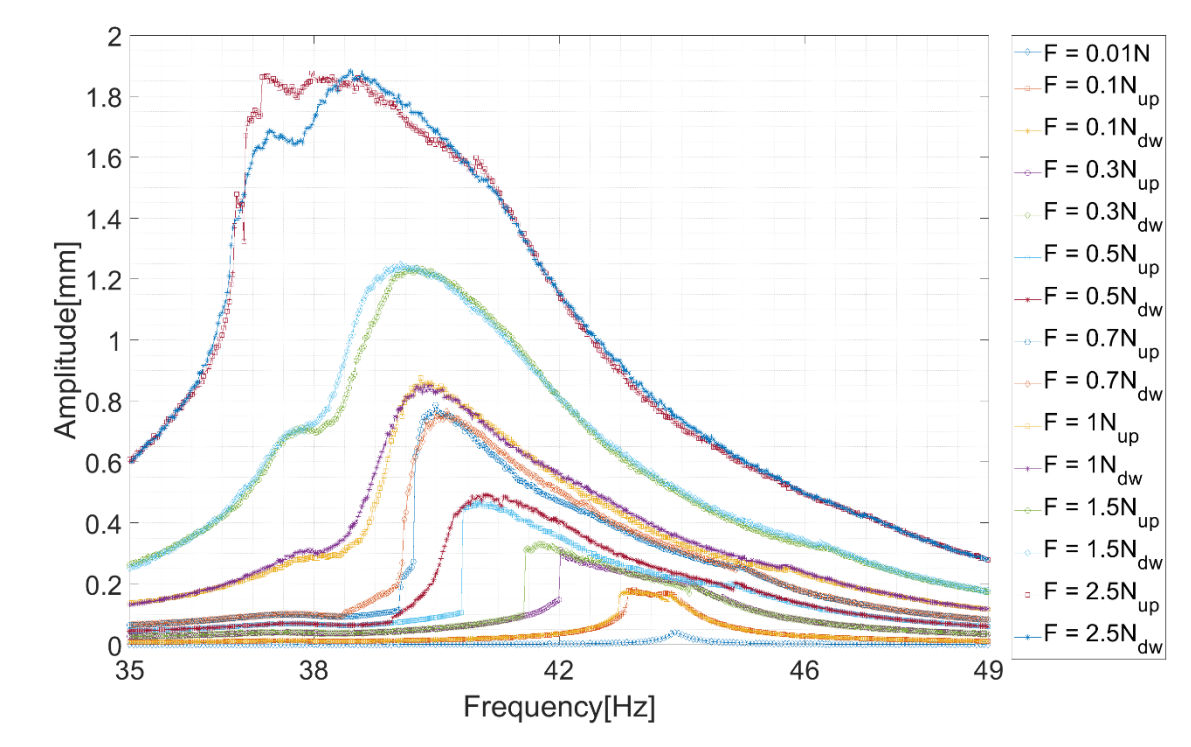


Fig. 10: Frequency – Amplitude curves for the driven mode of the empty rod in air, UP and DOWN directions.

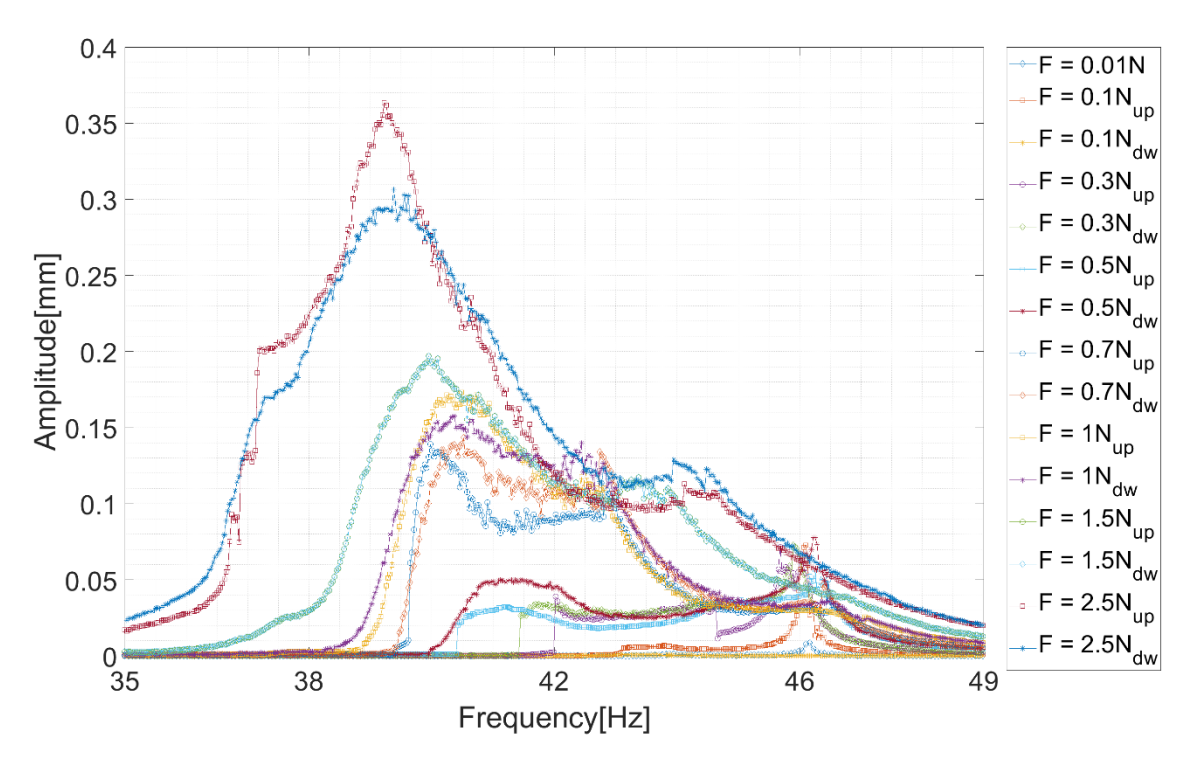


Fig. 11: Frequency – Amplitude curves for the companion mode of the empty rod in air, UP and DOWN directions.

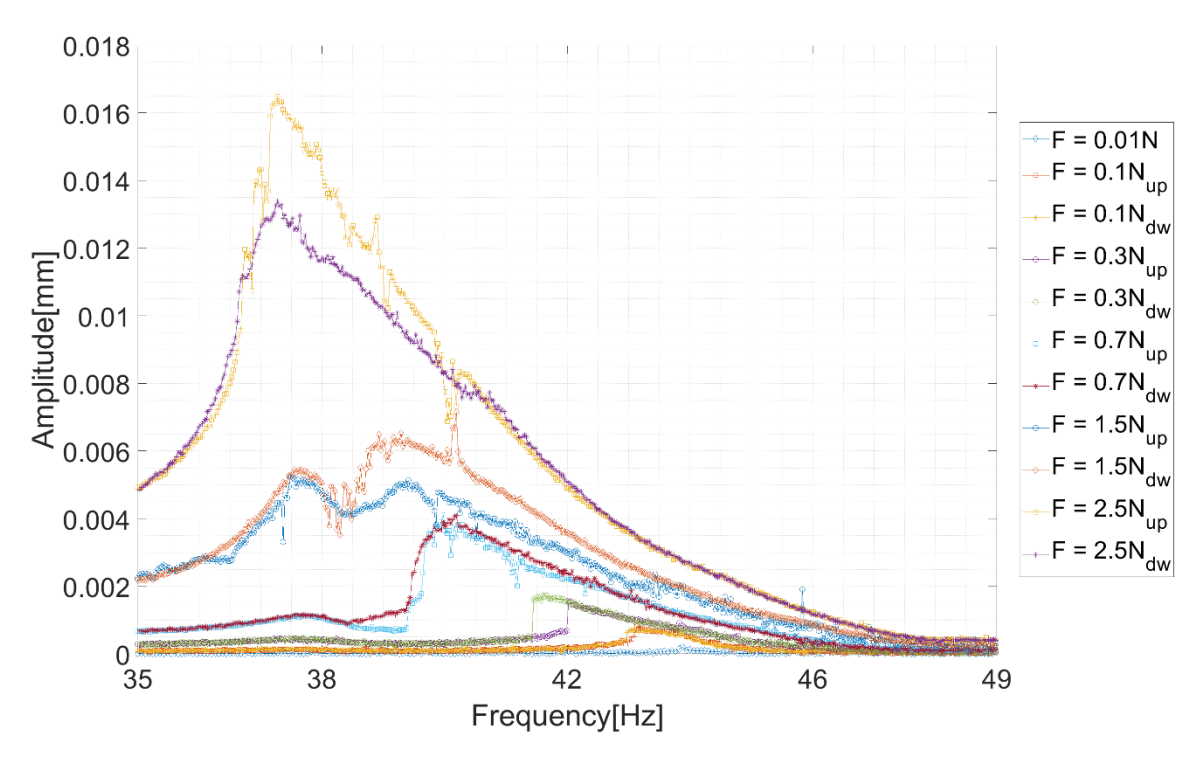


Fig. 12: Frequency – Amplitude curves for the axial mode of the empty rod in air, UP and DOWN directions.

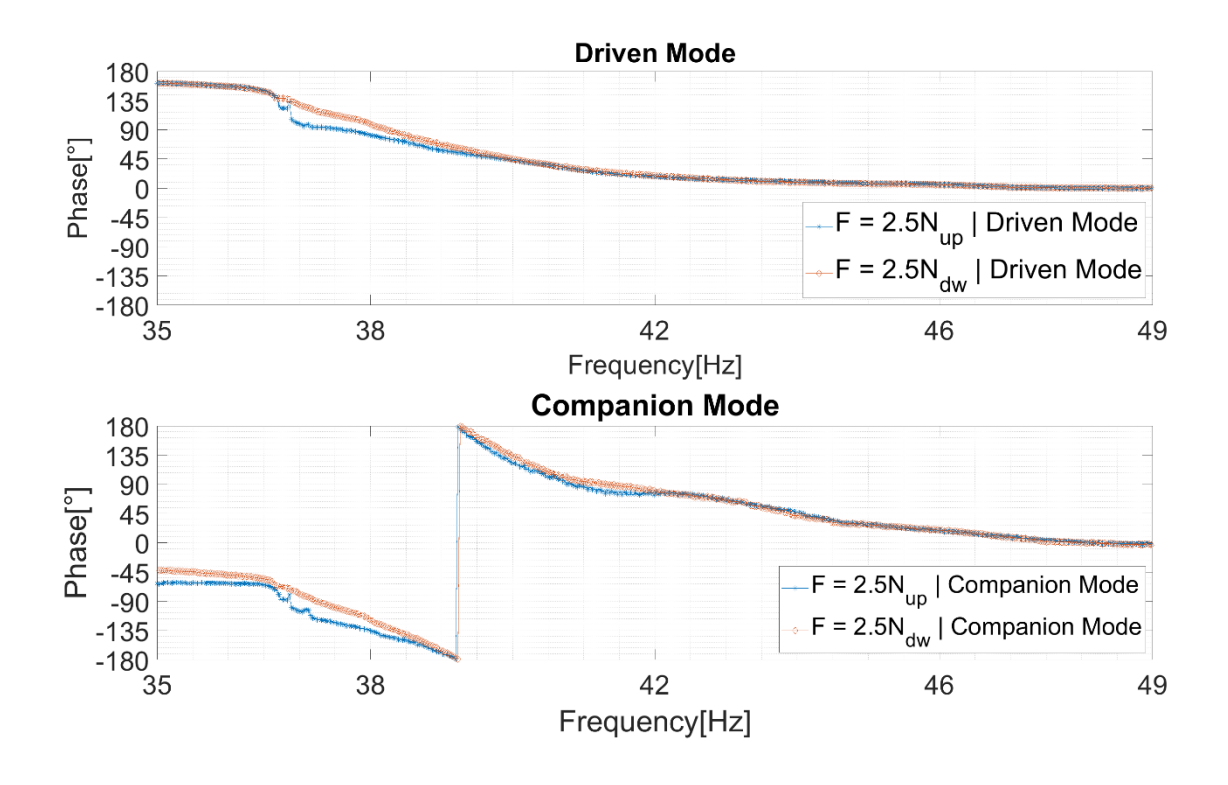


Fig. 13: Frequency – Amplitude and Phase curves for chosen force levels of the driven and companion modes.

3.2. Rod with freely moving pellets in air

The mass of the tungsten pellets, not balanced by a stiffness increase, has as a consequence the reduction of the natural frequencies of the system. This reduction in the frequency values is presented in Table 3. As expected, since energy is dissipated in the free motion of the pellets, modal damping values are higher than in the previous case and larger forces are required to reach the same amplitude levels in the nonlinear regime. Hysteresis cycles of very modest amplitude and few nonlinear hardening jumps are detected but the overall nonlinear behavior is of the softening type (Fig. 14 and Fig. 15). The companion mode remains much smaller than the driven mode; the latter is not influenced by the former. The axial vibration is linked to the driven mode, but it is not comparable in amplitude (Fig. 16).

 Table 3

 Modal parameters of the free-pellets rod in air

Mode	No. half waves	Frequency (Hz)	Damping (%)
I	1	17.2	1.23
П	2	96.9	0.78
III	3	157	0.79
IV	4	233	1.47

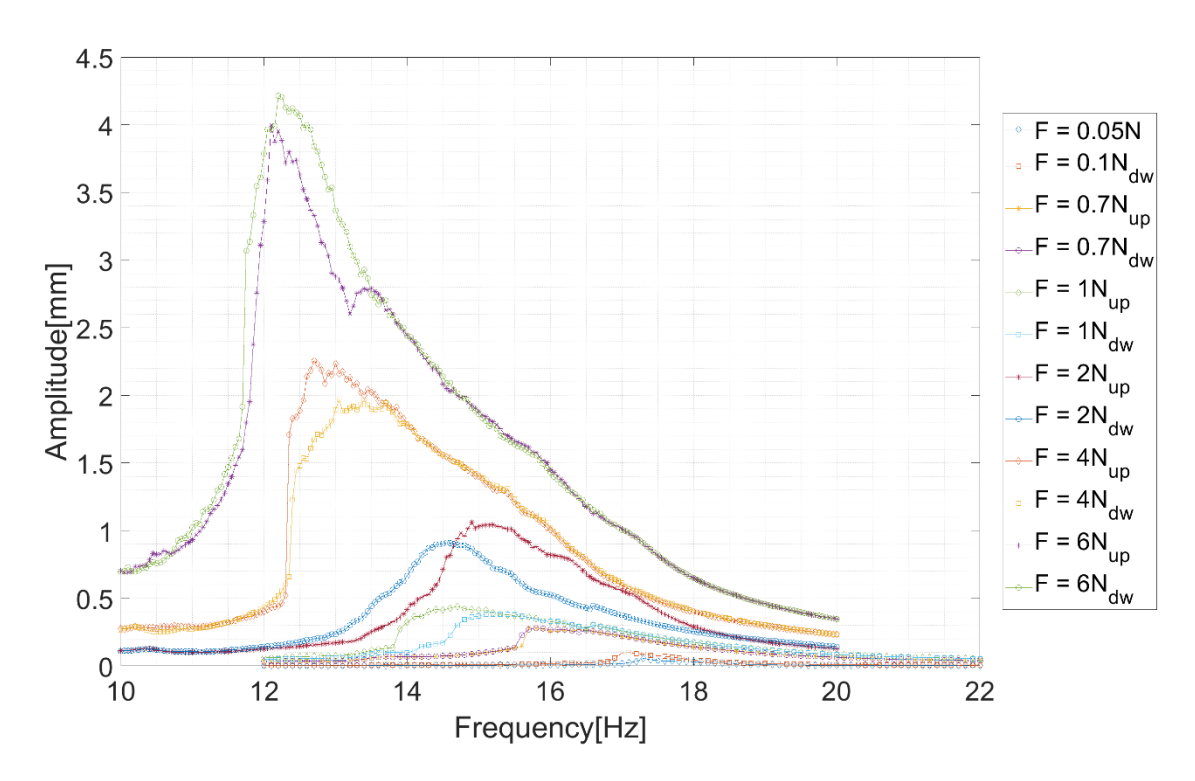


Fig. 14: Frequency – Amplitude curves for the driven mode of the free-pellets rod in air, UP and DOWN directions.

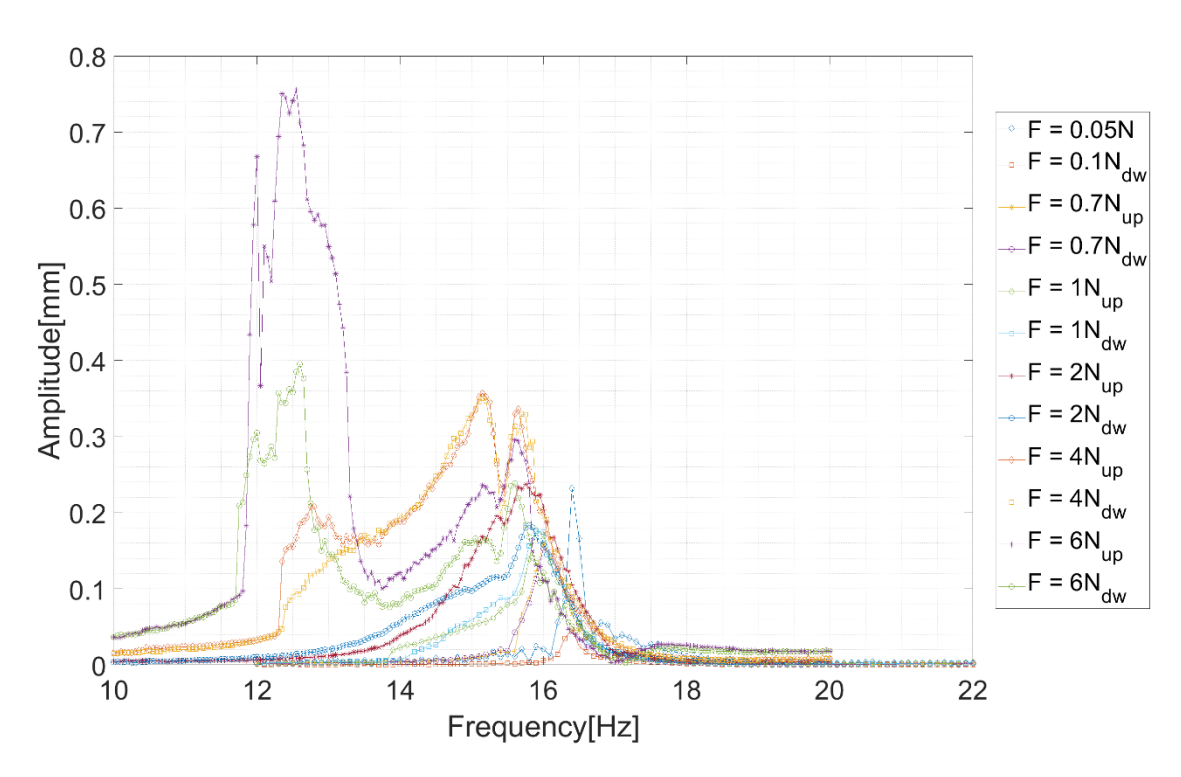


Fig. 15: Frequency – Amplitude curves for the companion mode of the free-pellets rod in air, UP and DOWN directions.

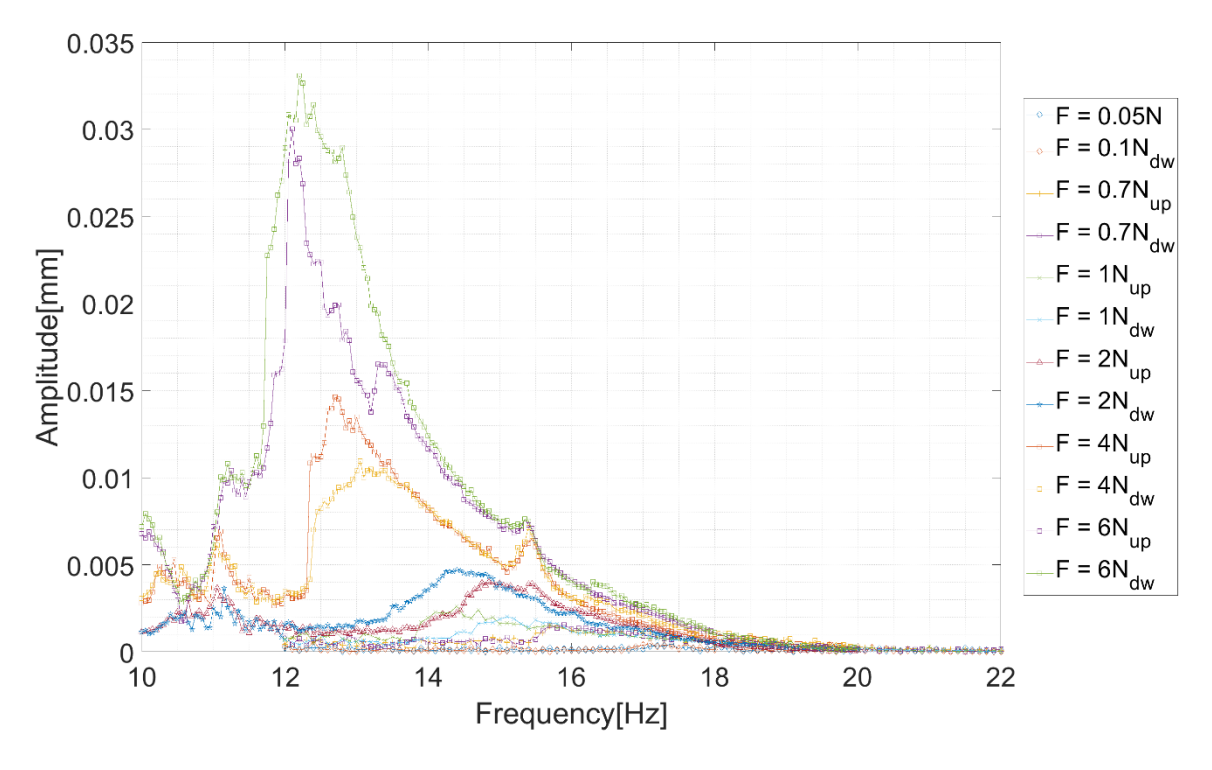


Fig. 16: Frequency – Amplitude curves for the axial mode of the free-pellets rod in air, UP and DOWN directions.

3.3. Rod with fixed pellets in air

With respect to the previous case, natural frequencies are mostly lower; an explanation for this phenomenon is unclear since the mass is unchanged while the stiffness of the system should be increased through the threaded device acting on the pellets. Similarly, the constraint on the movement of the pellets should decrease dissipation, but damping values are similar instead (Table 4). The slots occupied by the rod in the two spacer grids do not change, and the number of cycles the rod is subjected to is totally insufficient to justify a change in the retainment force. Since it is necessary to remove the rod with free pellets and to install the rod with fixed pellets to pass from the tests on the former to the tests on the latter, it is possible to conjecture that the boundary conditions are sensitive to assembly conditions.

Observing the driven mode in the UP and DOWN directions (Fig. 17) it is possible to notice that the behavior becomes softening and some nonlinear jumps appear. The resonance of the companion mode is higher in frequency than that of the driven mode (Fig. 18). The influence of the driven mode on the companion mode is actually higher in amplitude than the resonance of the companion mode itself. The axial vibration is extremely modest in amplitude, but it is influenced by both transversal vibration modes (Fig. 19).

 Table 4

 Modal parameters of the fixed pellets rod in air

Mode	No. half waves	Frequency (Hz)	Damping (%)
I	1	19.85	1.34
П	2	56.9	0.8
Ш	3	114	0.8
IV	4	181	0.73

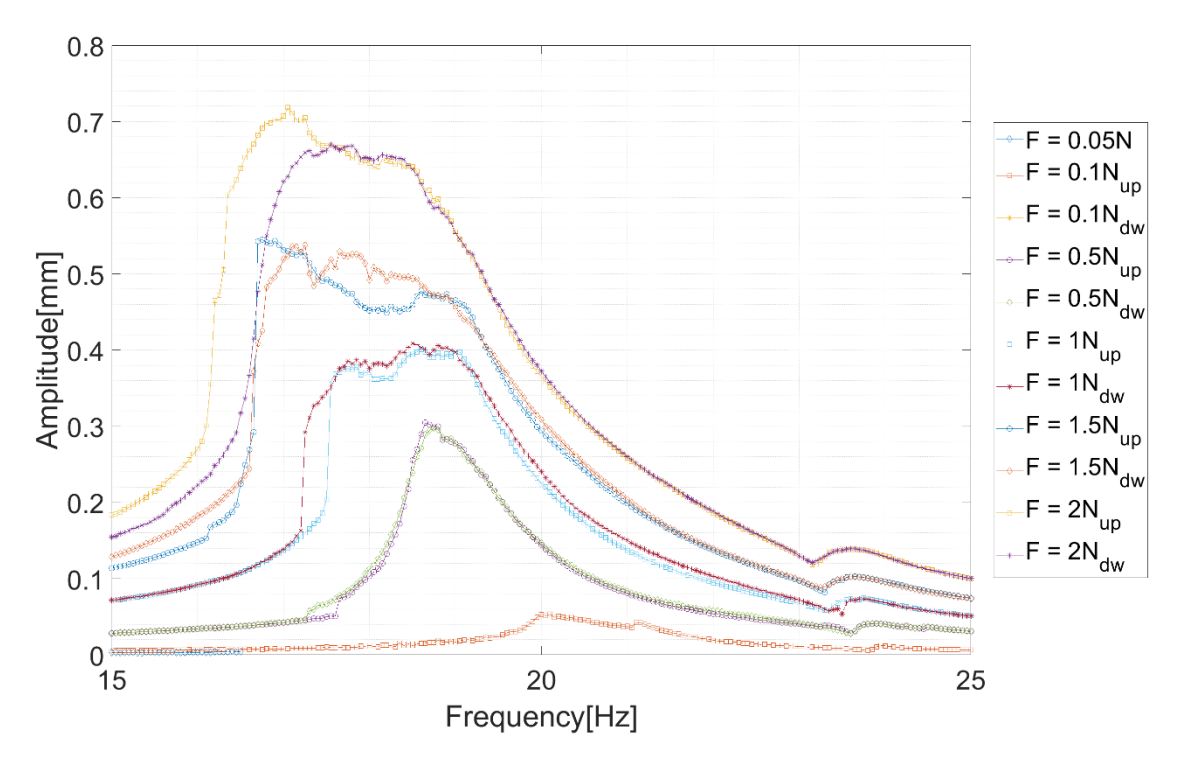


Fig. 17: Frequency – Amplitude curves for the driven mode of the fixed-pellets rod in air, UP and DOWN directions.

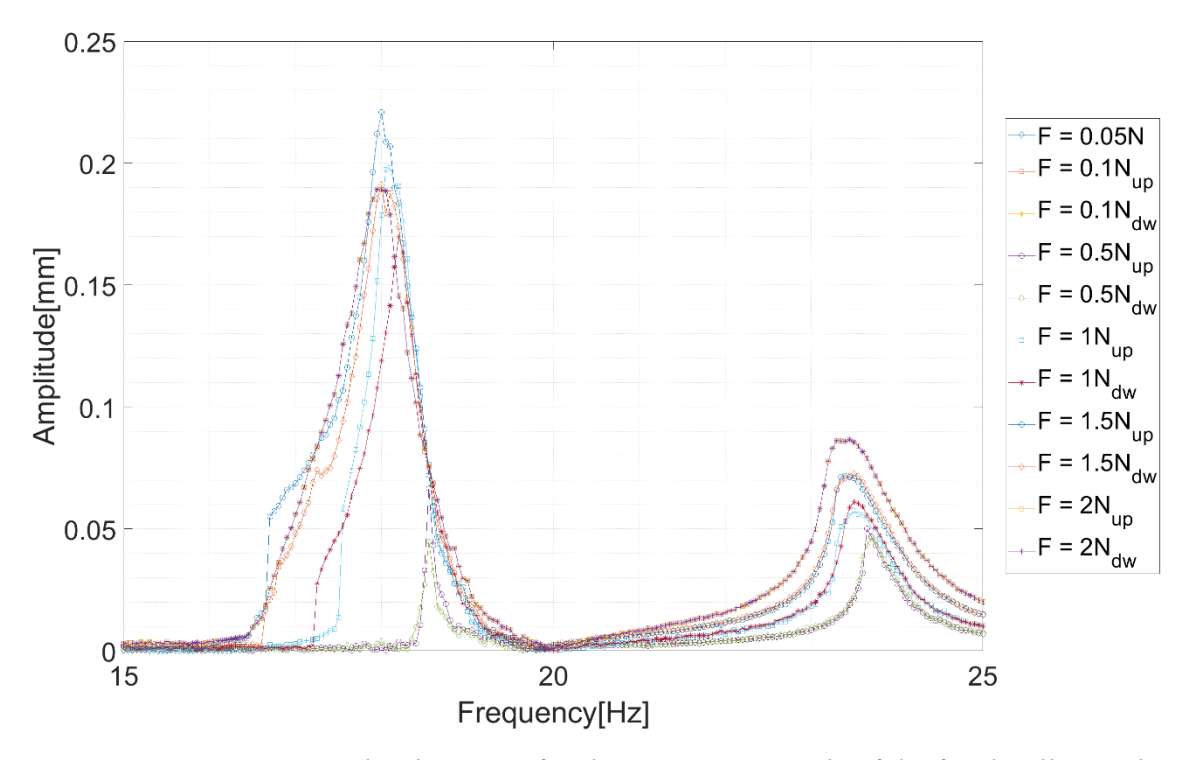


Fig. 18: Frequency – Amplitude curves for the companion mode of the fixed-pellets rod in air, UP and DOWN directions.

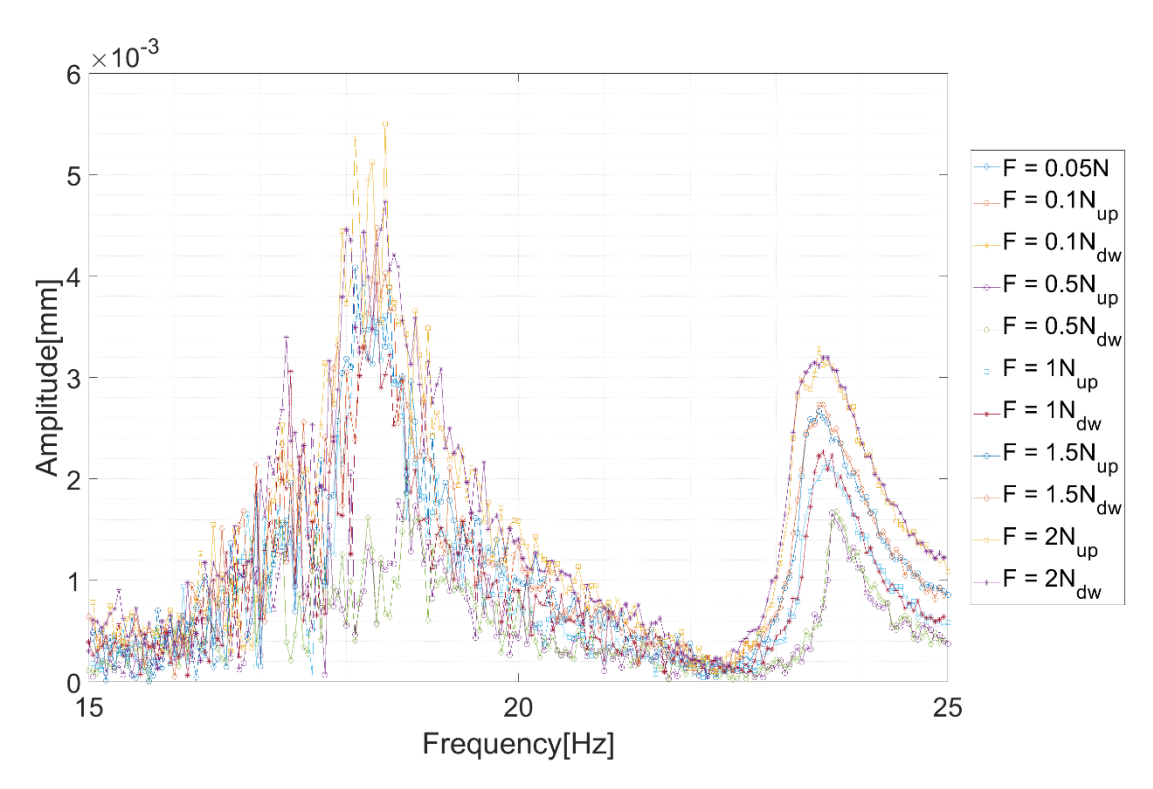


Fig. 19: Frequency – Amplitude curves for the axial mode of the fixed-pellets rod in air, UP and DOWN directions.

3.4. Empty rod in water

Predictably, the introduction of water, through a virtual mass effect, decreases the frequencies with respect to the same configuration in air (see Table 5). It must be also noted from linear results that the values of modal damping are much larger. Frequency-amplitude curves in the nonlinear regime show that in presence of water slightly higher forces are required to achieve specific levels of vibration amplitude (Fig. 20). A nonlinear softening behavior appears from the lowest levels of force, even if the vibration amplitude remains smaller than the external diameter of the rods. The companion mode is characterized by higher frequencies and smaller amplitudes than the driven mode (Fig. 21). The axial vibration is much smaller and follows the trend of the driven mode (Fig. 22).

 Table 5

 Modal parameters of the empty rod in water

Mode	No. half waves	Frequency (Hz)	Damping (%)
ı	1	34.15	1.06
Ш	2	70.52	0.64
Ш	3	95.26	0.89
IV	4	186.93	1.33

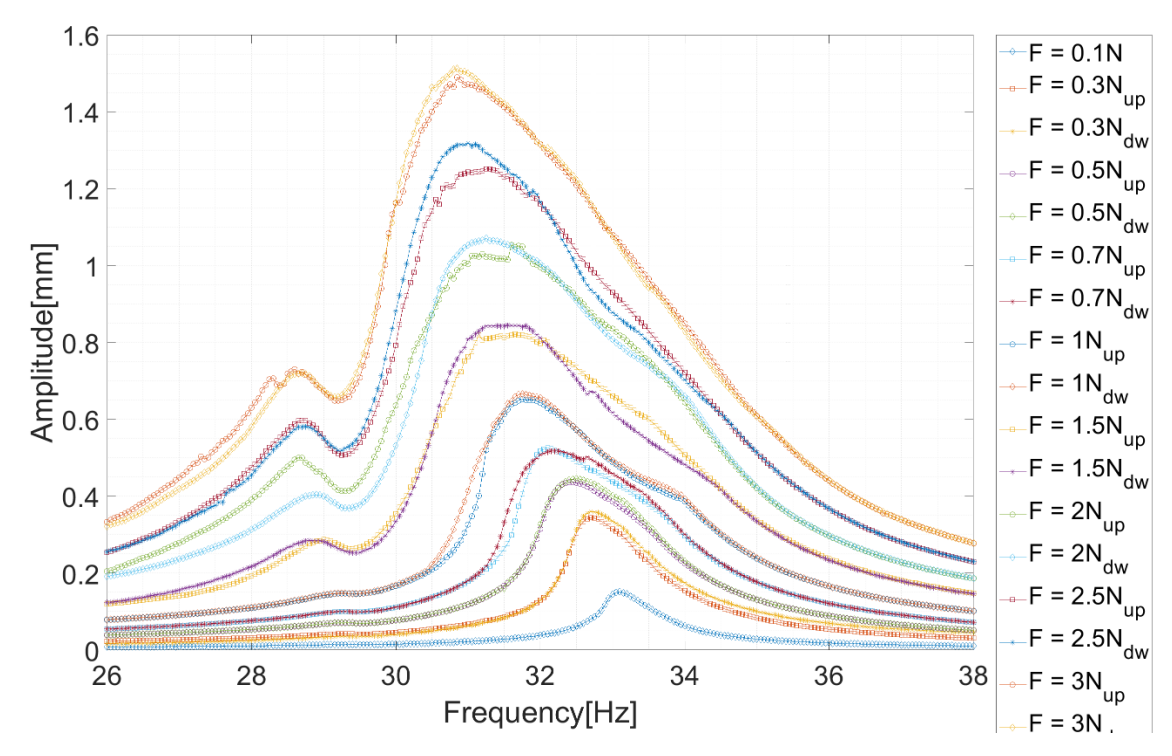


Fig. 20: Frequency – Amplitude curves for the driven mode of the empty rod in water, UP and DOWN directions.

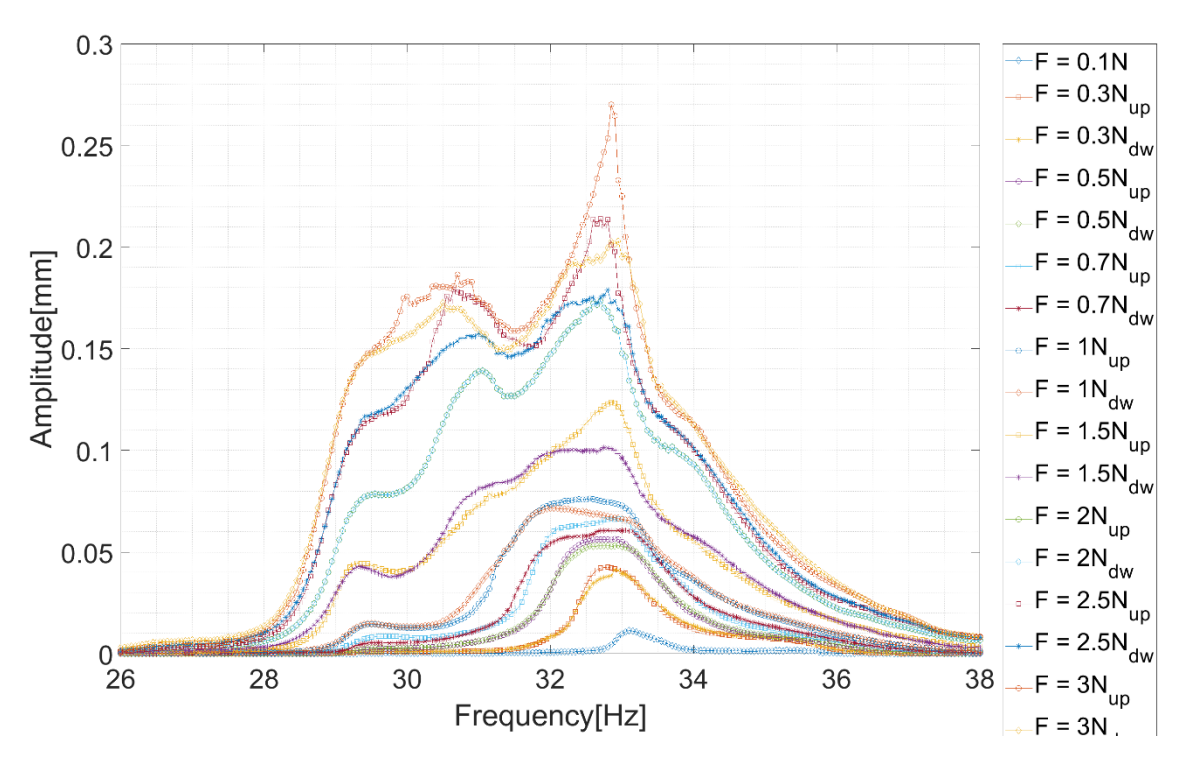


Fig. 21: Frequency – Amplitude curves for the companion mode of the empty rod in water, UP and DOWN directions.

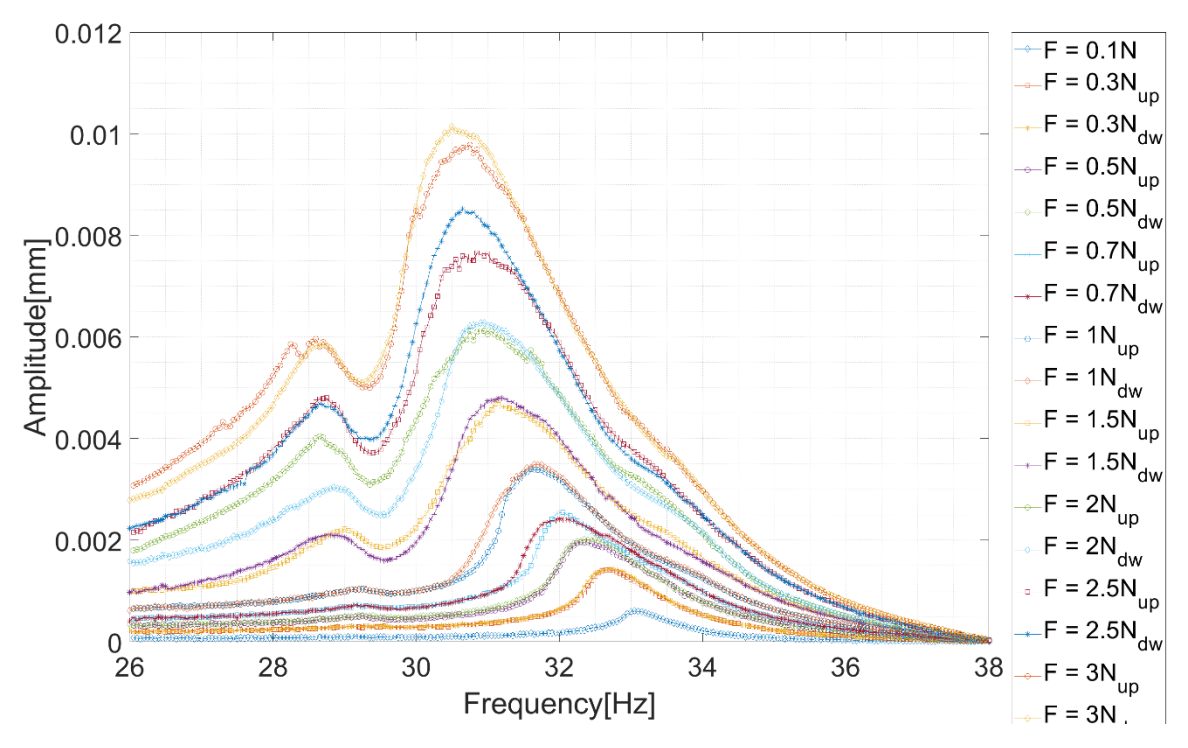


Fig. 22: Frequency – Amplitude curves for the axial mode of the empty rod in water, UP and DOWN directions.

3.5. Rod with freely moving pellets in water

With respect to the corresponding configuration in air, the resonant frequencies decrease and damping increases, with the exception of the first mode (Table 6). The nonlinear curves show a monotonically softening behavior of the driven and companion modes, with a negligible hysteresis and with no development of jumps (Fig. 23 and Fig. 24). Nonlinearity is already evident beyond 0.5 N and the softening frequency shift is larger than that in air. The driven and companion modes are well separated in the frequency domain; the companion mode remains much smaller in amplitude and does not affect the peak amplitude reached by the driven mode. The driven mode, however, affects greatly the companion mode. The axial mode is negligible and is affected clearly by both the horizontal and by the vertical vibration (Fig. 25).

Table 6Modal parameters of the rod with freely moving pellets in water

No. half waves	Mode number	Frequency (Hz)	Damping (%)
1	I	15.59	0.84
2	II	44.17	1.13
3	III	91.34	1.12
4	IV	148 61	1 66

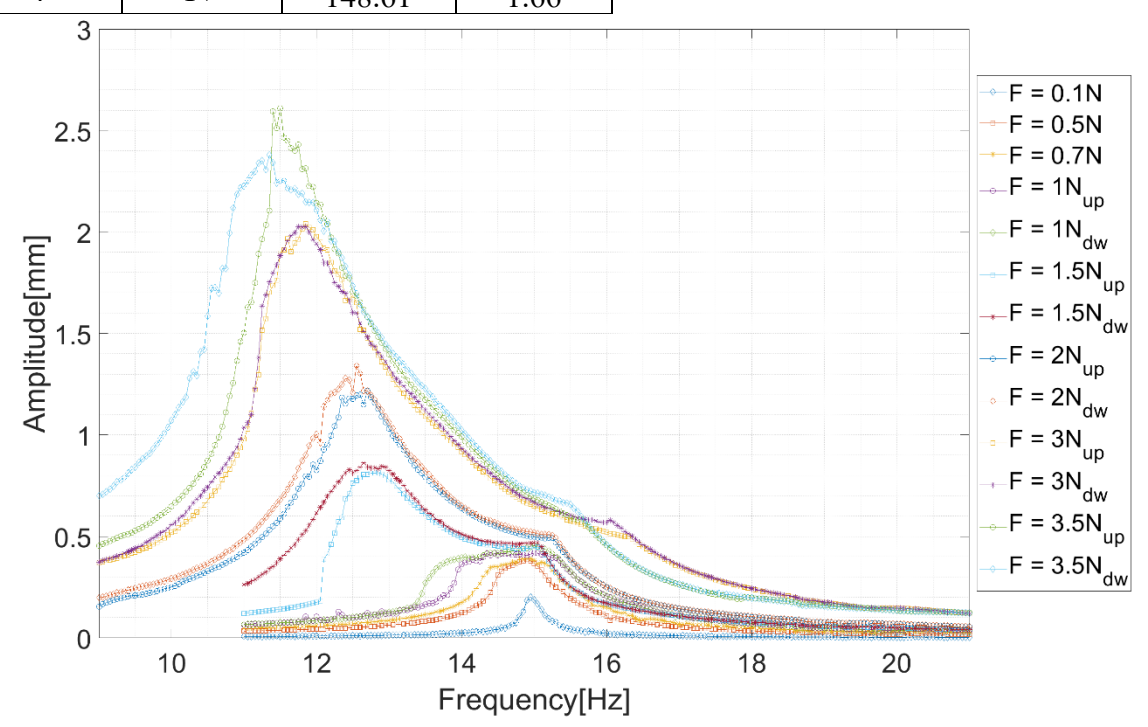


Fig. 23: Frequency – Amplitude curves for the driven mode of the freely moving pellets rod in water, UP and DOWN directions.

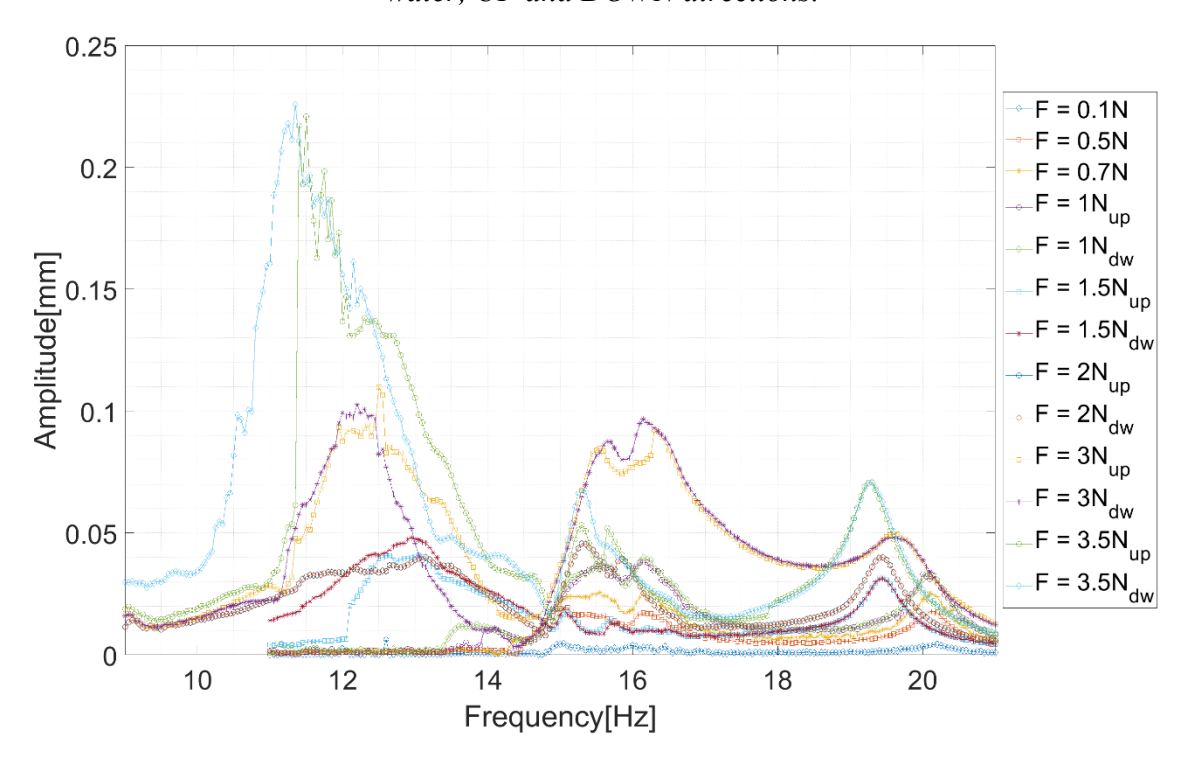


Fig. 24: Frequency – Amplitude curves for the companion mode of the freely moving pellets rod in water, UP and DOWN directions.

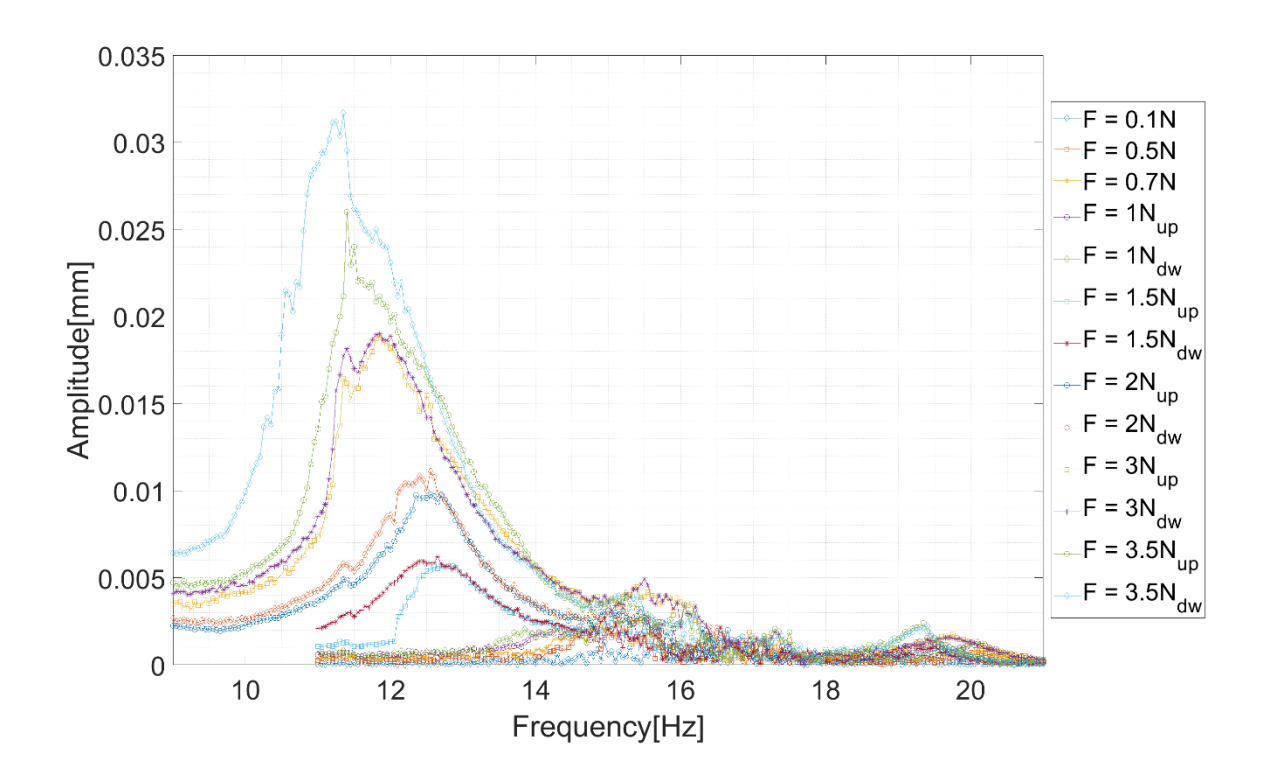


Fig. 25: Frequency – Amplitude curves for the axial vibration of the freely moving pellets rod in water, UP and DOWN directions.

3.6. Rod with fixed pellets in water

The natural frequencies for this configuration are mostly lower than in the corresponding configuration in air, while the opposite happens for the modal damping values (Table 7). Both behaviors are reasonable in presence of water. The nonlinear curves show a very important softening frequency shift, similar to that in air. The amplitude of the nonlinear frequency-amplitude curves is extremely similar to the amplitude reached in air for an excitation of 2 N (Fig. 26). Interestingly, the companion mode presents two different nonlinear peak frequencies, both higher than that of the driven mode (Fig. 27). At approximately 21 Hz, the companion mode presents its resonant peak. While the driven mode vibrates at 14-15 Hz at the largest excitation levels, the companion mode has its vibration peak at approximately 17 Hz. The shift between the two frequencies is caused, as in the other cases, by a symmetry break between the horizontal and the vertical plane, which can be given by the boundary conditions or by the effect of gravity. The companion mode, anyway, remains much smaller than the driven mode, and the latter is not affected. The axial vibration is negligible and repeats the vibration pattern of the driven and companion modes (Fig. 28).

Table 7 *Modal parameters of the rod with fixed pellets in water*

No. half	Mode	Frequency	Damping
waves	number	(Hz)	(%)
1	I	19.19	1.32
2	II	54.30	1.07
3	III	109.13	1.20
4	IV	184.11	1.81

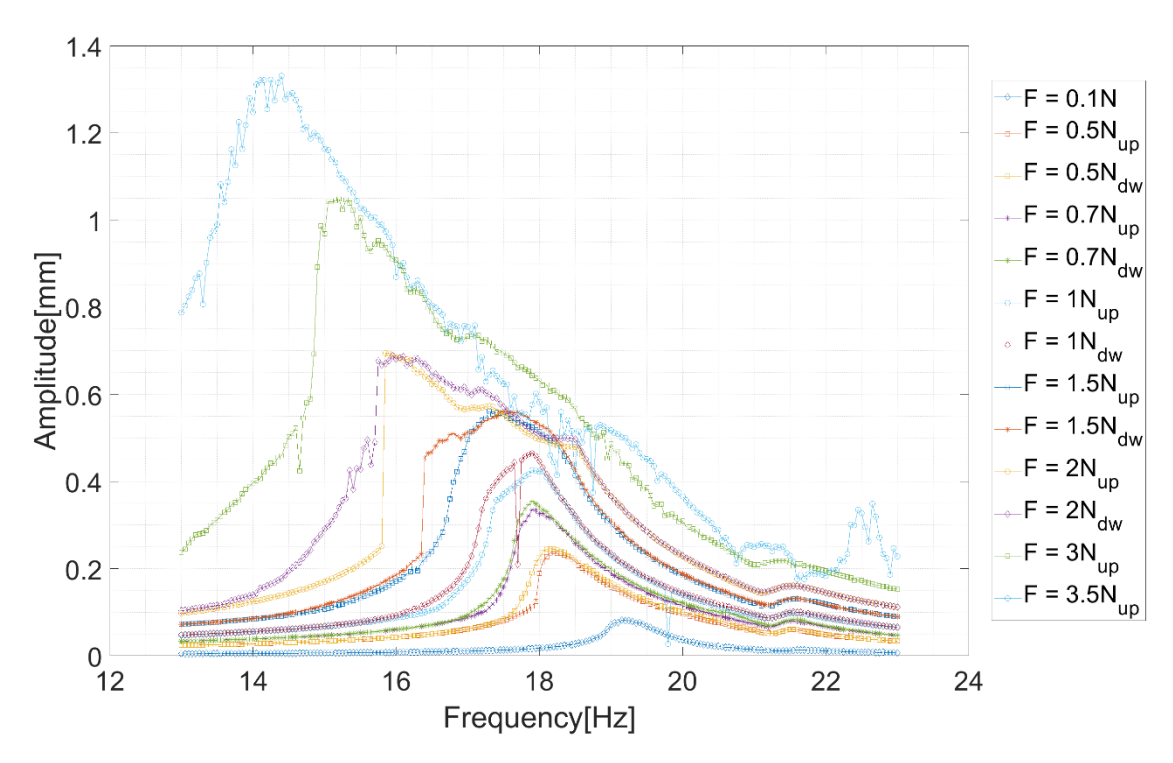


Fig. 26: Frequency – Amplitude curves for the driven mode of the fixed pellets rod in water, UP and DOWN directions.

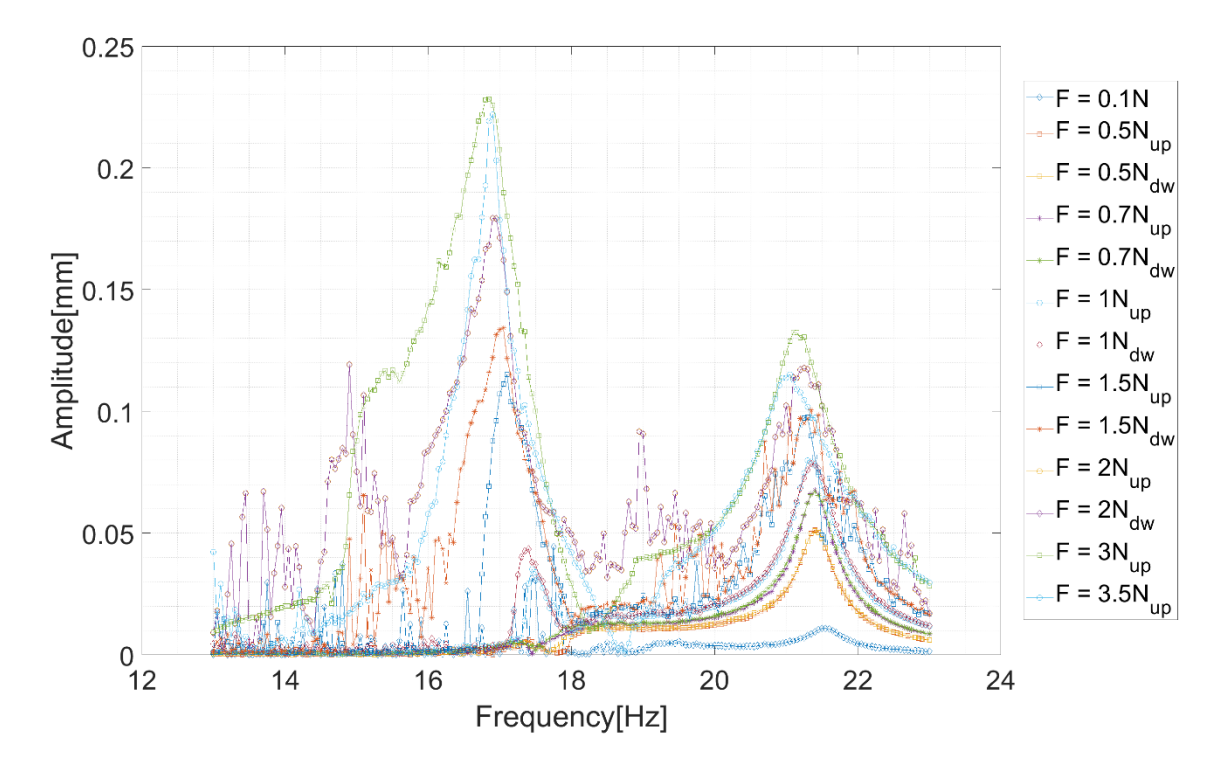


Fig. 27: Frequency – Amplitude curves for the companion mode of the fixed pellets rod in water, UP and DOWN directions.

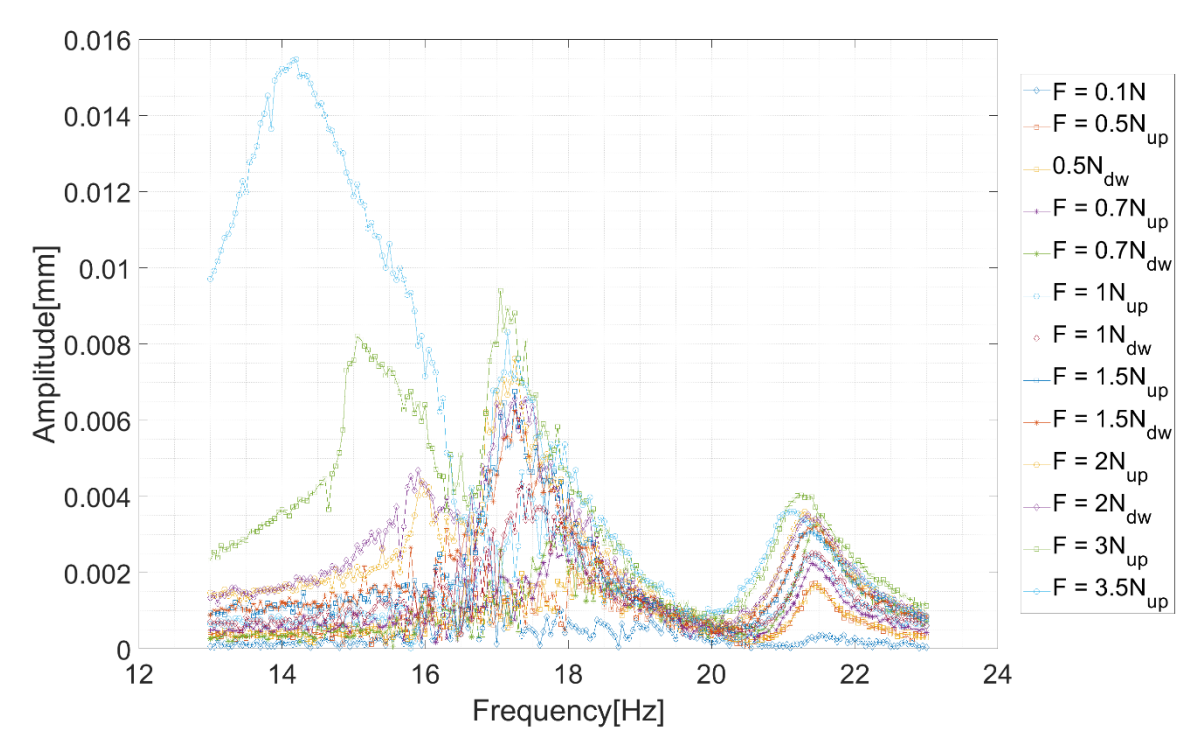


Fig. 28: Frequency – Amplitude curves for the axial vibration of the fixed pellets rod in water, UP and DOWN directions.

4. Damping identification

4.1. Identification process

The single or two-degrees-of-freedom identification procedure for nonlinear frequency responses developed by Le Guisquet and Amabili (2019¹) is valid for most geometric nonlinearities arising from large-amplitude vibrations. Moreover, if a companion vibration (perpendicular to the excitation) is present, it is required that the one-to-one internal resonance between driven and companion mode is perfect—*i.e.*, the two modes must share a perfectly identical frequency. However, the experimental responses presented before feature a significant frequency split between driven and companion mode. Moreover, the evolution of the equivalent nonlinear stiffness—discernible from the shift of resonant frequency with increasing excitation levels—is too strong to be described by a nonlinear model including only stiffness proportional to the square

¹ Mechanical Systems and Signal Processing, submitted.

and the cube of the displacement. This is probably due to the complex boundary conditions at the spacer grids and to the internal motion of the pellets, which introduce phenomena that have to be taken into account by a more accurate numerical model, which is not available yet.

Therefore, in order to describe the evolution of damping with vibration amplitude, a single DOF linear oscillator is fit on the experimental frequency response curves for the driven mode at the minimum and at the maximum levels of excitation. This way, the equivalent modal damping ratio of one response in the small-amplitude domain can be compared with the equivalent modal damping ratio in the large-amplitude domain. As the vibration of the companion mode remains much smaller than that of the driven mode, it was assumed that the former does not affect the global energy dissipation of the structure and it was excluded from the study.

The dimensionless equation of motion of the equivalent single DOF system is

$$r^2\ddot{q} + 2r\zeta\dot{q} + q = \lambda\cos(t),\tag{1}$$

where q is the displacement divided by the wall thickness h of the rod, r is the circular frequency of excitation divided by the natural circular frequency ω_n , ζ is the damping ratio and λ the dimensionless force, defined as

$$\lambda = \frac{F}{hm\omega_n^2},\tag{2}$$

where m is the modal mass. The displacement is approximated by its first harmonic, which in fact is the only one experimentally measured during stepped-sine tests.

The dimensionless equation of motion is applied first on the lowest response and then on the largest response. For the lowest responses, the value of ω_n is determined as the frequency corresponding to the peak amplitude while, for the largest responses, it is taken as the value giving the best fit; consequently, the low-amplitude and the large-amplitude curves have two different values for ω_n . In the equation of motion, ζ and λ remain unknown (λ depending on the unknown modal mass). Both unknowns could be estimated by means of a least-squares method developed for this purpose, which would provide the closest fit of the simulated and of the experimental responses over the entire frequency range. However, this would result in an unsatisfactory trade-off between the peak amplitude reached and a good fit in the entire frequency range. Nonlinear amplitude responses, in fact, are in general not symmetric in the frequency domain with respect to their peak frequency ω_n , so they cannot be fitted closely by a linear model. A discrepancy in the amplitude of the peak of the nonlinear curve would be particularly harmful in the scope of this study. Consequently, only

 λ is provided by the least-squares algorithm. The damping ratio, instead, is set so that the simulated and the experimental response reach exactly the same amplitude at their peak.

Table 8Identified natural frequencies, dimensionless forces and damping ratios at the minimum and maximum excitation amplitude for each experimental case.

	imental ase	Force (N)	Peak frequency (Hz)	Frequency decrease (%)	Equivalent modal damping ratio ζ	Damping increase
	Empty	0.01	43.88	11.14	0.37×10^{-2}	12.27
	rod	2.50	38.99	11.14	4.54×10 ⁻²	12.27
Air	Free	0.05	17.30	25.95	1.40×10 ⁻²	5.01
Alf pellets	pellets	6.00	12.81	23.93	7.01×10 ⁻²	5.01
Fixed	0.10	20.10	8.96	2.54×10 ⁻²	2.11	
	pellets	2.00	18.30	0.90	5.36×10 ⁻²	2.11
	Empty	0.10	33.10	3.99	1.00×10 ⁻²	4.11
	rod	3.00	31.78	3.99	4.11×10 ⁻²	4.11
water pe	Free	0.10	14.95	23.08	0.74×10^{-2}	8.15
	pellets	3.50	11.50		6.03×10 ⁻²	
	Fixed	0.10	19.15	23.29	1.58×10 ⁻²	6.61
	pellets	3.50	14.69	23.29	10.45×10 ⁻²	6.61

4.2. Results and discussion

Table 8 shows force, peak frequency and equivalent modal damping ratio for each case both at the minimum and at the maximum force level. Fig. 29 and Fig. 30 feature the experimental and the simulated responses in terms of amplitude (a_1) and phase (ϕ_1) of the first harmonic of the dimensionless displacement at the highest excitation level for each case.

Despite some discrepancies between the identified and the experimental responses, the linear oscillator enables a first approximation of the frequency response of the rod for a specific magnitude of excitation. The natural frequencies obtained for the linear responses are predictably close to the ones obtained previously by experimental modal analysis. However, with the exception of the empty rod in air, the estimated damping ratios of the linear responses are 8% to 33% lower than the ones from experimental modal analysis. This can be explained by the fact that: i) some linear responses show one-to-one internal resonance, hence a truncation of the peak amplitude of the driven mode;

ii) the stepped-sine sinusoidal signal provides excitations too large to remain in the linear field; and, iii) the system may change slightly, for example because of changes in temperature, between the moments of the modal analysis and of the stepped-sine analysis.

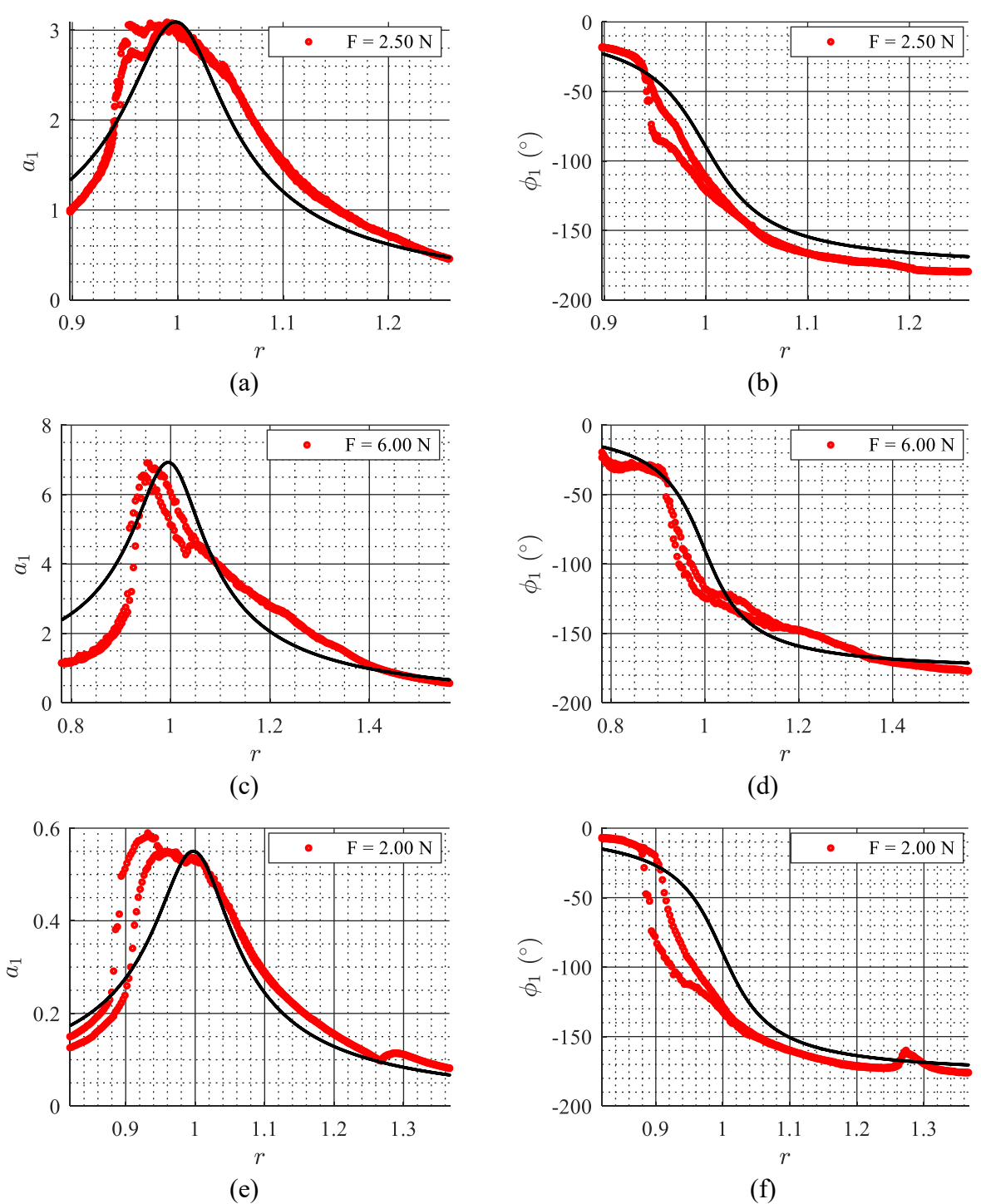
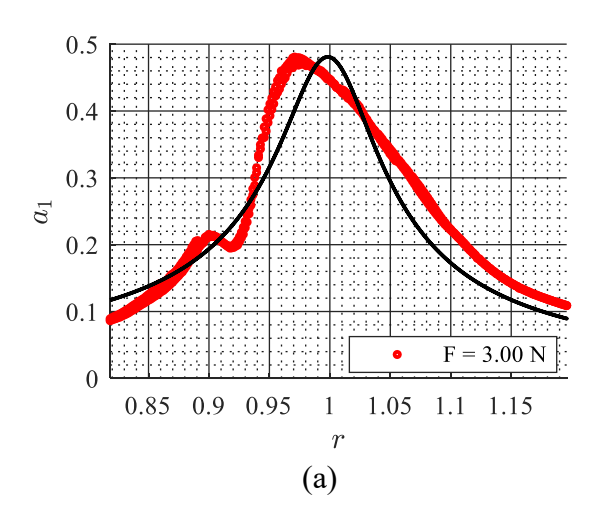


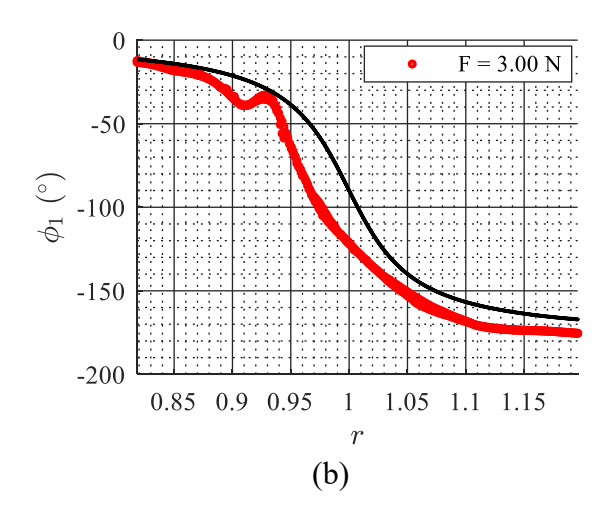
Fig. 29: Frequency-response of the first harmonic of the dimensionless displacement for the experiments in air: (a) amplitude and (b) phase of the empty rod; (c) amplitude and (d) phase of

the rod with freely moving pellets; (e) amplitude and (f) phase of the rod with fixed pellets.

Experimental data represented by markers and identified data represented by continuous line.

On the other hand, it is clear that the damping ratios estimated for the largest responses present a significant increase (they are 2 to 12 times higher) with respect to the ones extracted from responses at the lowest excitation levels. These figures highlight the need of taking into account a nonlinear increase of the damping with the magnitude of excitation and with the peak amplitude of the response by means of nonlinear models, as applied phenomenologically by Eichler *et al.* (2011); Jeong *et al.* (2013); Le Guisquet and Amabili (2019²); Lu *et al.* (2019) and as developed theoretically by Amabili (2018a, 2018b, 2018c, 2019a). Comparing damping ratios in water and in air at the lowest excitation levels does not show any clear trend. The increase of the damping value for nonlinear excitation is highest for the empty rod in air and lowest for the rod with fixed pellets in air; other configurations feature instead similar values of the increase. The reduction of the natural frequencies between linear and nonlinear field is softening, but much larger than that modeled by typical Duffing equations with nonlinear quadratic stiffness; in fact, here the decrease reaches a value of almost 26% in air.





² Mechanical Systems and Signal Processing, submitted.

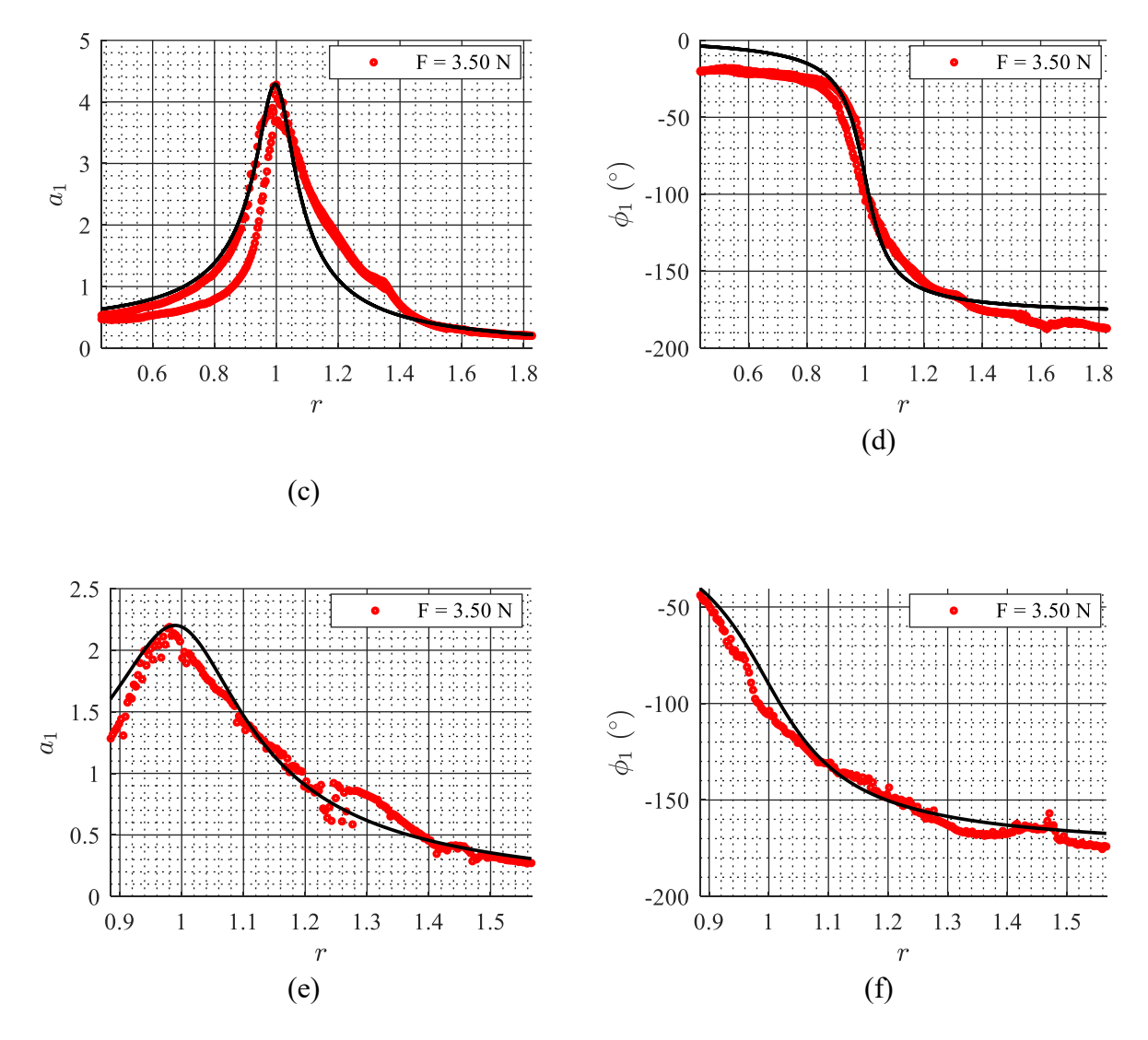


Fig. 30: Frequency-response of the first harmonic of the dimensionless displacement for the experiments in water: (a) amplitude and (b) phase of the empty rod; (c) amplitude and (d) phase of the rod with freely moving pellets; (e) amplitude and (f) phase of the rod with fixed pellets. Experimental data represented by markers and identified data represented by continuous line.

5. Conclusions

The current work proceeds from the past characterization of single fuel rods with fixed-fixed boundary conditions and precedes the study of bundles of fuel rods in quiescent and flowing water. Consequently, it does not take into account the fluid structure interaction of flowing water on a cluster of fuel rods. Flowing water is, *inter alia*, the likely cause of broadband excitation. This

problem is investigated in detail by the same authors in Ferrari *et al.* (2019). While the present investigation provides limited insight on the nonlinear vibrations of operative PWR bundles, it is particularly suitable for the determination of the specific influence of spacer grids. Such elements showed a remarkably nonlinear static characteristic. It was reasonable therefore to expect an important influence of the boundary conditions on the dynamics of the structure. Compared to the fixed-fixed boundary conditions discussed by Ferrari *et al.* (2018), a much larger damping increase is in fact observed passing from the linear to the nonlinear field. This is probably due to the friction forces and to the impacts occurring at the boundary conditions. The increase of nonlinear damping contributes to the overall safety of the system against excessive vibration amplitudes.

Although axial symmetry is broken and damping increases, the presence of spacer grids does not inhibit the appearance of vibrations perpendicular to the direction of the excitation (companion mode), along with vibrations parallel to the excitation (driven mode). The composition of driven and companion mode for axisymmetric structures is explained in detail in Ferrari *et al.* (2018). However, in presence of spacer grids the companion mode does not reach vibration amplitudes comparable to the driven mode; consequently, proper traveling wave phenomena do not appear. Nevertheless, this seems to suggest that bi-directional flexural vibrations may appear during the operation of nuclear reactors as well. Since spacer grids allow axial displacements, opposed by dry friction only, the axial vibration at the constraints was measured. As expected, the measured axial displacements were several times smaller in amplitude than those of the driven and companion modes. While the driven and the companion modes appear at different frequencies and interact in a complex manner (influenced, perhaps, by the vibration of the nuclear fuel pellets as well), the axial vibration occurs always at the same frequencies corresponding to the two main vibration modes. This seems to suggest that no specific vibration mode is present in the axial direction.

The presence of nuclear fuel pellets is the main factor influencing the vibration in the linear field by means of added mass and stiffness. The trend of nonlinear vibration is always strongly softening. This is an important difference with respect to what happened in case of fixed-fixed boundary conditions (Ferrari *et. al.*, 2018). The hysteresis here is negligible, most likely because of damping phenomena. Similarly, nonlinear jumps are not found, with the exception of small areas in the frequency charts. Highly damped curves without nonlinear jumps and such a softening behavior, unfortunately, were not described successfully by the one DOF model based on a modified Duffing oscillator developed by this research group. Therefore, it was not possible to

characterize the trend of the damping increase between the two extreme values of the excitation level. Such study will be undertaken in the future as experimentation on friction and impacts at the spacer grids is anticipated. Experimental data on the interaction between spacer grids and rods will in fact allow the development of lumped parameter models for the nonlinear boundary conditions. These models will constitute the inputs for reduced order models of the nuclear systems and for modified forms of the single DOF Duffing oscillator proposed in this study.

The experimental setup, inherited from previous tests without spacer grids, allowed successfully the measurement of the linear and nonlinear dynamics of the rods in air and in water. Therefore, this system will be adapted to more complex dynamic experiments on nuclear fuel bundles. However, the measurement of axial vibrations proved remarkably difficult. In fact, these vibrations are not existent in the linear field, while they increase sharply, reproducing the trend of larger flexural vibrations. A dedicated in-plane vibration measurement will be developed to measure the vibration at the spacer grids instead of the overall extension and contraction of the ends of the rods. The availability of reliable non-contact methods for the measurement of the axial motion of nuclear fuel rods is particularly important, because it allows the estimation of the amount of friction at the boundary conditions.

Given the moderate difference between free and fixed pellets conditions, the former may not be taken into account in future studies. During the operation of nuclear reactors, pellets are in fact packed axially. However, the presence of pellets is the primary cause of large softening frequency decreases, which indicates the utility of taking pellets into account by the inclusion of additional degrees of freedom into future models and simulations.

Acknowledgements

The authors would like to thank the NSERC CRD Grant Program for its financial support. The authors would also like to thank Framatome Canada Ltd. for their support.

References

Adams, D.E., and Randall, J.A. (1998). Survey of Nonlinear Detection and Identification Techniques for Experimental Vibrations. Proceedings of the 23rd International Conference on Noise and Vibration Engineering, ISMA, Leuven, Belgium.

Adhikari, S. and Woodhouse, J. (2001). Identification of damping: Part 1, viscous damping. Journal of Sound and Vibration, 243, 43-61.

Adhikari, S. and Woodhouse, J. (2001). Identification of damping: Part 2, non-viscous damping. Journal of Sound and Vibration, 243, 63-88.

Alijani, F., Amabili, M., Balasubramanian, P., Carra, S., Ferrari, G., Garziera, R. (2016). Damping for large-amplitude vibrations of plates and curved panels, part 1: modelling and experiments. International Journal of Non-linear Mechanics, 85, 23-40.

Amabili M. (2008). Nonlinear vibrations and stability of shells and plates. Cambridge University Press, New York, USA.

Amabili M. (2018a). Nonlinear Mechanics of Shells and Plates: Composite, Soft and Biological Materials. Cambridge University Press, New York, USA.

Amabili, M. (2018b). Nonlinear damping in large-amplitude vibrations: modelling and experiments. Nonlinear Dynamics, 93(1), 5-18.

Amabili, M. (2018c). Nonlinear damping in nonlinear vibrations of rectangular plates: derivation from viscoelasticity and experimental validation. Journal of the Mechanics and Physics of Solids, 118, 275-292.

Amabili, M. (2019). Derivation of nonlinear damping from viscoelasticity in case of nonlinear vibrations. Nonlinear Dynamics, 97, 1785-1797.

Amabili, M., Alijani, F., Delannoy, J. (2016). Damping for large-amplitude vibrations of plates and curved panels, part 2: Identification and comparisons. International Journal of Non-Linear Mechanics, 85, 226–240.

Amabili, M., Balasubramanian, P., Ferrari, G. (2016). Travelling wave and non-stationary response in nonlinear vibrations of water-filled circular cylindrical shells: Experiments and simulations. Journal of Sound and Vibration, 381, 220-245.

Amabili, M., Carra, S. (2012). Experiments and simulations for large-amplitude vibrations of rectangular plates carrying concentrated masses. Journal of Sound and Vibration, 331, 155–166.

Au-Yang, M.K., Burgess, J.A. (2007). Critical velocity of a nonlinearly supported multispan tube bundle. ASME Pressure Vessel Technology, 129, 535-540.

Bakosi, J., Christon, M.A., Lowrie, R.B., Pritchett-Sheats, L.A., Nourgaliev, R.R. (2013). Large-eddy simulations of turbulent flow for grid-to-rod fretting in nuclear reactors. Nuclear Engineering and Design 262, 544-561.

Balasubramanian, P., Ferrari, G., Amabili, M. (2018). Identification and comparison of various damping models during large amplitude vibrations. Mechanicals Systems and Signal Processing 111, 376-398.

Balasubramanian, P., Ferrari, G., Amabili, M., del Prado, Z.J.G.N. (2017). Experimental and theoretical study on large amplitude vibrations of clamped rubber plates. International Journal of Non-Linear Mechanics, 94, 36-45.

Bennet, G., Antunes, J., Mendes, J., Piteau, Ph. (1997). Some issues on the identification of experimental fluid-elastic forces. Transactions of the 14th International Conference on structural Mechanics in Reactor Technology (SMiRT 14), Lyon, France.

Bhattacharya, A. (2013). Investigations on Flow and Flow-Induced Vibration of CANDU Fuel Bundles. Thesis. Ryerson University, Toronto, Ontario, Canada.

Brenneman, B. and Shah, S.J. (2000). Damping in fuel assemblies for axial flow. Emerging Technologies in Fluids, Structures, and Fluid/Structure Interactions – Volume 1, Seattle, Washington.

Campbell, W.R., Chen, J. (2017). An Analysis of GTRFW Initiation Using Finite Element Method. Nuclear Science, 2(3):82.

Chen, S.-S. (1975). Vibration of nuclear fuel bundles, Nuclear Engineering and Design, 35 (3), 399-422.

Chen, S.-S. (1985). Flow-Induced Vibration of Circular Cylindrical Structures. Argonne National Laboratory, Report ANL-85-81, USA.

Choi M. H., Kang H. S., Yoon K. H. and Song K. N. (2004). Vibration analysis of a dummy fuel rod continuously supported by spacer grids. Nuclear Engineering and Design, 232(2), 185-196.

Collard, B., Pisapia, S., Bellizzi, S., Broc, D. (2004). Flow induced damping of a PWR fuel assembly. Transactions of 8th International Conference on Flow-Induced Vibration, FIV2004, Paris, France.

Connors, H.J., Savorelli, S.J., Kramer, F.A. (1982). Hydrodynamic damping of rod bundles in axial flow. Pressure Vessel and Piping, 63, 109-124.

De Pauw, B., Weijtjens, W., Vanlanduit, S., Van Tichelen, K., Berghmans, F. (2015). Operational modal analysis of flow-induced vibration of nuclear fuel rods in a turbulent axial flow. Nuclear Engineering and Design, 284, 19-26.

De Santis, D., Shams, A. (2017). Numerical modeling of flow induced vibration of nuclear fuel rods. Nuclear Engineering and Design, 320, 44-56.

Delannoy J., Amabili M., Matthews B., Painter B., Karazis K. (2015). Non-linear damping identification in nuclear systems under external excitation. ASME 2015 International Mechanical Engineering Congress and Exposition. Houston, Texas, USA.

Delannoy J., Amabili M., Matthews B., Painter B., Karazis K. (2016) Identification of Non-Linear Damping of Nuclear Reactor Components in Case of One-to-One Internal Resonance, ASME International Mechanical Engineering Congress and Exposition, Pittsburgh, Pennsylvania, USA.

Dragunov, Yu.G., Solonin, V.I., Perevezentsev, V.V., Petrov, I.V. (2013). Vibrations of fuel-element bundles in VVER fuel assemblies excited by turbulent coolant flow. Atomic Energy, 113, 153-162.

Eichler, A., Moser, J., Chaste, J., Zdrojek, M., Wilson-Rae, I., & Bachtold, A. (2011). Nonlinear damping in mechanical resonators made from carbon nanotubes and graphene. Nature nanotechnology, 6(6), 339.

Fardeau, P., Barbier, D., de Langre, E., Rigaudeau, J. (1997). Damping from axial coolant flow in the response of PWR fuel assemblies to horizontal seismic loads. Transactions of the 14th International Conference on Structural Mechanics in Reactor Technology (SMiRT 14), Lyon, France.

Ferrari, G., Balasubramanian, P., Le Guisquet, S., Piccagli, L., Karazis, K., Painter, B., Amabili, M. (2018). Non-linear vibrations of nuclear fuel rods. Nuclear Engineering and Design, 338, 269-283.

Ferrari., G., Franchini, G., Faedo, L., Giovanniello, F., Le Guisquet, S., Balasubramanian, P., Karazis, K., Amabili, M. (2019, under internal review). Nonlinear vibrations of a PWR fuel assembly supported by spacer grids.

Hassan, M.A., Rogers, R.J., Gerber, A.G. (2011). Damping-controlled fluidelastic instability forces in multi-span tubes with loose supports. Nuclear Engineering and Design, 241, 2666-2673.

Hofstede, E.ter, Kottapalli, S., Shams, A. (2017). Numerical prediction of flow induced vibrations in nuclear reactor applications. Nuclear Engineering and Design, 319, 81-90.

Hu, Z., Thouless, M.D., Lu, W. (2016). Effects of gap size and excitation frequency on the vibrational behavior and wear rate of fuel rods. Nuclear Engineering and Design, 308, 261-268.

Jeong, B., Cho, H., Yu, M. F., Vakakis, A. F., McFarland, D. M., & Bergman, L. A. (2013). Modeling and measurement of geometrically nonlinear damping in a microcantilever–nanotube system. ACS nano, 7(10), 8547-8553.

Kaneko, S., Nakamura, T., Inada, F., Kato, M., Ishihara, K., Nishihara, T., Mureithi, Njuki, W.M., Langthjem, M.A. (2013). Flow-Induced Vibrations: Classifications and Lessons from Practical Experiences: Second Edition, Academic Press.

Kang H., Song K., Kim H.-K., Yoon K. and Jung Y. H. (2001). Verification Test and Model Updating for a Nuclear Fuel Rod with Its Supporting Structure. Nuclear Engineering and Technology, 33(1), 73-82.

Kim, H.K., Kim, M.S. (2005). Vibration analysis of PER fuel rod. Journal of Sound and Vibration, 282, 553-572.

Kim, K.T. (2010). The effect of fuel rod supporting conditions on fuel rod vibration characteristics and grid-to-rod fretting wear. Nuclear Engineering and Design, 240, 1386-1391.

Le Guisquet, S., & Amabili, M. (2019). Identification by means of a genetic algorithm of nonlinear damping and stiffness of slender and thin-walled structures subjected to large-amplitude vibrations. Part I: single-degree-of-freedom responses. Mechanical Systems and Signal Processing. Submitted.

Liu, C.C., Ferng, Y.M., Shih, C.K. (2012). CFD evaluation of turbulence models for flow simulation of the fuel bundle with a spacer assembly. Applied Thermal Engineering, 40, 389-396.

Liu, H., Chen, D., Hu, L., Yuan, D., Gao, H. (2017). Numerical investigations on flow-induced vibration of fuel rods with spacer grids subjected to turbulent flow. Nuclear Engineering and Design, 325, 68-77.

Lu, Z. Q., Hu, G. S., Ding, H., & Chen, L. Q. (2019). Jump-based estimation for nonlinear stiffness and damping parameters. Journal of Vibration and Control, 25(2), 325-335.

Païdoussis, M.P. (2006). Real-life experiences with flow-induced vibration. Journal of Fluids and Structures, 22, 741-755.

Païdoussis, M.P., and Curling, LL.R. (1985). An analytical model for vibration of clusters of flexible cylinders in turbulent axial flow. Journal of Sound and Vibration, 98, 493-517.

Park, N.-G., Rhee, H., Park, J.-K., Jeon, S.-Y., Kim, H.-K. (2009). Indirect estimation method of the turbulence induced fluid force spectrum acting on a fuel rod. Nuclear Engineering and Design, 239, 1237-1245.

Rehme, K. and Trippe, G. (1980). Pressure drop and velocity distribution in rod bundles with spacer grids. Nuclear Engineering and Design, 62(1-3), 349-359.

Sandström, S. (1987). Vibration analysis of a heat exchanger tube row with ADINA. Computers & Structures, 26, 297-305.

Schettino, C. F. M. (2017). Evaluation of spacer grid spring characteristics by means of physical tests and numerical simulation. INAC 2017: International Nuclear Atlantic Conference, Brazil.

Simoneau, J.-P., Sageaux, T., Moussallam, N., Bernard, O. (2011). Fluid structure interaction between rods and a cross flow – Numerical approach. Nuclear Engineering and Design, 241, 4515-4522.

Vandiver, J.K. (2012). Damping parameters for flow-induced vibration. Journal of Fluids and Structures, 35, 105-119.

Viallet, E. and Kestens, T. (2003). Prediction of flow induced damping of a PWR fuel assembly in case of seismic and LOCA load case. Transactions of the 17th International Conference on Striuctural Mechanics in Reactor Technology (SMiRT 17), Prague, Czech Republic.

Weaver, D.S., Ziada, S., Au-Yang, M.K., Chen, S.S., Païdoussis, M.P., Pettigrew, M.J. (2000). Flow-Induced Vibrations in Power and Process Plant Components – Progress and Prospects. ASME Journal of Pressure Vessel Technology, 122, 339-348.

Chapter3

Nonlinear Vibrations of a 3x3 Reduced Scale PWR Fuel Assembly Supported by Spacer Grids

GIOVANNI FERRARI^A, GIULIO FRANCHINI^A, LUCA FAEDO^A, FRANCESCO GIOVANNIELLO^A, STANISLAS LE GUISQUET^A, PRABAKARAN BALASUBRAMANIAN^A, KOSTAS KARAZIS^B, MARCO AMABILI^A

^AMcGill University, Dept. of Mechanical Engineering, Macdonald Engineering Bldg., 817 Sherbrooke St. W, Montreal H3A 0C3, Quebec, Canada ^BFramatome Inc., 3315 Old Forest Rd., Lynchburg, 24501 VA, USA

Running headline: Non-linear vibrations of a nuclear fuel bundle supported by spacer grids

Keywords: PWR fuel rods, Non-linear vibrations, Fluid-structure interaction, Dynamic parameter identification, Damping identification, Spacer grids

Abstract

The core of Pressurized Water Reactors (PWR) is composed by nuclear fuel assemblies, bundles of slender fuel rods containing uranium pellets, kept in position by spacer grids equipped with elastic elements for retention, and coupled to an axial flow of coolant pressurized water. Fuel bundles are subjected to fluid-induced vibrations causing fretting at the interface with spacer grids; events such as earthquakes may also constitute an external excitation resulting in large-amplitude vibrations of the fuel rods, which may bring to loss-of-coolant accidents. The relationship between the excitation amplitude and the damping during large-amplitude vibrations of nuclear fuel assemblies in the presence of flowing fluid is not fully understood. The present experimental study investigated the vibrations of a 3×3 tube assembly composed by eight regularly spaced fuel rods installed around a guide tube and supported by spacer grids; tests were performed in quiescent and flowing water. In addition to experimental modal analysis under small random excitation, stepped-sine experiments at different levels of harmonic excitation that caused large-amplitude vibrations

were performed. The equivalent viscous damping ratios of the fundamental model at different excitation levels were extracted by fitting the results with a single degree-of-freedom model. The vibrations of the fuel bundle were strongly influenced by the vibrational behavior of the single rods, which constitute coupled oscillators. An increase of damping with the excitation amplitude was observed both in quiescent and in flowing water and acted in the direction of structural safety. The water flow did not cause instabilities in the operational range; instead, the increment of flow speed increased the damping ratios in the linear (small-amplitude vibrations) and nonlinear (large-amplitude vibrations) regime.

1. Introduction

Pressurized Water Reactors (PWRs) are installed in civil plants to produce electricity and to produce propulsion in military submarines and vessels. The cores of large PWRs are large vessels containing hundreds of nuclear fuel bundles, which in turn are constituted by hundreds of slender fuel rods organized in a structured array. Fuel rods are hollow cylindrical zirconium tubes filled with pellets of enriched uranium; their typical length is 4 meters while their diameter is approximately 10 mm. Uranium pellets are cylindrical, with a length close to 10 mm. Their diameter is slightly smaller than the internal diameter of the fuel rods to allow for thermal expansion. Axially, they are kept packed inside the rods by means of elastic elements pushing axially. Fuel rods are kept in structured arrays by means of spacer grids, square zirconium grids perpendicular to the axis of the rods. Spacer grids are spaced regularly along the fuel rods, so that in a typical bundle 8 spacer grids may be present. The cells of the spacer grids keep fuel rods at a relative distance of few millimeters and accommodate guide and control tubes as well. The cells of spacer grids are equipped with elastic elements such as springs, which support fuel rods by means of preload and consequent friction, while allowing thermal expansion. Moreover, they are equipped with fins to increase the mixing of the coolant water. Fuel bundles and fuel rods are in fact installed vertically and traversed by a coaxial flow of light water, which removes the heat due to irradiation, reaching typical speeds of 5 - 6 m/s. Water is kept at a pressure around 15 MPa and a temperature of 300 degrees Celsius, so that it remains liquid in the reactor. Correspondingly, fuel rods are pressurized internally by means of helium.

Axial water flow causes flow-induced vibrations of single fuel rods and of entire fuel bundles. In fact, fuel rods are free to vibrate between each couple of adjacent spacer grids. Axial flow is less prone to create instabilities and large amplitude vibrations than cross flow. However, in PWRs modest amplitude vibrations are dangerous because i) fuel rods are slender and, therefore, flexible; vibrations easily become comparable to the diameter of fuel rods, thus entering a region of geometric nonlinearity; ii) the distance between fuel rods and bundles is small, so that during vibrations these elements may enter in contact; this reduces momentarily or alters permanently the fluid flow of the coolant and damages the metallic surfaces; iii) the elastic elements of the spacer grids constitute loose boundary conditions and are the location of friction and impacts during vibrations; this may lead to fretting at the interface with the fuel rods with the spacer grids and the release of fissile material into the primary circuit. Important vibrations, then, may not be caused by fluid-structure interaction alone, but also by external excitations caused by accidents such as earthquakes. In these cases, the interaction between forced excitation and fluid-structure interaction may result in unexpected responses.

The Laboratory of Mechanical Vibrations and Fluid Structure Interaction at McGill University has undertaken, in collaboration with Framatome Canada, the experimental study of forced large vibrations of a 3x3 reduced-scale PWR fuel bundle. Given the complexity of the dynamic study, the investigation was divided into three phases:

- 1) The first phase involved forced vibrations of single fuel rods in reference boundary conditions (fixed-fixed), intended to investigate the relationship between peak vibration amplitude and forcing level in the geometrically nonlinear field (Ferrari *et al.*, 2018);
- 2) The second phase described forced vibrations of single fuel rods supported by spacer grids provided by Framatome, intended to investigate the effect on the vibration amplitude of the strongly nonlinear boundary conditions (Ferrari *et al.*, 2019);
- 3) The third phase (current paper) presents the results of forced vibrations of a 3×3 tube assembly composed by eight regularly spaced fuel rods installed around a guide tube and supported by spacer grids, intended to investigate the dynamics of arrays of identical fuel rods and the effect of flowing fluid.

Phase 3) is the object of the present paper. The main differences of the setup used in the current analysis vis-à-vis the setup presented in (Ferrari *et al.*, 2019) are related to the different configuration used in the experiments (here, a reduced scale 3x3 fuel assembly is used in the forced

vibration analysis vs. the single rod used in (Ferrari et al., 2019)) and to the additional tests with fluid flow conditions presented in the current analysis (in (Ferrari et al., 2019) the single fuel rod was tested only in air and in quiescent water). Because of this, for additional references detailing the estimation of damping and other parameters in the linear (small-amplitude vibrations) and in the nonlinear (large-amplitude vibrations) regime, the effect of nuclear fuel pellets and the dynamics, fretting and creep of spacer grids, the reader is directed to (Ferrari et al., 2018) and (Ferrari et al., 2019). The main findings of these two works on single fuel rods are: i) the rods exhibit a strongly nonlinear behavior under forced vibrations; this behavior is hardening for fixed-fixed rods (the peak frequency increases with the excitation amplitude) and softening (the frequency decreases) if spacer grids are employed; ii) the equivalent modal damping ratio for the fundamental resonant frequency is not constant but increases strongly with excitation amplitude; iii) a one-to-one internal resonance due to axial symmetry is present, giving rise to vibrations perpendicular to the direction of the excitation.

Vibrations of fuel bundles in PWRs

Most applications of axial fluid flow through clusters of arrays of cylindrical elements are found in the nuclear and energy sector. As a consequence, the flow-induced vibrations of such systems were often studied, theoretically and experimentally (Bhattacharya, 2013; Chen, 1975c; De Pauw *et al.*, 2015; Dragunov *et al.*, 2013). Notable numerical studies are also available (De Santis and Shams, 2017; Hofstede *et al.*, 2017; Kang *et al.*, 2001; Kim and Kim, 2005; Liu *et al.*, 2012; Liu *et al.*, 2017; Païdoussis and Curling, 1985).

A complete discussion of the phenomena experienced by structured bundles of rods with tapered ends in axial flow can be found in (Païdoussis, 2004). Axial flow in the energy sector was studied first by (Burgreeen *et al.*, 1958; Païdoussis, 1965 a,b,c; Pavlica and Marshall, 1966; Quinn, 1962 and1965; Roström, 1964; Roström and Andersson, 1964 a and b; Shields, 1960; SOGREAH, 1962). The first experiments were performed by (Chen and Wambsganss, 1972) and (Païdoussis, 1966a). Axial flow is inherently less disruptive than cross flow to slender elements; rods may reach conditions of buckling or flutter, but for extremely high flow velocities, rarely encountered in practical applications (>50 m/s for flowing water (Païdoussis, 1966b)). In subcritical conditions, slender cylinders are subjected to stochastic fluid-induced vibrations resulting in the excitation of

the lowest "dry" vibration modes. The change in the natural frequency induced by flow depends on the boundary conditions; however, the added-mass effect on the natural frequency caused by quiescent fluid alone is dominant. The phenomenon of subcritical vibrations remains unclear, but it may be understood as a random forced vibration of the fuel rods caused by the pressure oscillations of the turbulent fluid. Fluid flow in subcritical condition tends to increase the damping of externally induced vibrations proportionally to the velocity of the fluid. It must be noted that, for flow velocities different from zero, the eigenfunctions of the system are not orthogonal and the modal shapes vary with velocity; therefore, the usage of terms such as normal modes and natural frequencies is improper, although practically convenient.

Conditions of confined flow are obviously present because of the finite dimensions of the flow section in PWRs and because of the close distance between fuel rods. Confined flow corresponds to an increased added-mass effect, an increased flow damping and a lower flutter limit. Clustered cylinders were first studied by (Païdoussis, 1979; Païdoussis *et al.*, 1982 and 1983a and b; Païdoussis and Besançon, 1981; Païdoussis and Suss, 1977).

Clustered cylinders in axial flow feature hydrodynamic coupling. The phenomenon was studied by (Chen,1975a,b,c; Chung and Chen, 1977; Dalton, 1980; Lin and Chen, 1977; Lin and Raptis, 1986; Païdoussis *et al.*, 1977; Païdoussis and Besançon, 1981; Païdoussis and Suss, 1977; Weppelink, 1979; Yamamoto, 1976). Experiments were conducted by (Chen and Jendrzejczyk, 1978) and (Moretti and Lowery, 1976). A cluster of closely spaced cylinders, each one having the same sequence of natural frequencies $\omega_1, ..., \omega_m$ (truncating the infinite series of normal modes at the *m*-th mode), does not have the same series of frequencies of the rods $\omega_1, ..., \omega_m$. Instead, the generic *i*-th mode corresponding to the natural frequency ω_i splits into multiple modes consisting in different combinations of the corresponding modal motions of the single rods. Correspondingly, the Frequency Response Function of a bundle of *n* fuel rods will present, in a neighborhood of the natural frequencies, resulting in beating phenomena. This is a consequence of the fact that the fluid does not introduce a virtual added mass but a virtual added mass matrix due to inertial coupling.

Further complication is given by the fact that PWR fuel rods are not only clustered in an enclosed space, but also interconnected by flexible elements. Such architectures were investigated by (Païdoussis $et\ al.$, 1983 a and b). If a bundle of fuel rods is supported by a number k of spacer grids, the 1-st and the k-th spacer grids may be considered as boundary conditions, however a

number of k-2 spacer grids remains, constituting intermediate flexible supports. Intermediate flexible supports may contribute to the scatter of the flexural frequencies of the single rods into bands. Loose multi-span supports may result in localized vibration modes (Yeh and Chen, 1990). The flow across nuclear fuel bundles is strongly influenced by the presence of the bundles themselves; consequently, both in the parallel and in the perpendicular direction to the axis of the bundle, it is far from uniform. Contributing to this effect are the following factors:

- Flow experiences concentrated head losses while it encounters the spacer grids and the (tapered) ends of the fuel rods.
- Flow is accelerated when the presence of spacer grids and nuclear fuel rods reduces the flow section.
- The duct is not infinitely extended around the fuel bundles, therefore overall flow is, at various degrees, confined.
- Spacer grids present fins that impart a transversal mixing component to flow, increasing turbulence and random vibrations.
- Among the fuel rods, flow is strictly confined and is named *subchannel* flow. Subchannel flow velocity is largely different from "bulk" flow velocity; large spatial gradients of flow are present, contributing to turbulence and random vibrations.
- Since flow is confined, large pressure drops due to viscosity are present along the axial extension of the bundles.

Flow calculations are often proprietary, since they are related to the design of spacer grids. However, fluid flow across arrays of cylinders was already discussed by (Eifler and Nijsing, 1967) and (Hooper and Rehme, 1984). Currently, most investigations are carried out numerically (Chang and Tavoularis, 2007). (Rehme and Trippe, 1980) investigated the effect of spacer girds on the flow along fuel bundles. More recent numerical works are also available (Khan *et al.*, 2013; Ricciardi, 2016). Notable works on cross flow in heat exchangers (*e.g.* Brockmeyer *et al.*, 2019) also provide useful insight on the numerical approach to fluid-structure interaction problems involving bundles.

Lastly, the buoyancy of fuel bundles is in general may be neglected because 1) typical fuel bundles are installed in a vertical configuration; 2) if a horizontal configuration is chosen, the effects of the buoyancy and of the weight of fuel rods (which are, anyway, modest) tend to cancel each other out.

Identification of damping

Abundant literature is available about the identification of the parameters describing the vibration of nuclear structures immersed in fluid flow (e.g. Adhikari and Woodhouse, 2001a and b; Bennett et al., 1997). The reader can refer to (Ferrari et al., 2019). Damping has received particular attention as it determines the vibration amplitude in resonant conditions. Damping for fuel assemblies in water was studied by (Brenneman and Shah, 2000; Collard et al., 2004; Connors et al., 1982; Fardeau et al., 1997; Hassan, 2011; Vandiver, 2012; Viallet and Kestens, 2003). Amabili has investigated the apparent increase of modal damping in various structures of practical interest and the existence of a unified damping model describing it (Alijani et al., 2016; Amabili 2018a,b,c; Amabili et al., 2016; Amabili and Carra, 2012; Balasubramanian et al. 2017 and 2018; Delannoy et al., 2015; Delannoy et al., 2016).

Since the development of a reduced order model of a fuel bundle, including fluid-structure interaction, confined flow, hydrodynamic coupling and nonlinear boundary conditions would be impractical, it was chosen instead to apply a single DOF approximation; the latter has, as its main purpose, the determination of the evolution of damping with the excitation amplitude and with the coolant flow. This research group has developed with success a one (Delannoy *et al.*, 2015) or two (Delannoy *et al.*, 2016) degree-of-freedom model based on a modified Duffing oscillator with linear, quadratic and cubic stiffness and a viscous modal damping ratio. The model describes the large amplitude vibrations of PWR fuel rods in reference boundary conditions (Ferrari *et al.*, 2018) under forced excitation, provided that the damping parameter is modified at each forcing level applied to the structure. For nonlinear systems, in fact, the peak vibration amplitude is not proportional to the amplitude of the excitation.

Single DOF model for forced vibrations of fuel bundles around the fundamental frequency

The single DOF model developed in (Le Guisquet and Amabili, 2019) is based on the modified Duffing oscillator (here expressed in dimensionless form) describing the modal vibration of the system around its fundamental frequency under a forced excitation of dimensionless amplitude

$$r^{2}\ddot{x} + 2r\zeta\dot{x} + x + \eta_{2}x^{2} + \eta_{3}x^{3} = \lambda\cos(t), \tag{1}$$

where r is the circular frequency of excitation divided by the natural circular frequency ω_n , x is the first harmonic of the displacement, t is dimensionless time, ζ is the equivalent viscous modal damping ratio, η_2 and η_3 are the quadratic and cubic stiffness parameters, respectively. The dimensionless forcing amplitude is

$$\lambda = \frac{F}{hm\omega_n^2} \,, \tag{2}$$

where F is the force amplitude in Newtons, m is the modal mass and h is the characteristic dimension of the system. This model captures the vibration of isolated fuel rods with fixed-fixed boundary conditions (Ferrari $et \, al.$, 2018), but not those of isolated fuel rods installed in spacer grids (Ferrari $et \, al.$, 2019). The combination of linear stiffness, quadratic stiffness and cubic stiffness cannot follow the large-amplitude responses obtained with a stepped-sine excitation, because they feature a strong nonlinearity (manifested by the reduction of the peak frequency with the forcing amplitude) starting from the lowest forcing levels, without the appearance of nonlinear jumps (regions of unstable solution for nonlinear systems (Amabili, 2008)). It is believed that the springs at the spacer grids are the location of large nonlinear stiffness and damping components, which cannot be captured by the stiffness and damping terms in (1). In the future, the direct experimental investigation of the interaction spacer grids-fuel rods and the inclusion of higher-order stiffness and damping terms may solve this issue. In (Ferrari $et \, al.$, 2019), however, the identification of the stiffness evolution is abandoned and a simpler linear equation is applied to the lowest and the highest forcing levels of stepped sine experiments:

$$r^{2}\ddot{q} + 2r\zeta\dot{q} + q = \lambda\cos(t). \tag{3}$$

 ζ is chosen so that the maximum peak vibration is perfectly reproduced; ω_n and m, the only unknown parameters, are determined through a least-squares procedure fitting the model on the experimental curves on the available frequency range.

2. Experimental setup for the fuel assembly

2.1. Experiments in air and quiescent water

A welded assembly of three zirconium spacer grids and one open and hollow guide tube similar to those employed in PWRs was employed in this study. Each spacer grid is composed of 17x17 cells allowing the passage of 264 fuel rods and 25 guide tubes. The guide tube was point-welded to the central cell of each spacer grid. While the guide tube is welded, fuel rods are supported by springs and dimples present in the spacer grids (Fig. 1). The spring force acting on the fuel rods keeps them in position. For this study eight fuel rods were chosen, since it is the smallest number of fuel rods that can give a uniform and symmetrical distribution of rods around the guide tube. The middle spacer grid was cut removing vacant empty cells leaving intact only the central 9 cells. The two end spacer grids constitute two end conditions similar to the ones used on examining single rods in past studies by this same group (Ferrari *et al.*, 2019). Thanks to the middle grid, the 8 fuel rods move as a bundle and not independently between the boundary conditions at the two ends. In any case, in PWRs as well, fuel rods are inserted in spacer grids not only at the two extremities, but also in between the full rod length.

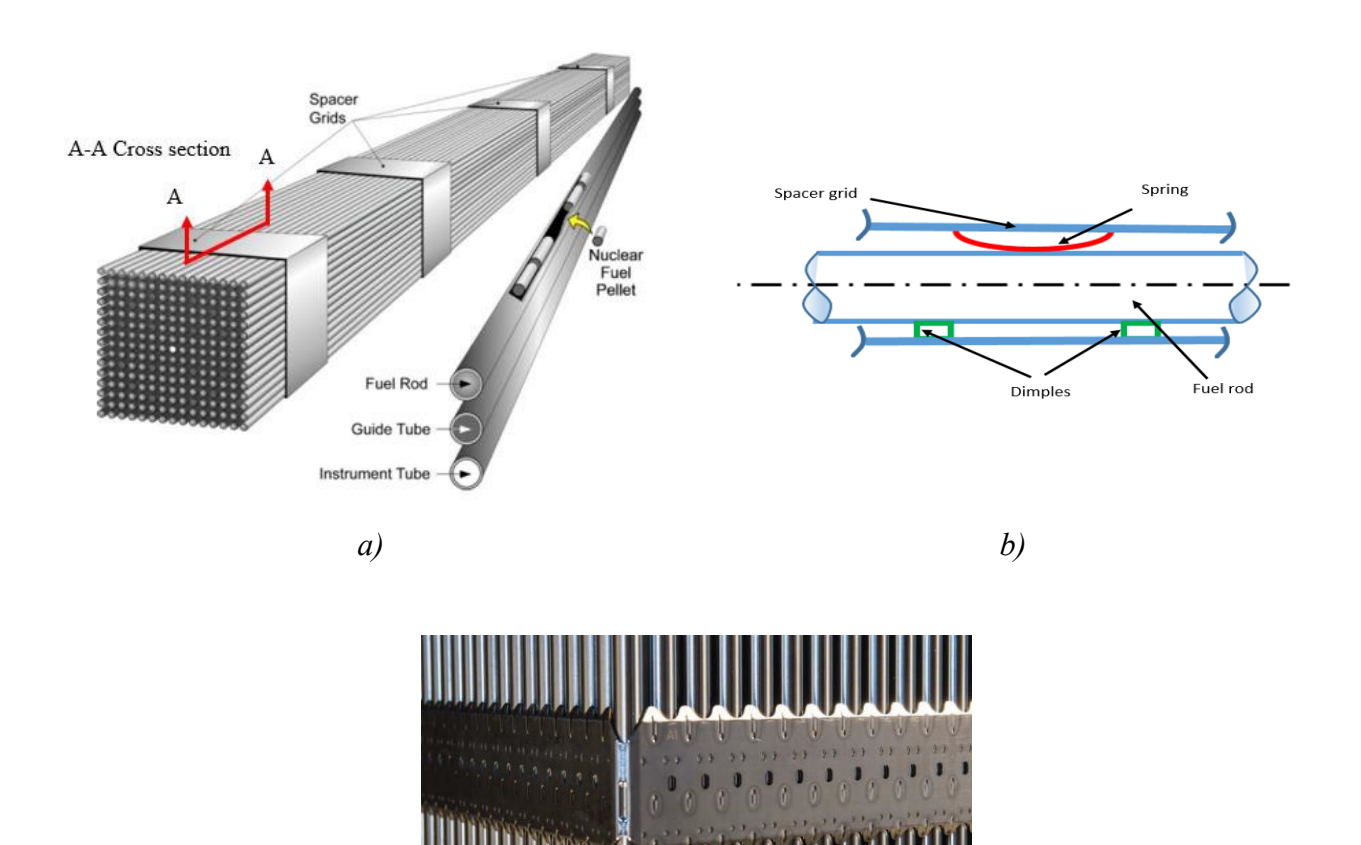


Fig. 31. (a) Typical PWR fuel assembly showing fuel rod and spacer grid (Source: energy.gov); (b) [A-A section] Boundary condition of fuel rod with spacer grid; (c) Photograph of fuel rods installed through a spacer grid (Ferrari et al., 2019).

The two end spacer grids were kept parallel at a distance of 900 mm by means of four ¾" threaded rods. The threaded rods were anchored to an acrylic frame (which has the secondary role of water tank if required) by means of bolts (Fig. 32). Great care was taken so that the spacer grids were not affected by compression, traction or torsion forces due to the bolts connecting the system to the acrylic frame. The axes of the rods were kept parallel to the ground, as gravity does not play a significant role in the dynamics of the beams, thanks to their light weight. To increase the realism of the tests, short dummy rods of the same diameter as the fuel rods were installed in the cells of the two end spacer grids adjacent to the fuel rods. The close presence of the dummy rods is likely to increase the stiffness of the constraint felt by the fuel rods under test. Since several cells of the spacer grids at the two ends remain unoccupied and unloaded outside the area occupied by fuel rods, guide tube and threaded rods, they were removed as necessary by means of pliers (Fig. 33).

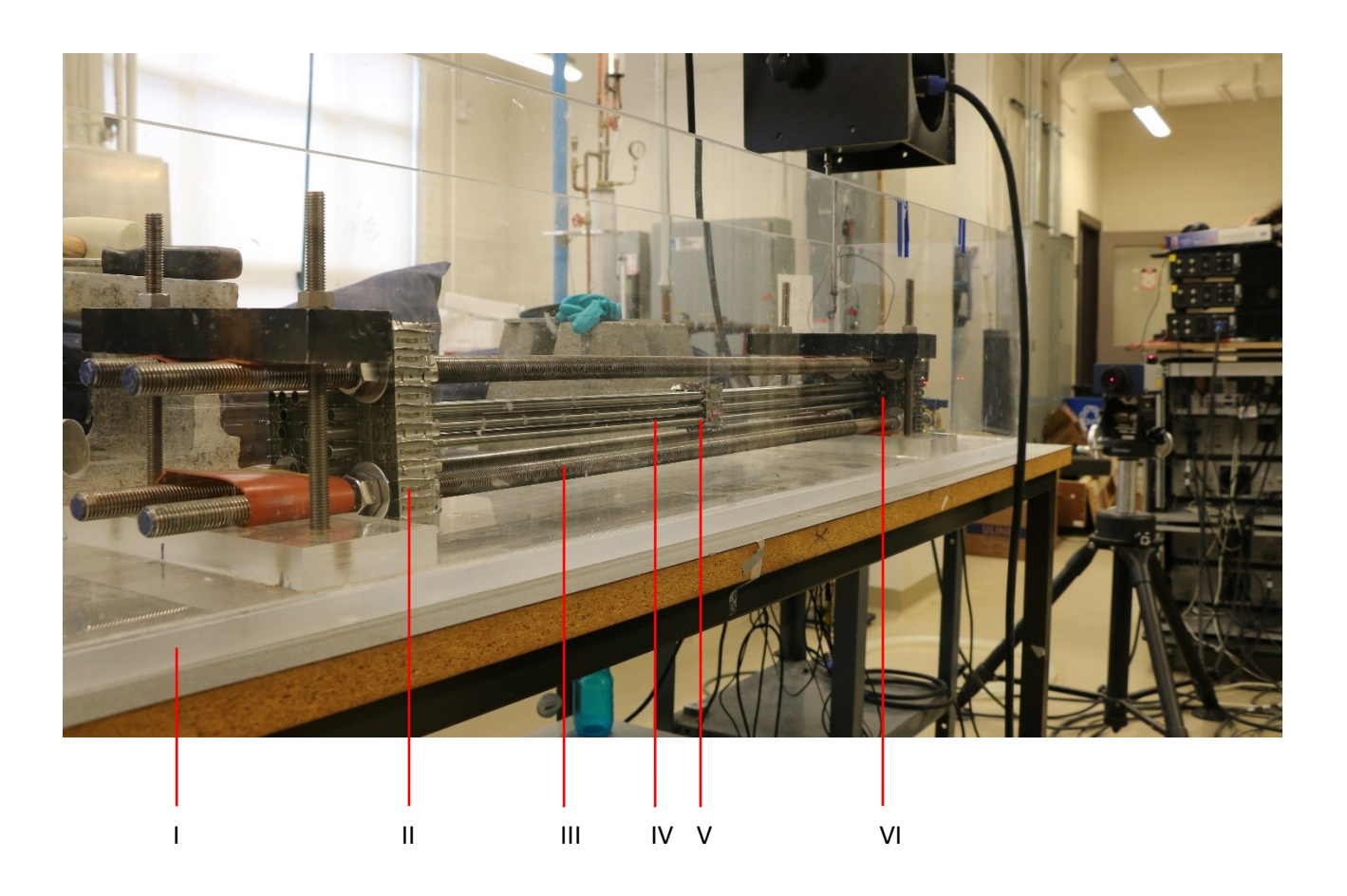


Fig. 32: Transversal view of the assembled system: I, acrylic frame/tank; II, left spacer grid; III, reinforcement threaded rods; IV, fuel rod bundle; V, middle spacer grid; VI, right spacer grid.

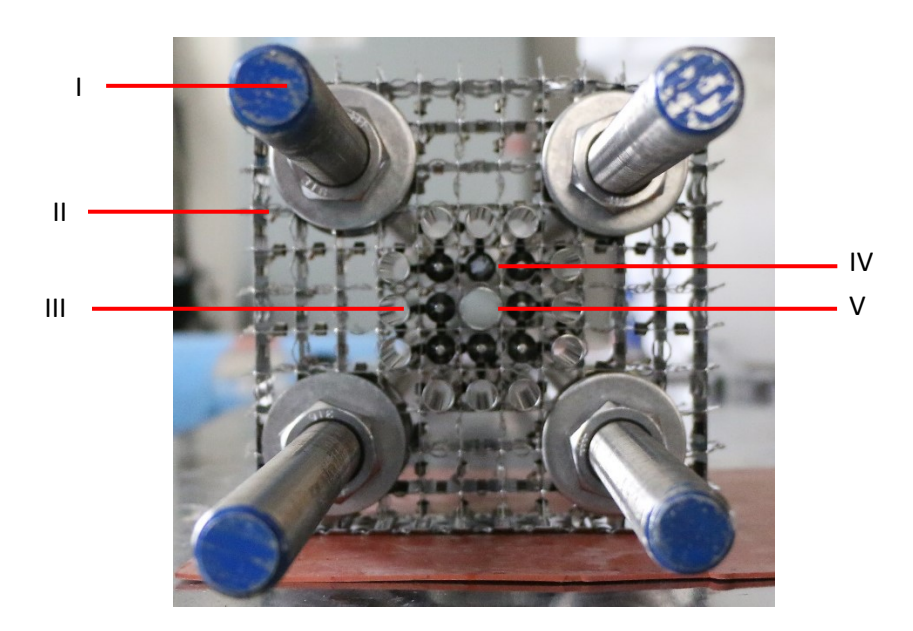


Fig. 33: Axial view of the disposition of the rods in the spacer grids: I, reinforcement threaded rods; II, spacer grid; III dummy rods, qty. 12; IV, fuel rods, qty. 8; V, guide tube.

The eight hollow zirconium rods that were sourced and employed for the experiments are shorter in length but otherwise identical to the ones used in the fuel assemblies of PWRs. The rods are 988 mm long and the length left free to vibrate between the two end spacer grids is 900 mm. The external diameter of the rods r is 9.50 mm and the wall thickness 0.61 mm. The material properties of the zirconium alloy are displayed in Table 1. One end of the zirconium rod is flared to facilitate the insertion into the spacer grids. The other end presents a clamping diameter. Fig. 3 shows one example of the fuel rod used in the test. At mid-length, the axial portion of the rods occupied by the thickness of the central grid is 32 mm.

Table 9. Material properties of a zirconium-alloy rod.

Density (kg.m³)	Young's modulus (GPa)	Poisson's ratio
6450	95	0.37

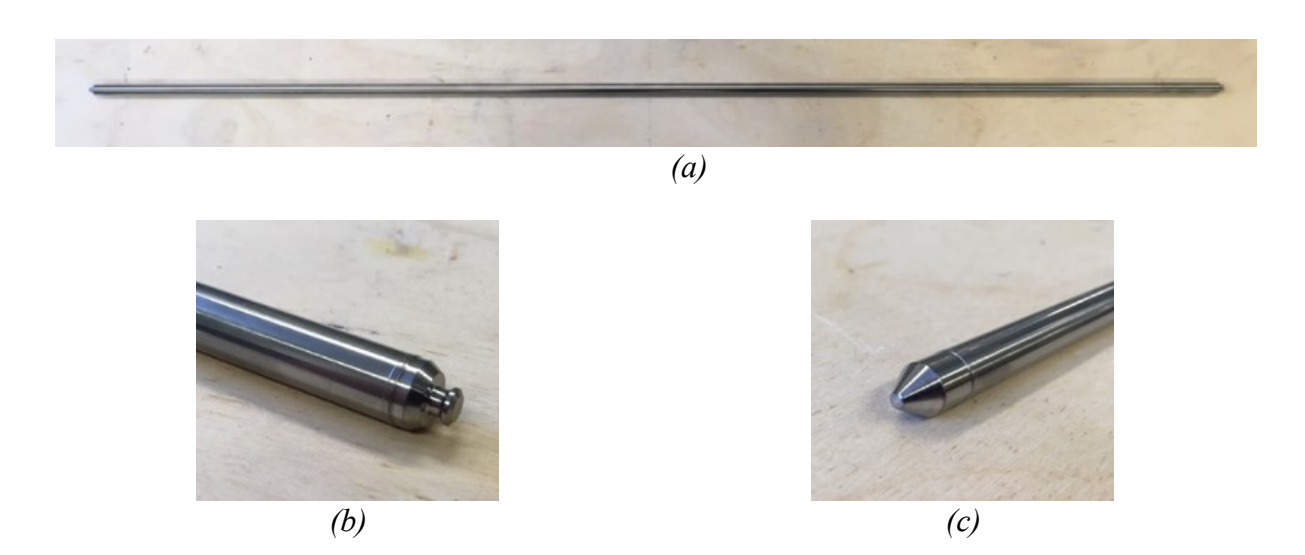


Fig. 34. (a), Zirconium fuel rod under test; (b) clamping end; (c) insertion end (Ferrari et al., 2018).

These test rods were provided by Framatome filled with cylindrical tungsten carbide pellets, which model uranium fuel pellets in terms of dimension and density. The weight of one rod complete with pellets is 5.80 times larger than in the empty configuration. A radial gap between the pellets and the internal wall of the zirconium rod is present. Being that the sum of the axial length of the pellets is slightly shorter than the axial clearance present inside the zirconium fuel rods, a modest axial gap is also present. In an operating nuclear reactor, axial springs keep fuel pellets tightly packed while allowing thermal expansion. The zirconium rods in the present study were tested without recovering the axial gap in some experiments, thus leaving the fuel pellets free to move axially and radially. In other experiments a simple threaded device (Fig. 6) was installed to keep the pellets in a tightly packed axial configuration. It must be noted that such precaution prevents axial play but does not prevent the radial motion of the pellets – although the latter becomes more difficult as the friction between the pellets limits or anyway modifies the radial motion.



Fig. 35: Threaded device used to pack fuel pellets axially (Ferrari et al., 2019).

Vibration experiments were conducted in presence of air and in presence of quiescent water surrounding the nuclear fuel rods. In this study the body of still water was large enough to be considered as infinitely extended around the fuel rods. The body of water is contained in the transparent acrylic tank, which is 1524 mm long, 300 mm wide and 300 mm deep. The tank constitutes the frame for the vibrating system even when it is not filled with water (experiments in air). The tank does not include a lid so that water presents a free surface. This allows the access of the instrumentation and of the measurement systems, while it was verified that no sloshing waves of any meaningful amplitude occur. The distance between the topmost fuel rod and the free surface of water is 100 mm.

An electrodynamic exciter (Brüel & Kjær model 4810) was used to apply in the vertical direction a punctual and perpendicular excitation 240 mm away from one terminal spacer grid; this distance was chosen so that the low frequency modes of the bundle were excited without giving excessive interaction between the exciter and the structure during large amplitude vibrations. In fact, beam-like transversal vibrations similar to those in (Ferrari *et al.*, 2019) were hypothesized for the entire fuel assembly. The excitation was applied to the central rod belonging to the horizontal row of three rods located on top in the experimental configuration. A force transducer (Brüel & Kjær model 8203) was interposed so that a real-time force measurement is obtained during vibration. The forced vibration excitation system is shown in Fig. 36.

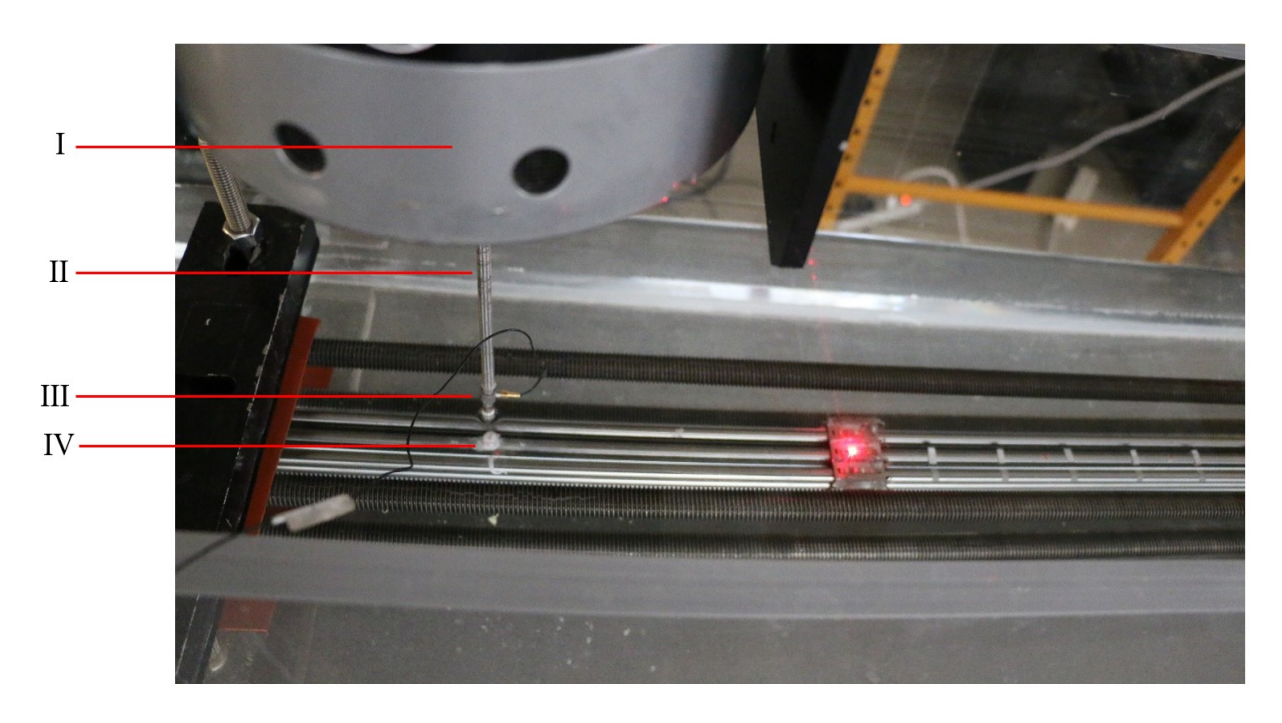
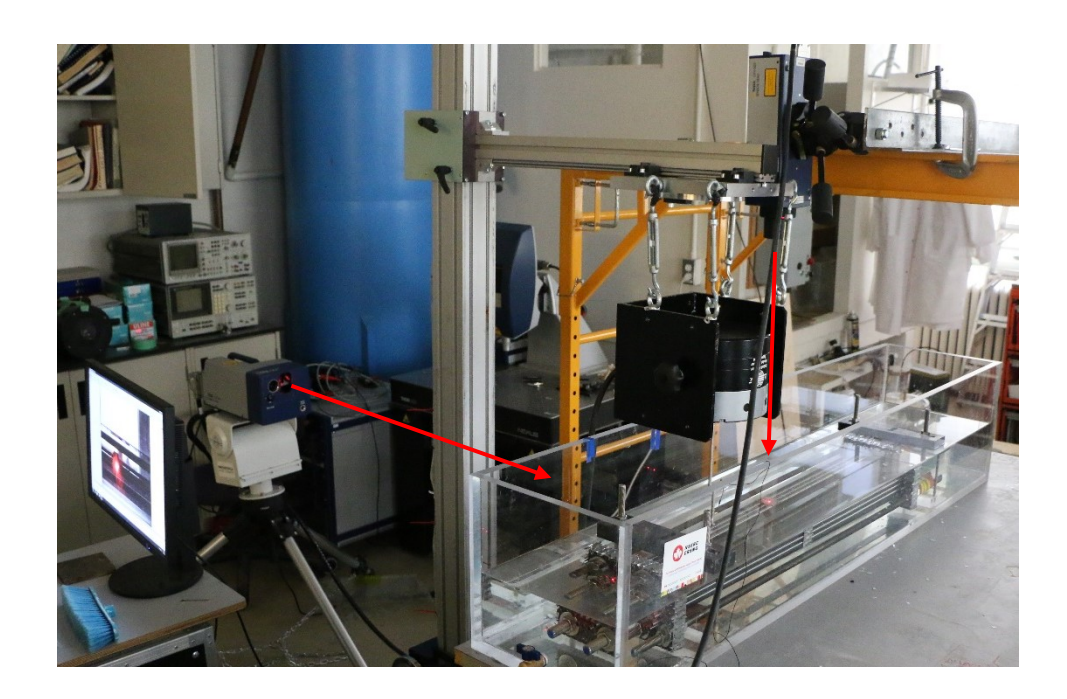


Fig. 36: Excitation system: I, electrodynamic exciter; II, extension rod; III, load cell; IV, glued connection to center-top fuel rod.

The weight of the vibrating structure is low; therefore, a non-contact measurement system based on laser Doppler vibrometry was employed to avoid the application of added massed. Laser Doppler vibrometers are capable of measuring the vibration of structures even in presence of surrounding water and clear acrylic walls. Laser heads by Polytec (Single point laser head model OFV-505 and Scanning laser head model PSV-400) were employed. One OFV-505 head was employed to measure the vertical vibration of the bundle, parallel to the direction of excitation. By aiming manually the head to several points along the bundle, the reconstruction of the mode shapes resulting from modal analysis was made possible. Broadband pseudo-random excitation signals were used to obtain the H1 Frequency Response Function averaged over 5 experiments with a frequency resolution equal to 0.193 Hz. For large-amplitude vibrations, one additional laser head (PSV-400) was also used to measure the horizontal vibration of the beam. Since the transversal section of the bundle is axisymmetric, normal modes are expected to appear in perpendicular couples sharing the same frequencies. Normal modes perpendicular to the direction of the excitation may be excited if the excitation amplitude is sufficient to activate nonlinear coupling. This justifies the presence of a laser directed horizontally (perpendicular to the direction of excitation). It must be noted that the structure is constituted by several identical rods coupled

energetically through the three spacer grids. Therefore, the system is coupled and may feature various combinations of the vibration modes of the single rods. If water is present, hydrodynamic coupling contributes further to the complex coupling of the rods. This study is mostly focused on the large-scale vibration modes of the entire bundle as observed on the intermediate spacer grid and only secondarily on the individual vibration of the fuel rods between spacer grids. The joint vibration of the bundle is allowed by the presence of the intermediate spacer grid. In fact, for all the vibration modes where the displacement of the fuel rods does not have a node at mid-length, this element tends to force all rods to move together. Since the first vibration mode of a bundle was expected (and verified) to be flexural, parallel to the excitation, with a maximum transversal displacement at one half of the free length, the horizontal and vertical laser heads were aimed correspondingly on the central grid (Fig. 37). The system under test, constituted by one spacer grid and two bundle spans moving among two side grids, constitutes the basic module of the multispan bundles present in PWRs. The dynamics of multi-span bundles, thus, may be reconstructed on the base of experiments on simpler subsystems, such as the ones under discussion, if suitable extrapolation models become available in the future.



a)

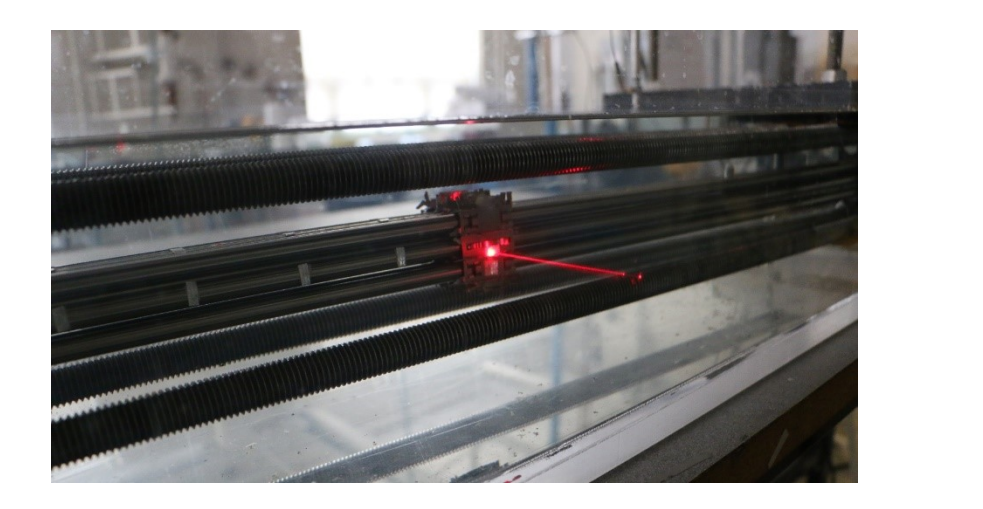


Fig. 37: Laser measurement system: (a), transversal measurement in the vertical and horizontal direction; (b) location of the laser beam on the middle spacer grid.

b)

A stepped-sine excitation technique was used to obtain frequency-amplitude curves at several forcing levels. A sinusoidal signal is employed to apply high energy levels at specific frequencies; the amplitude of the signal is kept accurately constant by means of a feedback control algorithm and the frequency varies slowly (by steps of 0.05 Hz) and monotonically in a neighborhood of the resonant frequency of interest – i.e., the fundamental one. At each frequency step, any transient is left to decay by discarding the initial 40 periods; afterwards, 10 periods are recorded and the frequency spectrum is reconstructed. Force feedback is required because the force generated by electrodynamic exciters is not proportional to the driving voltage around resonance. The monotonous variation of the frequency is required because hysteresis cycles and instabilities may arise. The stepped-sine algorithm is managed by a data acquisition and post-processing system (LMS TEST LAB) produced by Siemens. During the experiments the closed-loop control of the force was set with a tolerance of 0.5 %. The laser Doppler vibrometers are instead extremely precise.

2.2. Experiments in axially flowing water

The experiments in flowing water share several common elements with the setup developed for the experiments in quiescent environment. However, several additional pieces of equipment are required. The core of the test section (rods and spacer grids, reinforced by axial threaded rods), the excitation system and the measurement system were inherited from the experiments in quiescent water with minor modifications. However, the experiments in flowing water were performed inside a Kempf & Remmers water tunnel available at McGill University (Fig. 38). This closed loop tunnel is powered by an impeller with an electric motor and can generate flows as large as 12 meters per second. Deaeration capabilities are available so that the flowing fluid does not present bubbles during the experiments. The test section (Fig. 39), open to measurements, is a parallelepiped 260 by 260 by 1000 mm long, with the longest side parallel to the ground. The test section is provided with clear acrylic windows through which the beams of the laser Doppler vibrometers mentioned in the previous section can operate. The system under test was suspended at the center of the test section by means of eyelets and tie rods installed onto the 3/4" threaded rods (Fig. 40). The suspension is stiff under vibration while not applying considerable forces onto the spacer grids. The excitation system constituted by electrodynamic shaker, extension rod, stinger and load cell was maintained, however the extension rod had to pass through a neoprene membrane in the walls of the test section (Fig. 39). The presence of the membrane does not affect the results of the experiments as: 1) the force sensor is located between the membrane and the system under test, so it measures the actual force applied to the bundle; 2) the membrane does not feature resonances in the frequency range of interest. The load cell and its cable were protected by a layer of silicone for protection against water infiltration. While the excitation was directed vertically to exploit the presence of a free surface in still water, it was directed horizontally, instead, in the water tunnel because of practical constraints. Consequently, the main vibration direction (direction of the modal analysis) was the horizontal one and the secondary vibration direction was the vertical one. The load cell is located at a distance of 138 mm from one fixed spacer grid and is glued on the middle rod on the side of the rod bundle.

The water tunnel is equipped with a Venturi flowmeter; its accuracy is \pm 0.5 m/s at the velocities under exam. The bundle was tested inside water flowing at a maximum velocity of 5 m/s. This value was chosen because it corresponds, approximately, to the maximum velocity encountered in Framatome PWRs. It has to be noted that the flow velocity values mentioned in this article are measured by the Venturi effect and are, therefore, mean values over the inlet of the working section. Local velocity varies instead around and across the rods of the bundle because of the

presence of the rods, of the spacer grids and of the tunnel walls. However, the measurement of local speed values is not object of this study and will be included in future works.

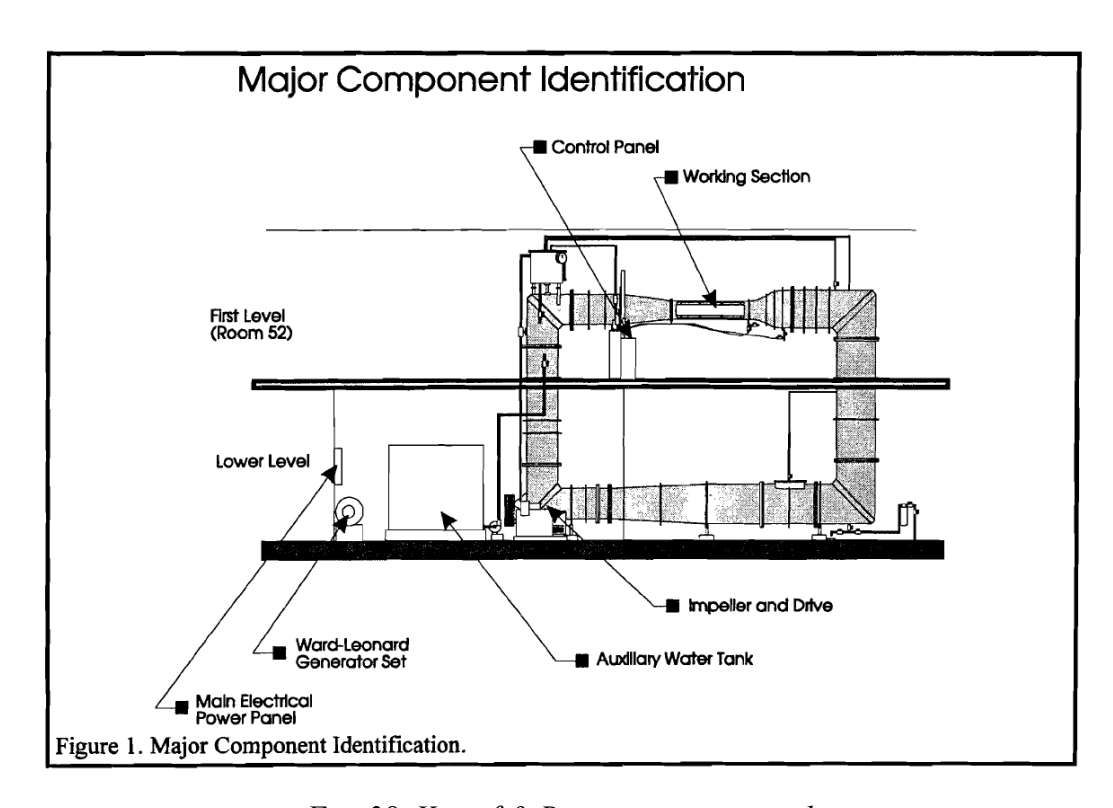


Fig. 38. Kempf & Renners water tunnel.

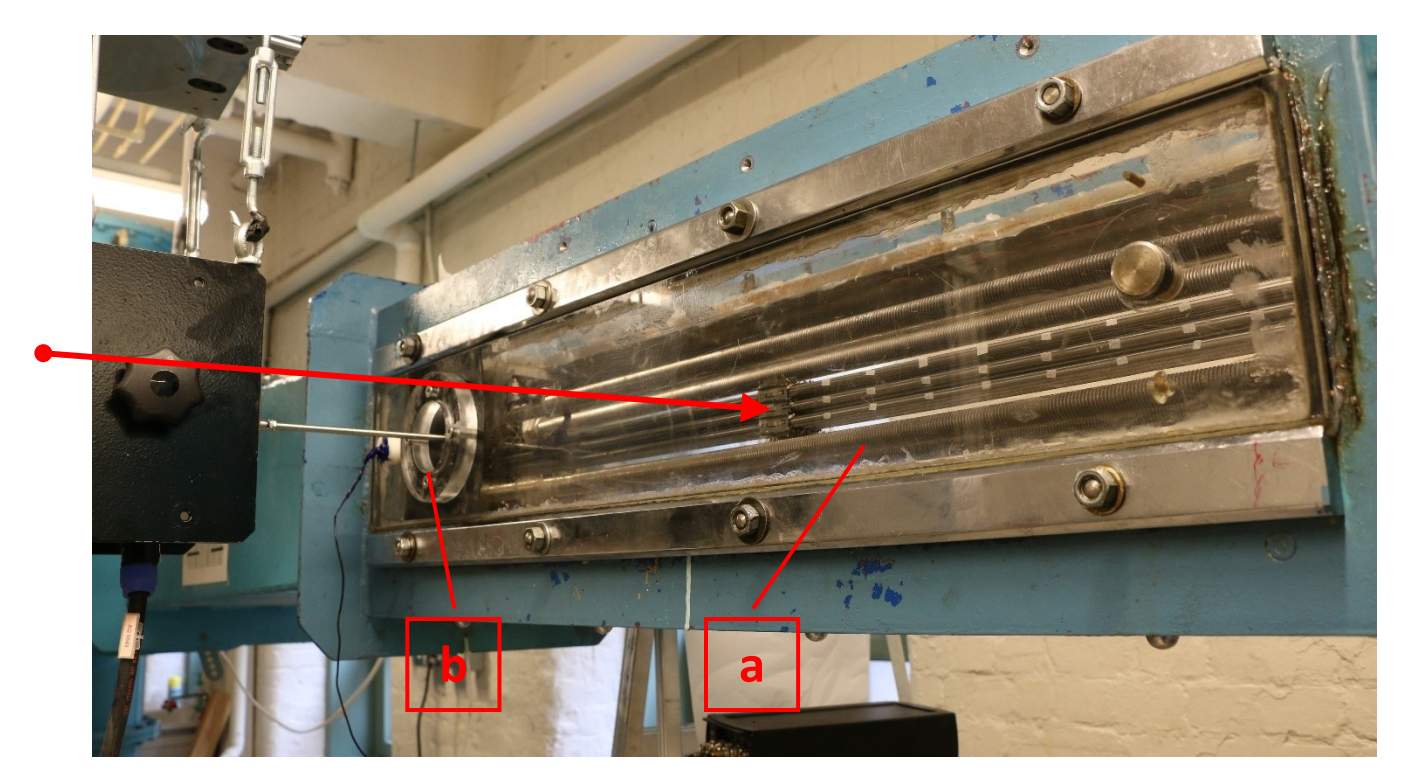
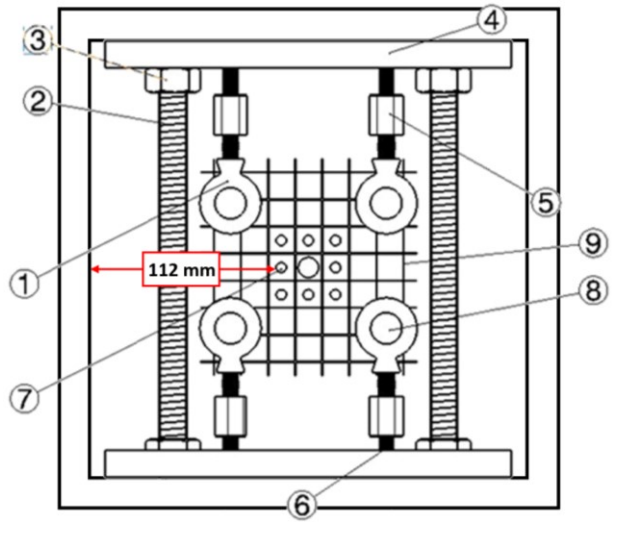


Fig. 39. Detail of the fuel bundle installed in the test section of the water tunnel. (a) Removable acrylic window; (b) passage of the excitation through neoprene membrane. The red arrow indicates the direction of the laser Doppler vibration measurement.





1	Eyebolt
2	Threaded vertical rod
3	Nut
4	Plate
5	Coupling Nut
6	Screw
7	Fuel rods
8	Threaded rod
9	Spacer grid
	· · · · · · · · · · · · · · · · · · ·

b)

Fig. 40. (a) Connection of the fuel bundle to the heavyweight walls of the water tunnel; (b) list of components. The minimum distance between the walls of fuel rods and the walls of the water tunnel is indicated.

2. Experimental results

The fuel assembly was tested in still air, in still water and in flowing water. In the first two cases, the pellets were first left free to move axially (freely moving pellets) and then they were blocked by an axial screw (fixed pellets). Inside the water tunnel, only fixed pellets were tested, because fuel bundles are not operated in PWRs with pellets left free to vibrate. Inside the water tunnel, more than one velocity value for the fluid flow was tested. A configuration of quiescent water was tested to ensure the compatibility of the experiments in the tank and in the water tunnel. Subsequently, a test at 2.5 m/s and a test at 5 m/s were performed. These mean velocities were chosen as they are approximately equal to 0.5 and 1 time, respectively, the maximum coolant velocity used in Framatome PWRs. Considering the local flow velocity equal to the mean, nominal value, and neglecting the mixing effect of the spacer grids, the approximate values of the Reynolds number for the subchannel flow can be estimated as 58900 at 5 m/s and 29450 at 2.5 m/s. In total, seven configurations were tested (four inside the acrylic tank and three inside the water tunnel). For each configuration, both linear (modal) and nonlinear analyses were performed. Linear and nonlinear experiments will be presented in two separate sections. Nonlinear experiments in quiescent media required the measurement of the vibrations in two directions: parallel to the excitation and perpendicular to the excitation. In fact, it was shown that the presence of spacer grids does not prevent through additional damping the appearance of vibrations perpendicular to the excitation, due to nonlinear coupling or other mechanisms. In flowing water, the vibration perpendicular to the excitation was not measured for practical reason: fluid-induced noise is larger than the vibration perpendicular to the excitation.

3.1. Small-amplitude vibrations (linear results)

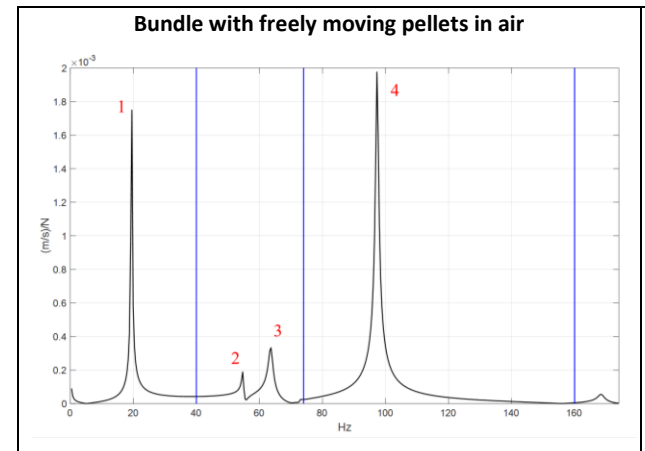
As anticipated, the PWR bundle is composed by identical fuel rods coupled through i) the central spacer grid; ii) the spacer grids at the two ends, connected to the frame; iii) hydrodynamic coupling. Consequently, the excitation of one fuel rod causes the vibrations of every other rod in the bundle. The normal modes of vibration of the bundle can be classified according to the corresponding vibration shape of the single rods. In (Ferrari *et al.*, 2019), it is in fact described how for one rod installed on spacer grids the *i*-th normal mode is characterized by *i*- flexural half-waves along the

length of the rod (Fig. 41). Each normal mode of the bundle tends to feature all fuel rods vibrating with the same number of flexural half-waves; however, several modes of the bundle can share the same number of flexural waves of the rods, while differing in the combination of the relative motion of the rods (which can be in-phase or with a phase of 180 degrees) and in the relative amplitude of the vibration of the single rods. The normal modes of the bundle characterized by the same underlying vibration shape of the single rods tend to group in one frequency band. Correspondingly, the FRF of the bundle can be divided into the areas of influence of the vibration shapes of the single rods. The order of these areas of influence respect the order of the modal shapes for the single rod and between these areas of influence there is no overlap. The tabular presentation of the modal parameters of each normal mode of the bundle will therefore divide the normal modes according to their type (the underlying vibration shape of the single rods) for convenience. It must be noted that the fundamental mode of vibration of the bundle is always the only one presenting no nodal points of the vibration of the single rods. Therefore, the fundamental mode of the bundle is not "split" into various modes of the same type. The study of the fundamental mode of vibration is the main objective of the PWR provider; the nonlinear investigation will focus correspondingly on the fundamental mode only. Moreover, PWR providers tend to measure the vibration in correspondence of the intermediate spacer grids. Thus, the study of modes other than the fundamental, and of even modes in particular (where the central spacer grid does not move) is considered less relevant. Lastly, it must be noted that it is possible to describe and divide the modes according to their number of flexural half-waves only because (as it was verified) the presence of quiescent and flowing water does not alter sensibly the shape of the normal modes with respect to the case in air.

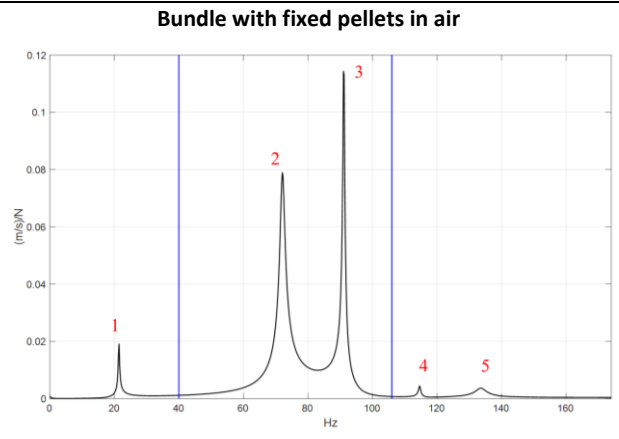
MODE I	
MODE II	
MODE III	
MODE IV	

Fig. 41. Lowest four normal modes of vibration for a single PWR fuel rod installed on spacer grids (Ferrari et al., 2019).

Table 10. Modal analysis for the bundle inside the tank.

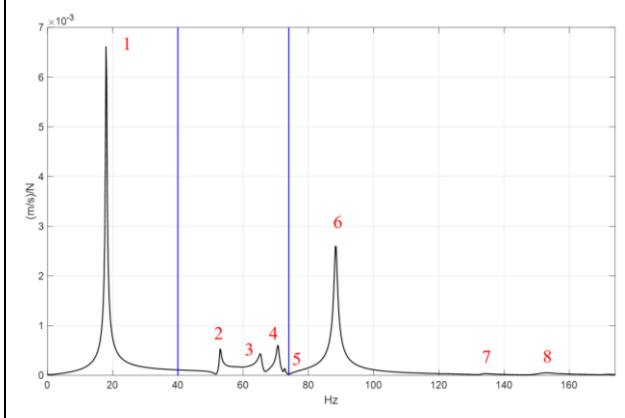


Mode	ode No. half Frequency waves (Hz)		Damping (%)	
1	1	19.42	0.70	
2	2	54.22	0.98	
3	2	64.13	1.68	
4	3	97.32	0.48	



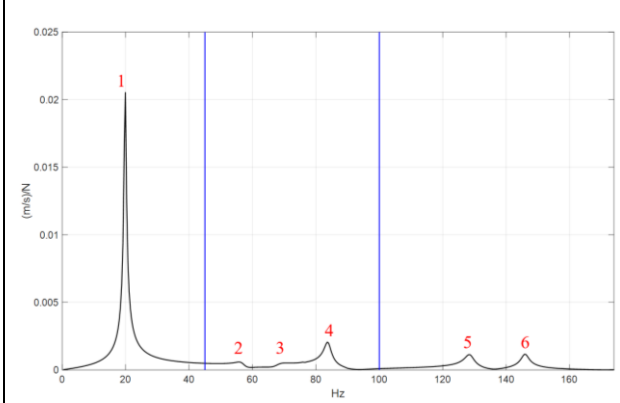
Mode	No. half waves	Frequency (Hz)	Damping (%)
1	1	21.47	0.79
2	2	72.10	1.08
3	2	91.12	0.3
4	3	114.63	0.27
5	3	133.58	1.21

Bundle with freely moving pellets in still water



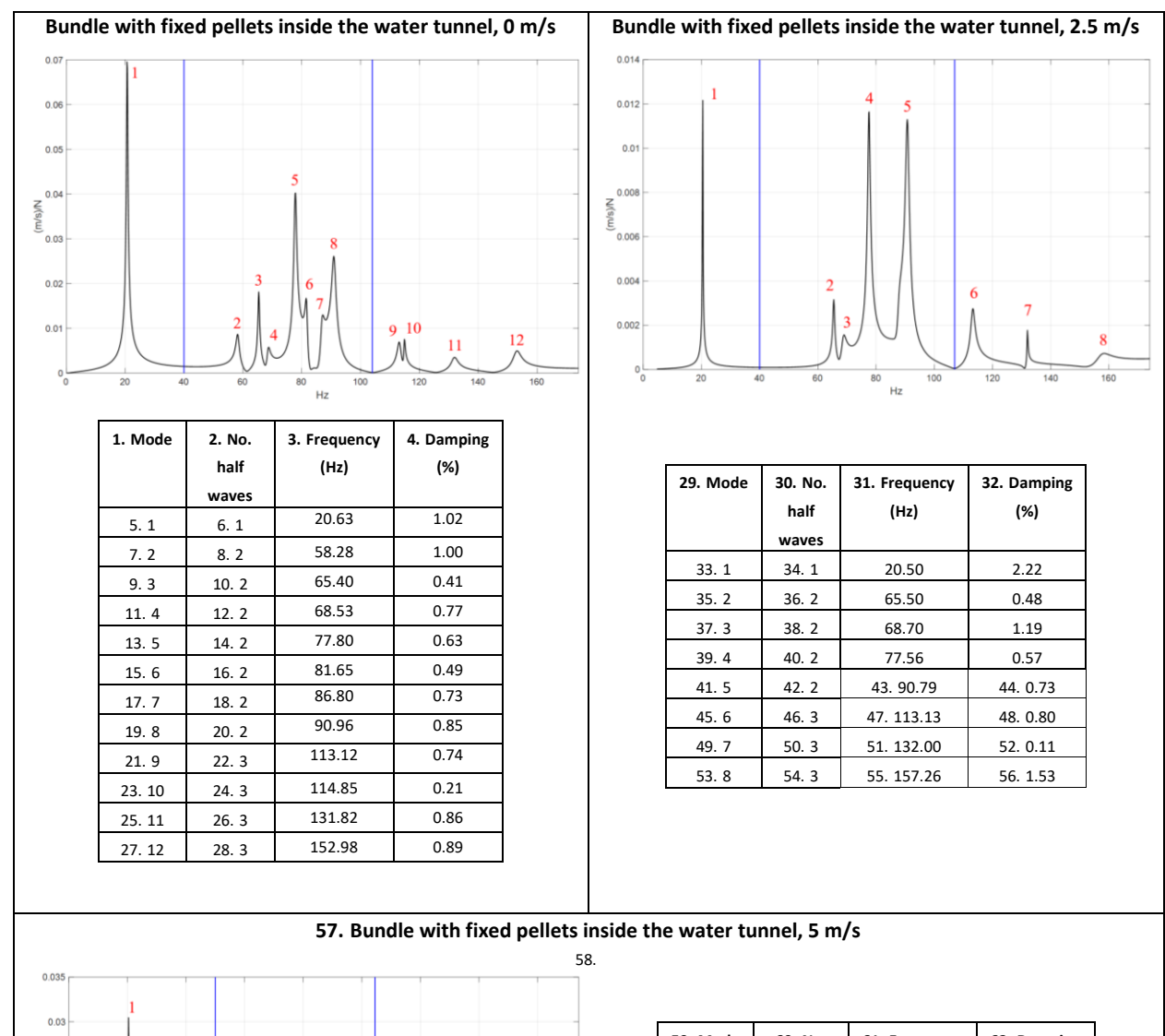
Mode	No. half waves	Frequency (Hz)	Damping (%)
1	1	17.97	0.97
2	2	52.93	0.54
3	2	65.42	0.84
4	2	71.25	1.46
5	2	72.69	0.3
6	3	88.37	0.60
7	3	133.65	0.88
8	3	152.1	1.52

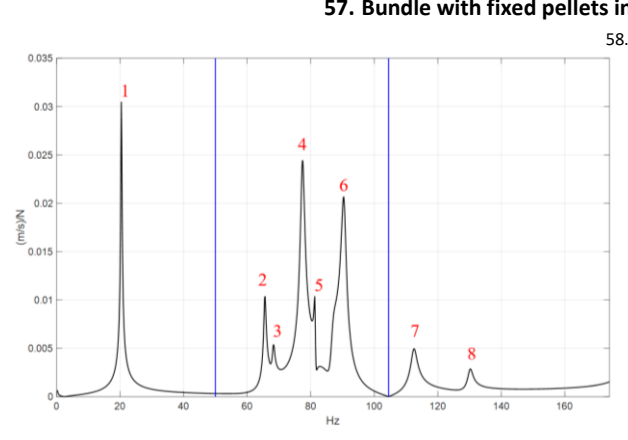
Bundle with fixed pellets in still water



Mode	No. half	Frequency	Damping
Wiode	waves	(Hz)	(%)
1	1	19.92	1.73%
2	2	56.72	2.65%
3	2	68.22	3.18%
4	2	83.79	1.36%
5	3	128.55	1.16%
6	3	146.49	0.91%

Table 11. Modal analysis for the bundle inside the water tunnel.





59. Mode	60. No. half	61. Frequency (Hz)	62. Damping (%)
	waves		
63. 1	64. 1	20.38	2.78
65. 2	66. 2	65.40	0.41
67. 3	68. 2	68.53	0.77
69. 4	70. 2	77.80	0.63
71. 5	72. 2	81.65	0.49
73. 6	74. 2	90.96	0.85
75. 7	76. 3	113.15	0.58
77. 8	78. 3	129.95	0.96

Table 10 and Table 11 show in a concise manner the Frequency Response Functions and the modal parameters extracted for the seven configurations under exam. The resonances of the FRFs are correlated to the rows of the tables of the modal parameters through progressive numbers. As anticipated, the modes are also classified according to the number of half-waves. The area of the FRFs is divided by two vertical lines into three regions, each one characterized by the same number of half-waves in the motion of the rods.

The modal analysis of the bundle with free rods in air shows a fundamental frequency remarkably close to that in (Ferrari *et al.*, 2019). However, the range of frequency of the other modes is different. The bundle with fixed pellets in air has higher natural frequencies. The introduction of still water gives lower natural frequencies and higher damping ratios for the fundamental mode. This is justified by the virtual added-mass effect of water and by the increased viscous dissipation in the liquid. The bundle with fixed pellets in water presents the highest damping ratios.

The bundle was tested in quiescent water in the water tunnel as well. The purpose of this test is to ensure the comparability of the boundary conditions in the water tunnel and in the acrylic tank. The natural frequencies and the modal damping values in the water tunnel are in effect compatible to the corresponding configuration in the acrylic tank. Damping values are slightly lower overall. Subsequently an average velocity of 2.5 m/s was chosen as it is intermediate between the quiescent condition and the approximate maximum velocity of the fluid flow encountered in Framatome PWRs. At this velocity damping increases with respect to the quiescent condition, in particular for the first mode (where it increases by more than 100%). At the maximum testing velocity of 5 m/s, the damping of the fundamental mode increases with respect to the 0 and 2.5 m/s conditions. This seems to suggest that an increasing fluid flow contributes to damping vibrations, at least up to the velocities tested in this study. The natural frequencies at 2.5 and 5 m/s remain practically unchanged with respect to the quiescent condition in the case under exam. The dependence of natural frequencies on the fluid velocity depends, however, on the specific boundary conditions, as it can be inferred in (Païdoussis, 1979).

The number of modes detected in the frequency range of interest increases with the presence of water, since the latter adds hydrodynamic coupling to the coupling due to the spacer grids. The number of modes is also larger in the tunnel, probably because of the confinement effect. However, it decreases with the flow speed as *i*- overall damping increases and some mode may not appear anymore and ii- flow-borne noise prevents the detection of the least prominent modes.

3.1.1 Modal shapes

As mentioned, the coupling between the rods constituting the bundle gives rise to vibration modes that can be divided according to the number of flexural waves in the rods. For any normal mode of the bundle, every rod presents the same number of flexural waves, but the vibrations of the rods are different in relative phase and amplitude. Moreover, the normal modes of the bundle are perfectly sorted in terms of the number of half-waves in the rods. Therefore, a normal mode characterized by a number i of half-waves in the rods will happen at a frequency lower than a normal mode with i+1 half-waves; and, as a consequence, the FRF of the bundle can be divided into the areas of influence on the underlying vibration shapes of the rods, and these areas do not overlap. As an example, Table 12 shows the vibration shapes corresponding to the normal modes presented in the section relevant to the bundle in the tunnel without water flow. This case was chosen as it presents the largest number of normal modes of vibration. It must be noted that the normal modes that were measured and presented in this section are in no way representative of the total number of normal modes that shall be expected in a coupled system. Some modes may, in fact, be too damped to be detected by the modal analysis system. Because of the multiple and complex sources of coupling, moreover, it would be difficult to predict theoretically the number of normal modes that the bundled system should present.

Table 12. Vibration shapes of the bundle in the water tunnel at a flow of 0 m/s. Only one half of the length of the bundle is represented (it has been verified that the vibration of the bundle is approximately symmetrical).

79. Mode number	80. Number of half-waves	81. Frequency (Hz)	82. Damping (%)	83. Mode shape
84. 85. 1	1	20.63	1.02	
86. 87. 2	2	58.28	1.00	
88. 89. 3	2	65.40	0.41	
90. 91. 4	2	68.53	0.77	
92. 93. 5	2	77.80	0.63	
94. 95. 6	2	81.65	0.49	
96. 97. 7	2	86.80	0.73	
98. 99. 8	2	90.96	0.85	
100. 101. 9	3	113.12	0.74	
102. 103. 10	3	114.85	0.21	
104. 105. 11	3	131.82	0.86	
106. 107. 12	3	152.98	0.89	

3.2. Large-amplitude vibrations (nonlinear results)

Non-linear vibrations with stepped-sine excitation can be described by frequency-amplitude curves and frequency-phase curves (amplitude and phase diagrams with several curves measured at different force amplitude levels). The phase curves are here omitted as they do not show any notable phenomenon. Results for an increasing and a decreasing direction of the excitation frequency (UP and DOWN curves, respectively) are presented together in the charts. UP and DOWN curves differ since the response of non-linear systems depends on the history of the system itself. It is anticipated that, as in (Ferrari et al., 2019), the nonlinear behavior is softening in nature (the peak frequency decreases with the amplitude of the excitation). All configurations were subjected to forces ranging in amplitude from a linear level ($0.1 - 0.5 \, \text{N}$) to a fully nonlinear level equal to $12 \, \text{N}$.

3.2.1 Bundle with freely moving pellets in air

Forces up to 12 N were applied to vibrate the bundle up to a vibration amplitude of approximately 3.5 mm, as shown in Fig. 42. A strong softening shift is present, which confirms the behavior of single rods in spacer grids observed in (Ferrari *et al.*, 2019). Hysteresis between UP and DOWN curves is negligible and no nonlinear jumps are found. The horizontal vibration is more than 30 times smaller in amplitude than the excited (vertical) vibration, see Fig. 43. It might be noted, anyway, that the peak vibration amplitude of the horizontal mode happens at a higher frequency than the vertical mode. This suggests that the horizontal vibration is not given by measurement errors but constitutes a proper example of weak internal resonance. However, due to the much smaller amplitude, the companion mode participation to the global vibration response results negligible.

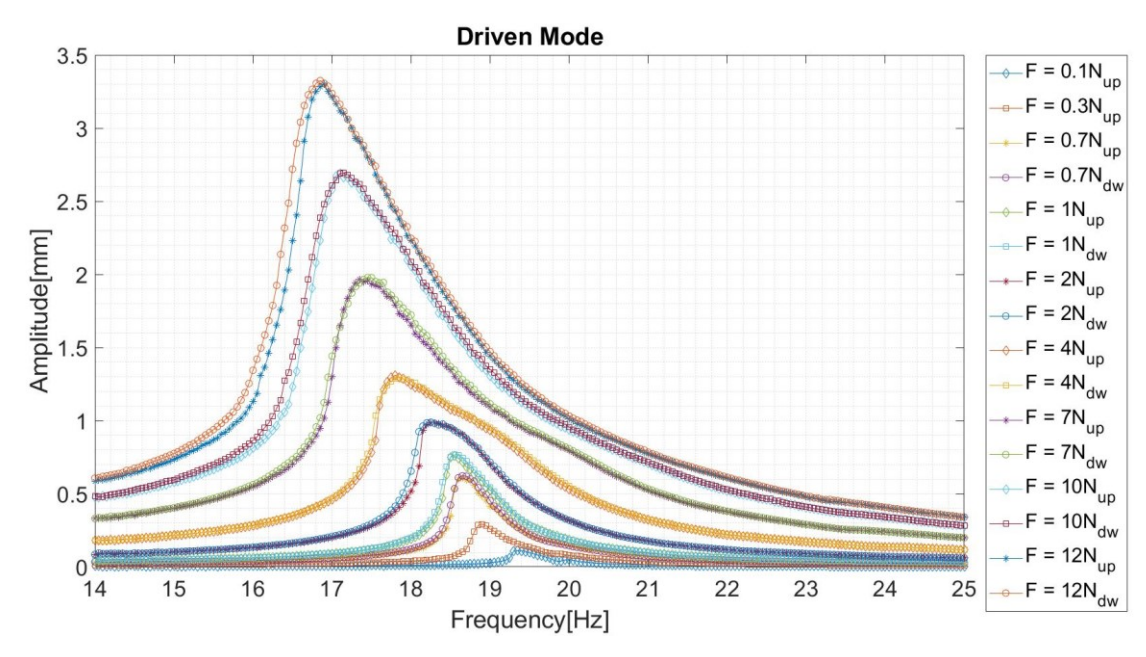


Fig. 42. Frequency-amplitude curves for the driven mode of the free-pellets rod in air, UP and DOWN directions.

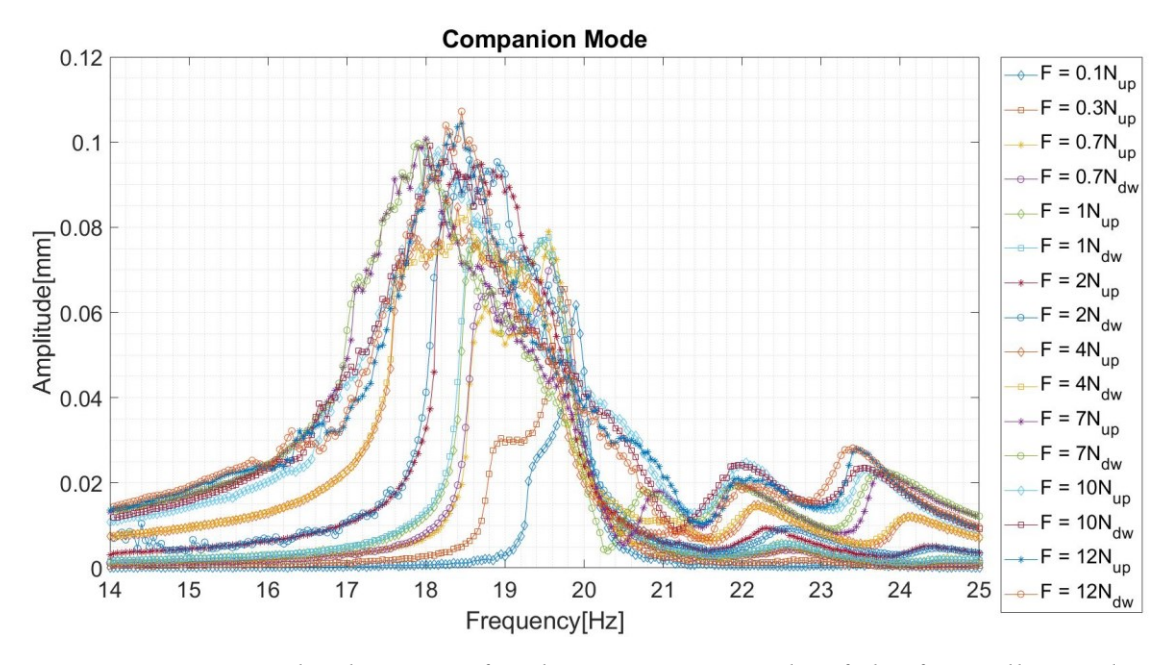


Fig. 43. Frequency—amplitude curves for the companion mode of the free-pellets rod in air, UP and DOWN directions.

3.2.2 Bundle with fixed pellets in air

The nonlinear vibration of is similar in character to that with free pellets. The behavior is again softening with no hysteresis; slightly lower amplitudes are reached, as shown in Fig. 44. A jump

behavior seems to develop in the 4-7 N range, but it disappears for higher forces. The horizontal vibration is 15 times lower than the vertical vibration in amplitude and the peak is at higher frequencies, see Fig. 45. In this case too, the companion mode can be neglected in the system dynamic response. With respect to the case with free pellets, the horizontal vibration has vibration peaks more clearly distinct from the driven mode.

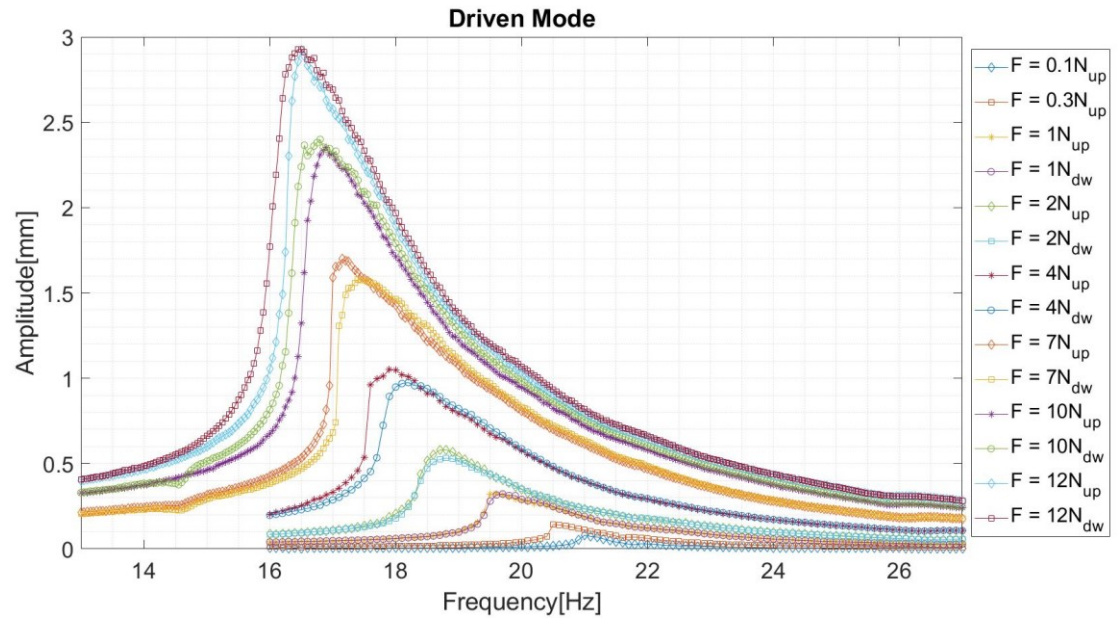


Fig. 44. Frequency—amplitude curves for the driven mode of the fixed-pellets rod in air, UP and DOWN directions.

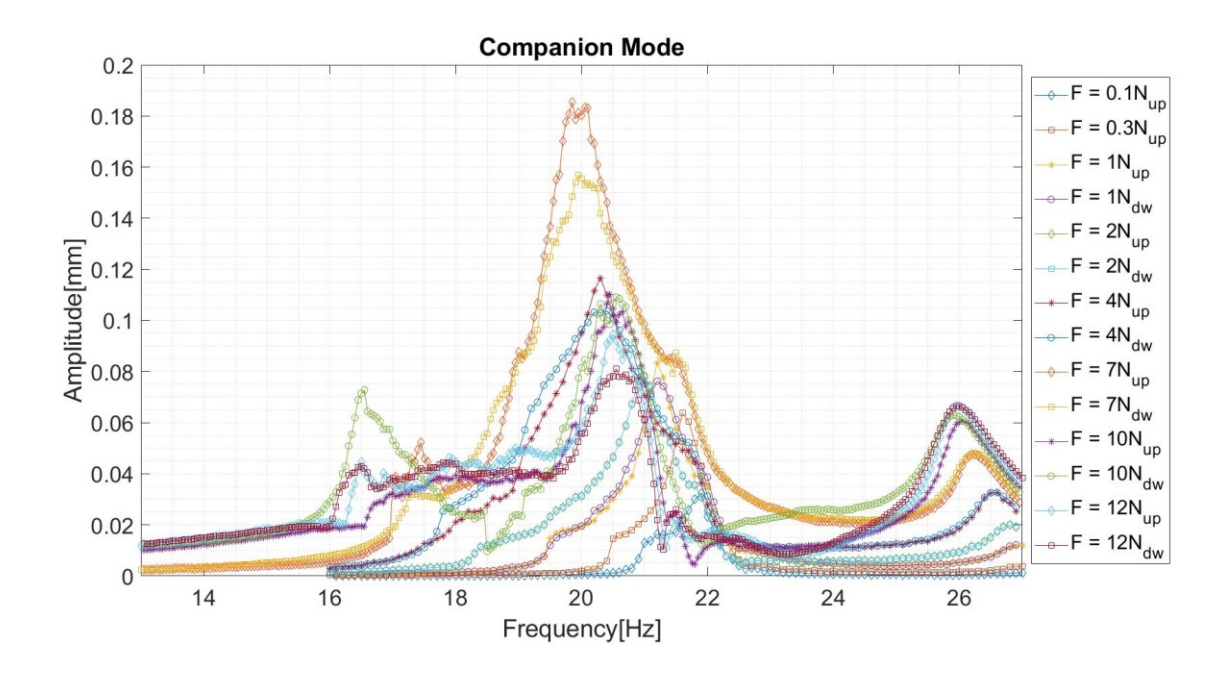


Fig. 45. Frequency—amplitude curves for the companion mode of the fixed-pellets rod in air, UP and DOWN directions.

3.2.3 Bundle with freely moving pellets in still water

The nonlinear vibration amplitude reached at the resonance peak by the freely moving pellets configuration in water for harmonic excitation of 12 N is smaller than for the same system in air, as it is shown comparing Fig. 12 and Fig. 46. This is associated with an increase of damping. The companion mode shows two main peaks at different frequencies and remains approximately 15 times smaller than the driven mode as displayed by Fig. 47. Therefore, companion mode is practically negligible.

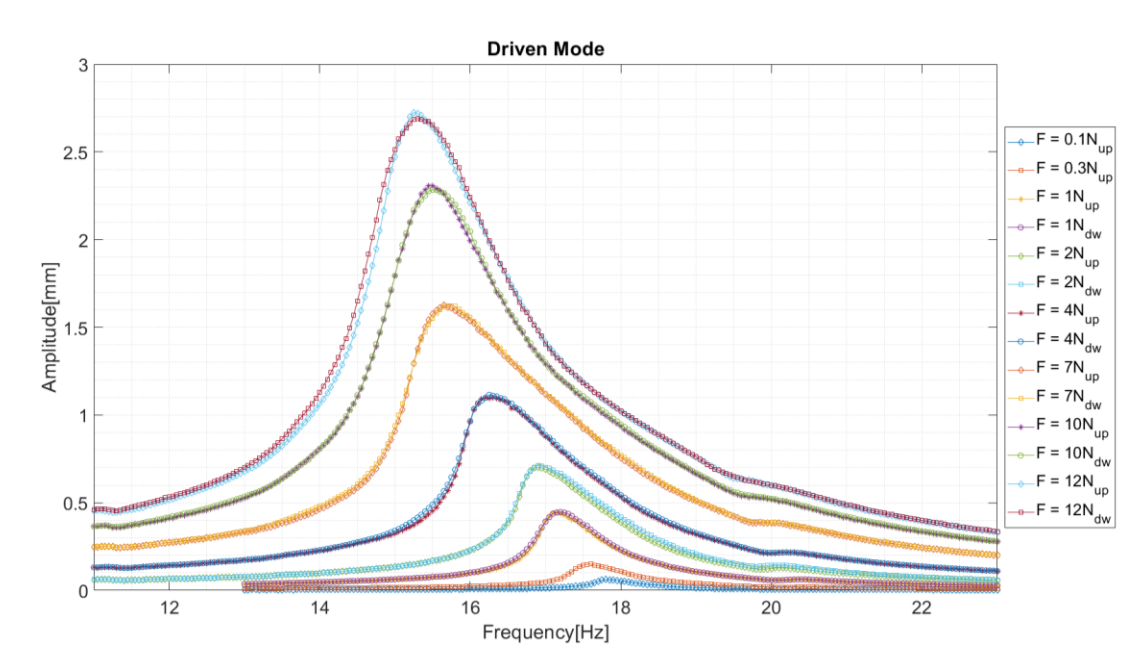


Fig. 46. Frequency – Amplitude curves for the driven mode of the free-pellets rod in water, UP and DOWN directions.

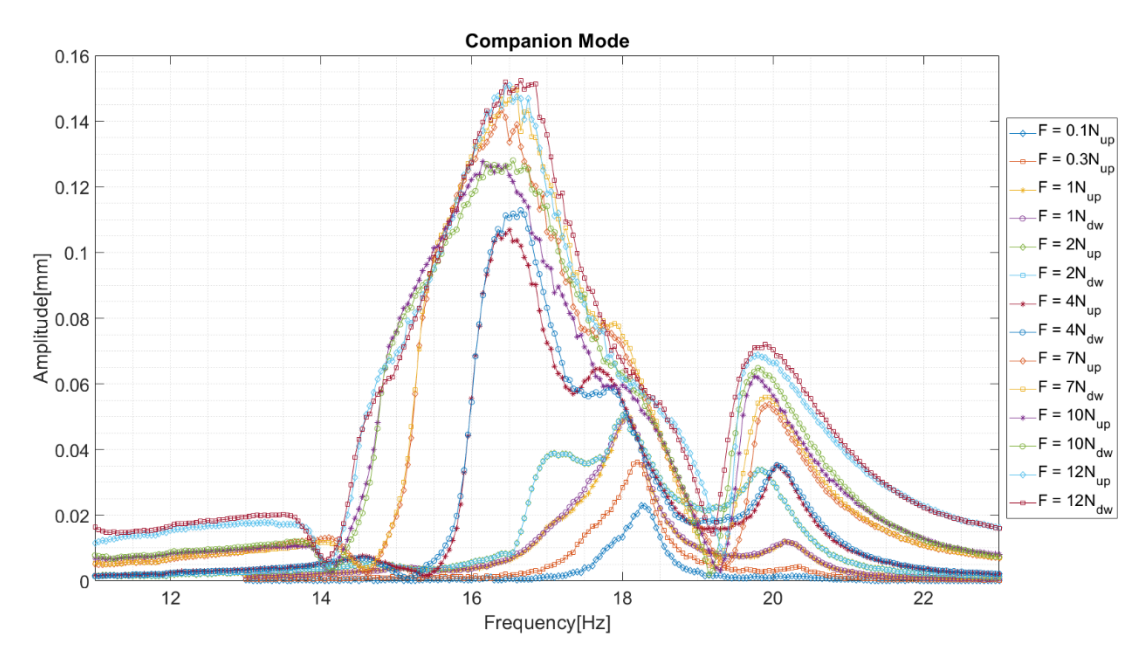


Fig. 47. Frequency—amplitude curves for the companion mode of the free-pellets rod in water, UP and DOWN directions.

3.2.4 Bundle with fixed pellets in still water

The peak vibrations reached by driven and companion vibration are not dissimilar from those measured in water with free pellets, see Fig. 48 and 19. Therefore, the companion mode, shown in Fig. 19, is practically negligible being one order of magnitude smaller than the driven mode, presented in Fig. 18. The amount of softening shift, about 4.5 Hz for the harmonic force of 12 N that gives a vibration amplitude of about 2.5 mm, is close to the value measured in air with fixed pellets and previously shown in Fig. 14.

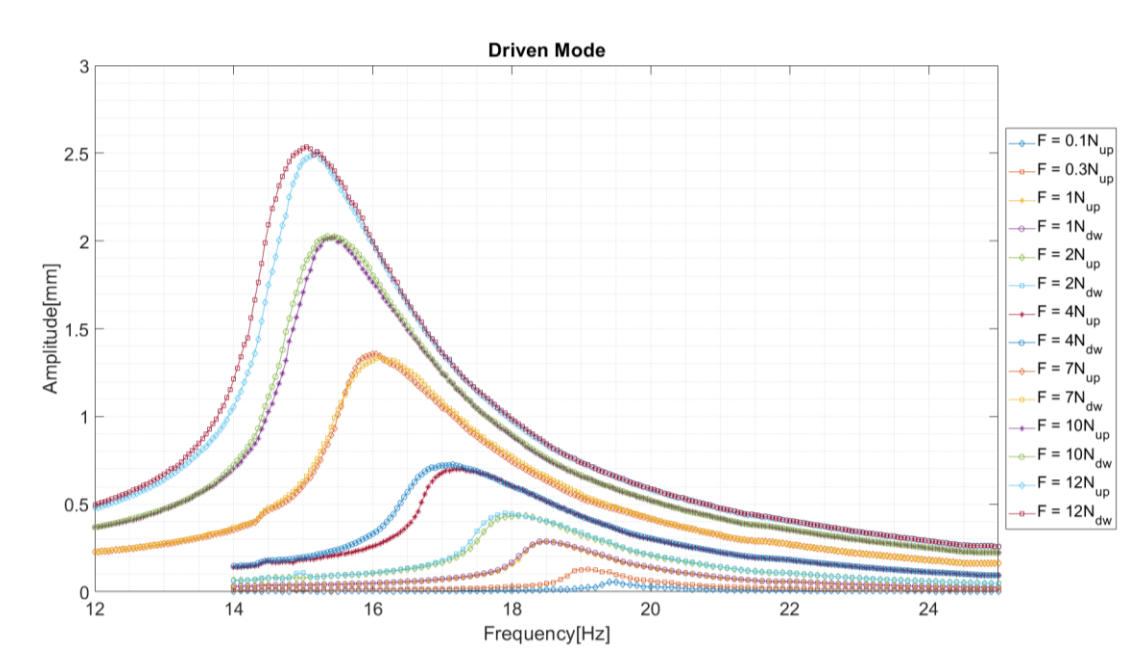


Fig. 48. Frequency—amplitude curves for the driven mode of the fixed-pellets rod in water, UP and DOWN directions.

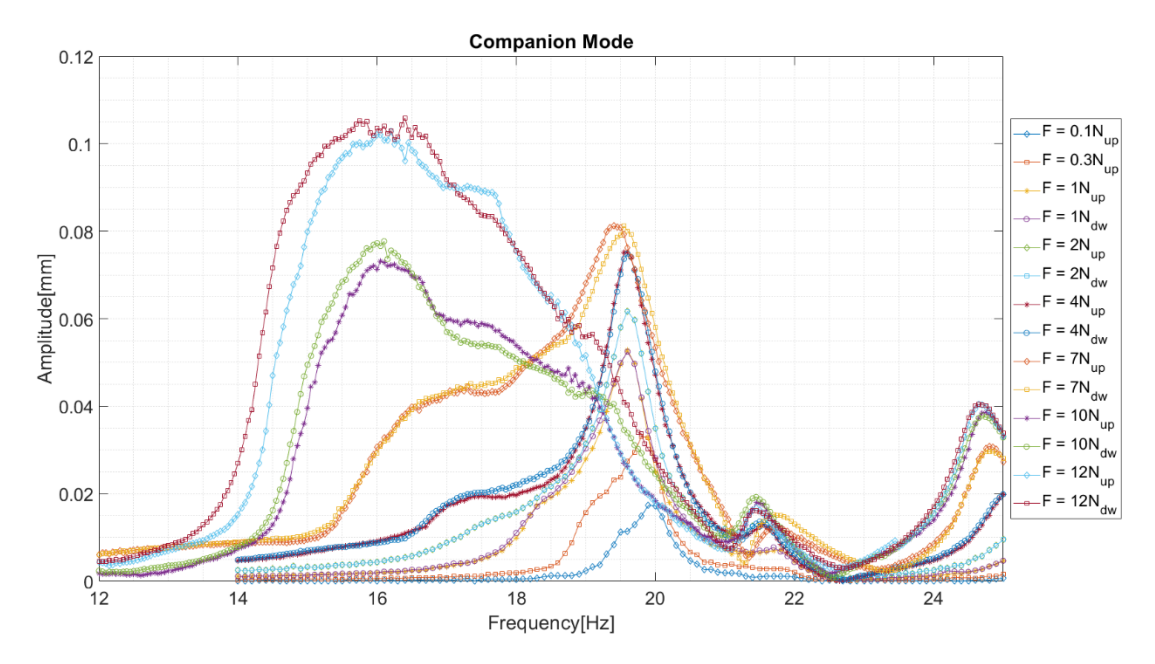


Fig. 49. Frequency–amplitude curves for the companion mode of the fixed-pellets rod in water, UP and DOWN directions.

3.2.5 Bundle with fixed pellets inside the water tunnel, 0 m/s (no flow)

The frequency-amplitude curves in Fig. 50 show again a softening frequency shift without nonlinear jumps. The softening frequency shift of about 3 Hz for harmonic excitation of 12 N is similar to the one observed in the water tank with fixed pellets at the same peak vibration amplitude, around 1.3 mm. However, the peak vibration amplitude reached, which is 1.3 mm, is significantly lower than the 2.5 mm obtained in that case for the same harmonic force of 12 N. The lower amplitude reached for the same harmonic force is due to the different setup in the tank and water tunnel, with different excitation point. In fact, damping of the fundamental mode of the fuel assembly is similar in the two cases and the natural frequency slightly increased (about 1 Hz) in the water tunnel.

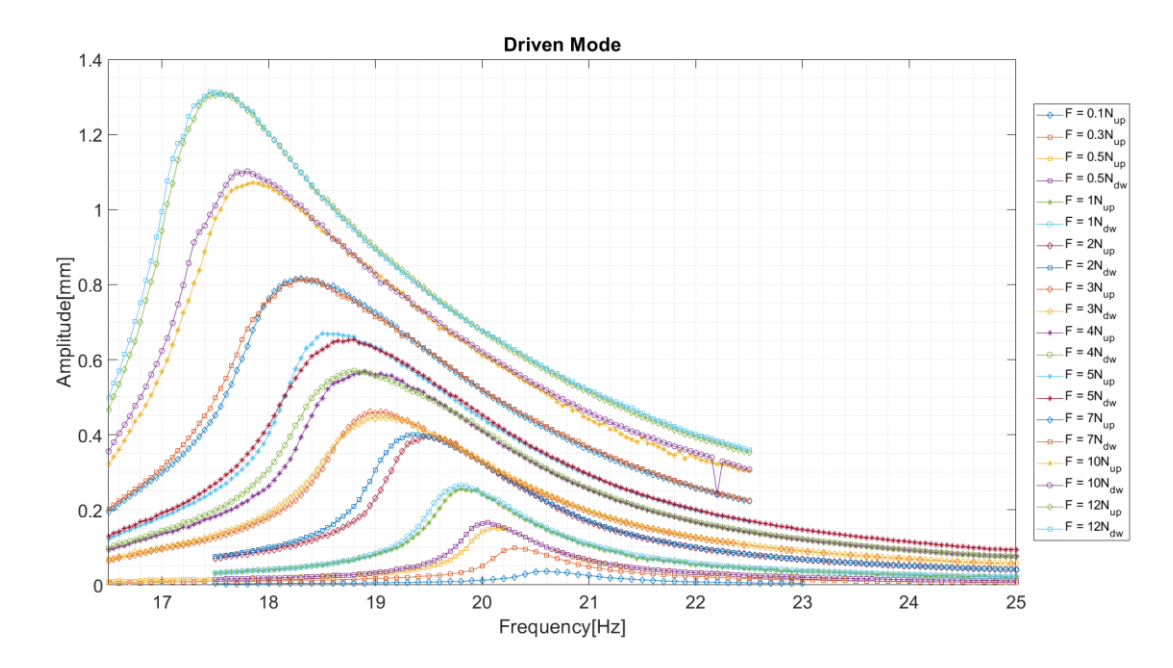


Fig. 50. Frequency—amplitude curves for the driven mode of the bundle inside the water tunnel, water velocity 0 m/s.

3.2.6 Bundle with fixed pellets inside the water tunnel, water velocity 2.5 m/s

The peak amplitude of the nonlinear curves in Fig. 51 for the largest harmonic force is almost unchanged with respect to the case of zero water flow velocity. This indicates that the equivalent damping associated to large-amplitude vibration is not far apart in these two cases. However, the peak amplitude for low forces is significantly reduced with respect to the case of no flow in the water tunnel. While the lowest forcing level is 0.1 N in quiescent water, with fluid flow it has to

be increased to 0.5 N. In effect, the random vibrations due to fluid flow appear as random vibrations, thus rendering the measurement of the response to low forcing levels excessively noisy and not meaningful.

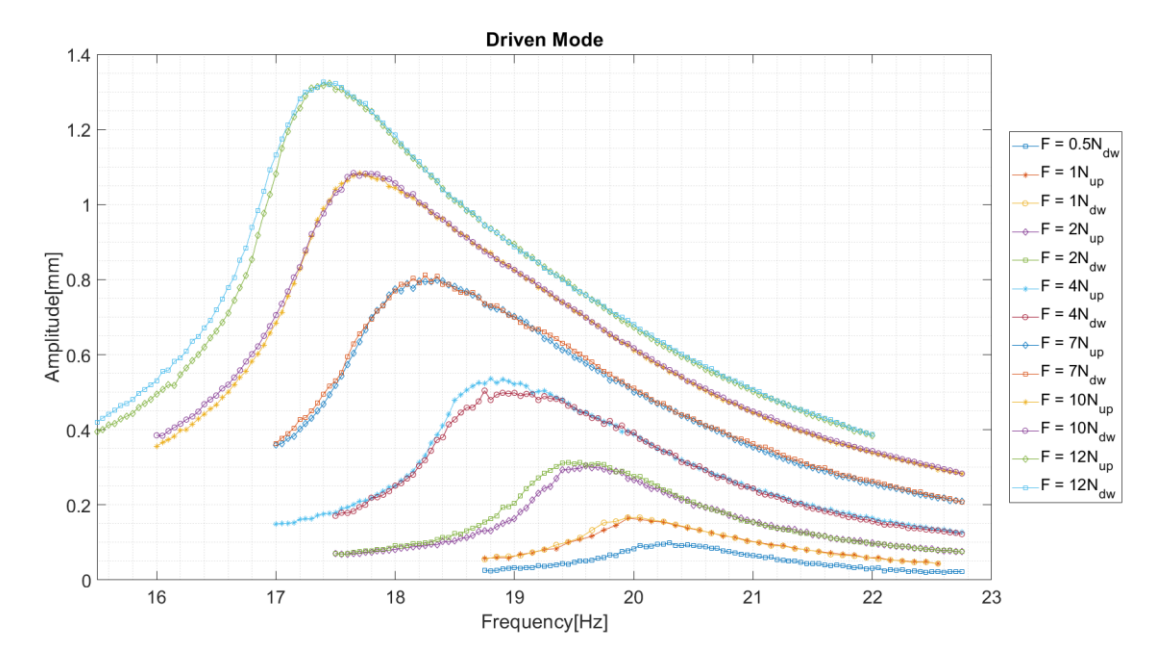


Fig. 51. Frequency—amplitude curves for the driven mode of the bundle inside the water tunnel, water velocity 2.5 m/s.

3.2.7 Bundle with fixed pellets inside the water tunnel, water velocity 5 m/s

Again, the peak amplitude and frequency shift of the nonlinear curve for 12 N remain very similar to those obtained in the water tunnel for water velocity of 0 and 2.5 m/s. In effect, it is remarkable that, by increasing the flow velocity from 2.5 to 5 m/s, the peak frequencies at each forcing level change by less than 1% and the peak vibration amplitudes are approximately 3% lower. Also, there is absence of nonlinear jumps and nonlinear UP/DOWN hysteresis, as shown in Fig. 52. In addition, the curves for all the excitation levels are substantially noisier. This is due to flow-induced vibration creating "noise" since the water speed is relevant.

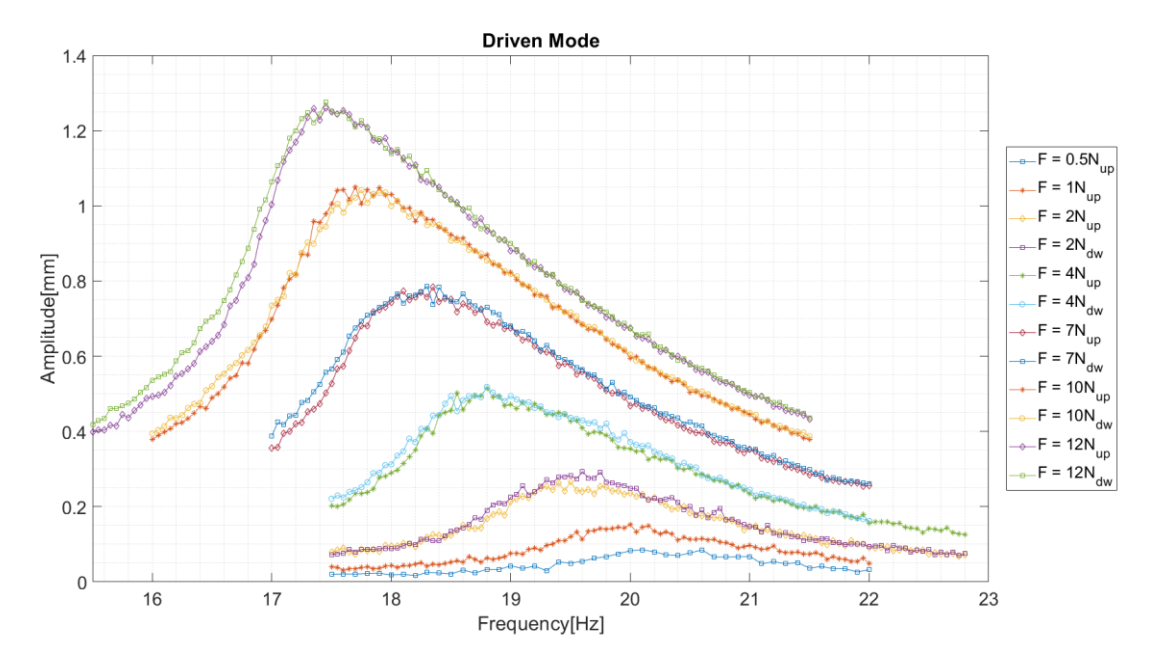


Fig. 52. Frequency—amplitude curves for the driven mode of the bundle inside the water tunnel, water velocity 5 m/s.

4. Discussion

4.1. Small-amplitude (linear) experiments

With comparison to the results in (Ferrari *et al.*, 2019), it was found that the bundle has fundamental frequencies extremely close, but slightly higher than the equivalent single rod. The damping values in the bundle are lower in air, but higher in water. Obviously, the fixed rods in (Ferrari *et al.*, 2018) have higher frequencies, but much lower damping values. The comparison of modes other than the fundamental is difficult, since in the bundle the rod modes split into several modes because of coupling.

Besides, water tends to increase slightly damping and to reduce natural frequencies. The small difference between quiescent conditions in the tank and in the tunnel is not explained, but it must be noted that natural frequencies are extremely sensitive to the conditions of the installation and to thermal changes. The estimation of modal damping, even if estimated by advanced algorithms

such as LMS Polymax (Peeters et al., 2004), presents some uncertainty due to the parameters of the estimation itself.

Flowing water appears to reduce the natural frequency by no more than 2.5 % (likely because viscous friction creates a state of compression between the constraints) and increases modal damping dramatically (by 1.8 times at 2.5 m/s and by 2 times at 5 m/s).

4.2. Large-amplitude (nonlinear) experiments

Nonlinear curves show a softening behavior, extremely similar to the one attributed to single rods in (Ferrari *et al.*, 2019). The decrease in the stiffness of the system for increasing forcing and vibration amplitudes has not been explained physically, so far, if not by a decrease in stiffness of the constraints at the spacer grids. Fuel rods in fixed-fixed boundary conditions show instead a hardening behavior (Ferrari *et al.*, 2018), given by the axial tension built during flexural vibration. Compared to fixed rods, rods and bundles in spacer grids show a reduced if not negligible hysteresis: UP and DOWN curves share an almost identical path and no nonlinear jumps are detected. This is attributed to a much higher value of overall damping.

The damping and the symmetry break introduced by spacer grids is not sufficient to impair completely the appearance of vibrations perpendicular to the direction of excitation. These vibrations may appear in nuclear reactors as well. However, they do not reach amplitudes comparable to those of the directly driven excitation direction. Contrary to what shown in (Ferrari *et al.*, 2018) for fixed rods, it is not possible to mention a proper companion mode or proper traveling waves due to axial symmetry and one-to-one internal resonance.

4.3. Identification of nonlinear parameters

Fig. 53, 24 and 25 feature the experimental responses for different cases and identified linear models in terms of amplitude (a_1) and phase (ϕ_1) of the first harmonic of the dimensionless displacement (obtained by dividing by the tube thickness) at the highest excitation level for each case. Despite some discrepancies between the identified and the experimental responses, the linear oscillator enables a first approximation of the frequency response of the rod for a specific

magnitude of excitation. In this case, it is used to identify the equivalent damping ratio in nonlinear regime.

Table 13 gives the frequency of the maximum vibration response and the equivalent modal damping ratio for each experimental configuration; data obtained for both the minimum and maximum levels of harmonic force are presented. The natural frequencies identified at the smallest excitations are predictably close to the ones obtained by experimental modal analysis. However, the estimated damping ratios of the linear responses are different (mostly higher) than the ones from experimental modal analysis. This discrepancy can be explained by the facts that: (i) some small responses show one-to-one internal resonance, hence a truncation of the peak amplitude of the driven mode; (ii) the stepped-sine test with sinusoidal signal provides excitations too large to remain in the linear field; (iii) the system may change slightly, for example because of changes in temperature, between the moment when the modal and the stepped-sine analyses are run.

Table 13. Identified natural frequencies and damping ratios of the minimum and maximum excitation for each experimental case.

_	rimental case	Force (N)	Vibration amplitude of the peak (mm)	Frequency of the peak (Hz)	Frequency decrease (%)	Equivalent modal damping ratio ζ	Damping increase
	Free	0.1	0.11	19.35	12.92	0.88×10^{-2}	6.06
Air	pellets	12.0	3.32	16.85	12.72	5.33×10 ⁻²	0.00
All	Fixed	0.1	0.08	21.00	21.67	1.19×10 ⁻²	5.06
	pellets	12.0	2.93	16.45	21.07	6.97×10 ⁻²	5.86
	Free	0.1	0.06	17.80	14.33	1.48×10 ⁻²	4.26
Still	pellets	12.0	2.72	15.25		6.30×10 ⁻²	
water	Fixed	0.1	0.06	19.50	22.82	1.46×10 ⁻²	5 44
	pellets	12.0	2.54	15.05	22.82	7.94×10 ⁻²	5.44
	0 m.s ⁻¹		0.04	20.60	15.29	1.34×10 ⁻²	(07
Water 0 m.s	12.0	1.31	17.45	13.29	8.13×10 ⁻²	6.07	
flow	2.5 m.s ⁻¹	0.5	0.10	20.30	14.20	2.41×10 ⁻²	2.00
Fixed	2.3 III.S	12.0	1.33	17.40	14.29	7.18×10 ⁻²	2.98
pellets 5.0 m.s ⁻¹	5.0 m a-1	0.5	0.09	20.10	13.18	2.74×10 ⁻²	2.00
	12.0	1.28	17.45	13.18	7.13×10 ⁻²	2.60	

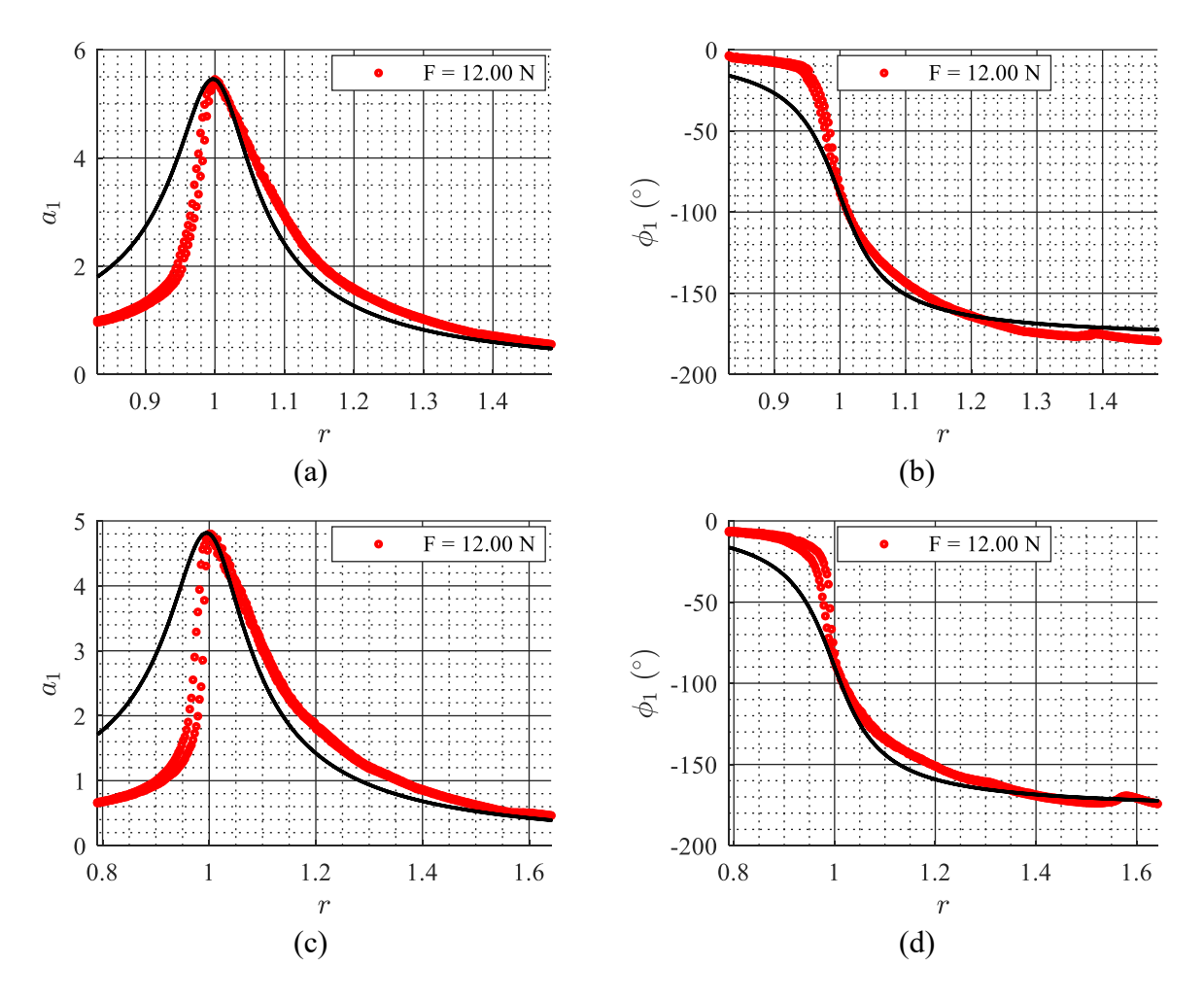


Fig. 53. Frequency-response of the first harmonic of the dimensionless displacement for the experiments in air: (a) amplitude and (b) phase of the bundle with freely moving pellets; (c) amplitude and (d) phase of the bundle with fixed pellets. Experimental data are represented by red markers while identified data are represented by continuous black line.

Natural frequencies, as mentioned, are larger for the bundle in the tunnel than in the tank. The softening shift of frequency of the peak is very similar in the tank and in the water tunnel when taking data for the same vibration amplitude. In fact, the column in Table 5 that gives the frequency changes, show data for different vibration amplitudes. Therefore, this column must be considered together with the column showing the vibration amplitude of the peak.

The softening natural frequency shift is also larger with fixed pellets and in presence of water instead of in air. While it is expected that water gives an added mass effect resulting in an increased

softening behavior, the possible stiffness given by the axially fixed pellets should have an opposite effect. It must be concluded that the pellets do not increase the stiffness of the system. Flow velocity barely affects the natural frequencies and softening behaviour for larger excitation levels. With regards to the identified damping, the axial constraint on pellets increases damping for the largest responses both in air and in water by approximately 26%. The presence of water affects positively the overall damping value as well. At the largest vibration amplitude, damping in water is 18% larger in the free-pellets configuration.

Damping ratios increase in the water tank with respect to the ones of comparable experiments in air, with an increase from the 14 % to the 68 %. The effect on the damping ratio of the water confinement in the tunnel at 0 m/s is negligible at both the minimum and at the maximum excitation levels. However, flowing water influences damping substantially at small excitations (linear regime). At the lowest forces, damping presents an 80% increase at 2.5 m/s and a 100% increase at 5 m/s. However, at the largest forces, the equivalent damping does not become higher than that identified without flow. In fact, at 12 N, the damping values are similar enough, considering possible identification errors. In conclusion, damping starts at a value twice higher in the water tunnel at 5 m/s with respect to the quiescent condition; afterwards, it increases by one half of how much it would increase in quiescent water, with a final result extremely similar to the one in still water and not far from the ones identified in the other configurations (the farthest large-amplitude damping value is measured in air with free pellets, and it is 33% lower). This seems to suggest that, in the small-amplitude regime, part of the excitation energy is dissipated because of the flow; afterwards, the damping increase is different in still and flowing water, up to reach similar values at the maximum excitation level tested.

As expected, damping ratios estimated for the largest nonlinear responses (12 N) present a significant increase with respect to the ones at the lowest excitation levels (0.1/0.5 N) for all the cases under investigation. This increase is of the range 400% - 600% in quiescent fluids and 200% - 300% in flowing water. These figures highlight the need of taking into account a nonlinear increase of the damping with the magnitude of excitation by means of nonlinear models, as applied phenomenologically by (Eichler *et al.*, 2011; Jeong *et al.*, 2013; Le Guisquet and Amabili, 2019; Lu *et al.*, 2019) and as developed theoretically by (Amabili, 2018b,c and d). This increase of damping ensures a safer behavior of nuclear bundles by limiting the increase of amplitude in case of large excitation.

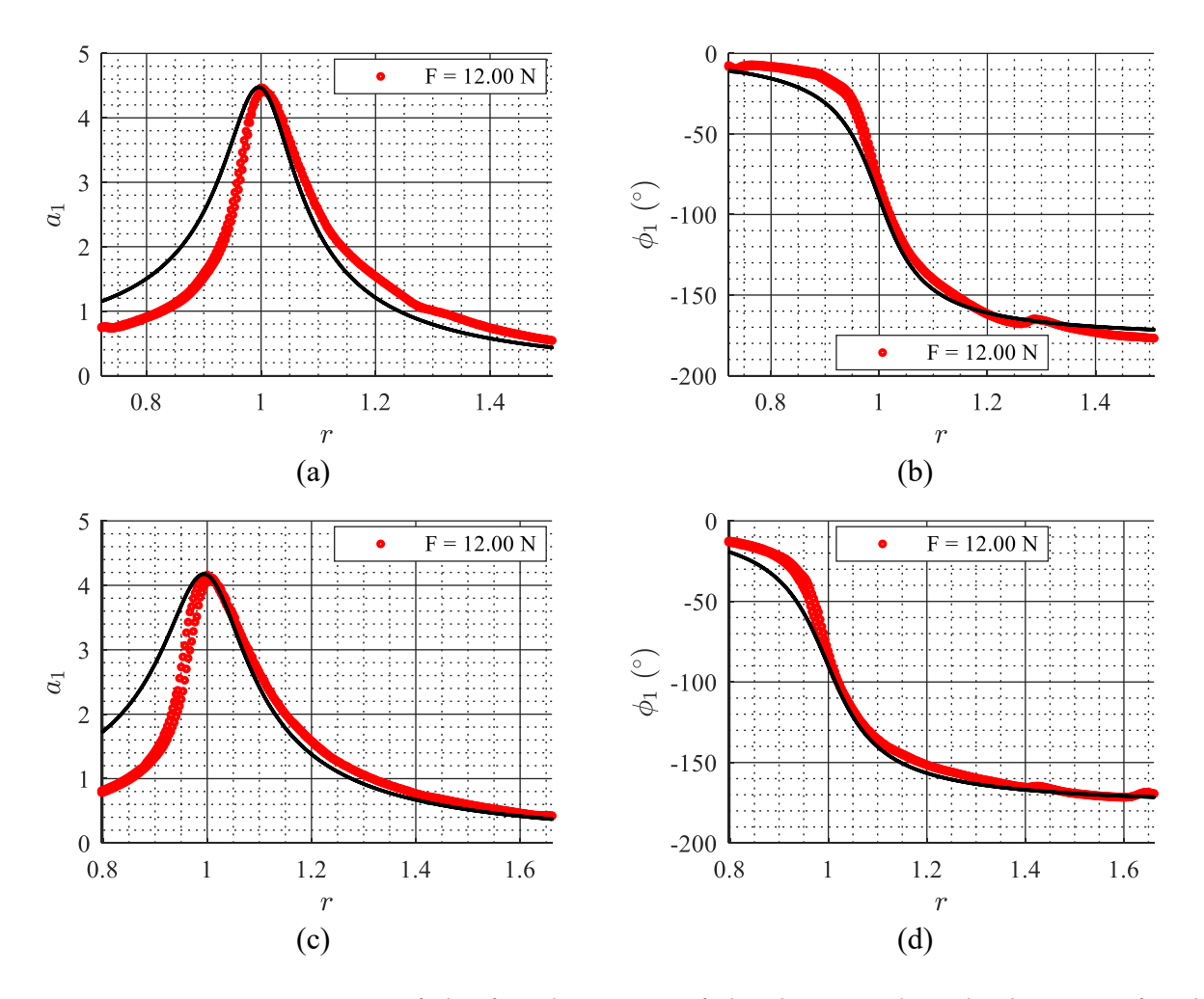


Fig. 54. Frequency-response of the first harmonic of the dimensionless displacement for the experiments in quiescent water: (a) amplitude and (b) phase of the bundle with freely moving pellets; (c) amplitude and (d) phase of the bundle with fixed pellets. Experimental data are represented by red markers while identified data are represented by continuous black line.

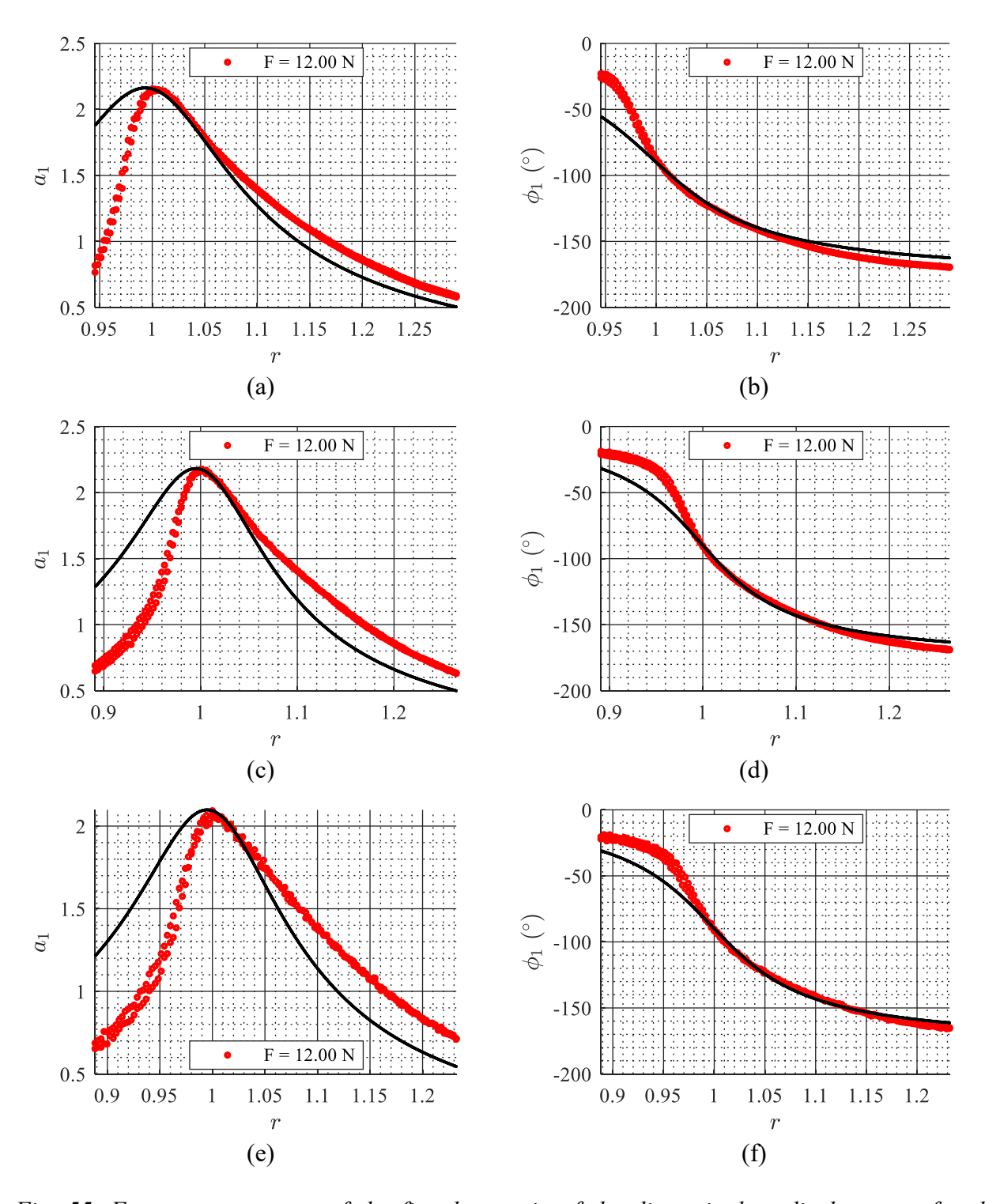


Fig. 55. Frequency-response of the first harmonic of the dimensionless displacement for the experiments in flowing water in the water tunnel for the bundle with fixed pellets: (a) amplitude and (b) phase at a velocity of 0 m.s⁻¹; (c) amplitude and (d) phase at a velocity of 2.5 m.s⁻¹; (e) amplitude and (f) phase at a velocity of 5.0 m.s⁻¹. Experimental data are represented by red markers while identified data are represented by continuous black line.

5. Conclusions

A recent study investigated experimentally the dynamic response and damping of a single fuel rod supported by spacer grids (Ferrari *et al.*, 2019). The experimental procedure was adapted successfully with few variations to a 3×3 cluster of nuclear fuel rods with a central guide tube in order to study the effect of the bundled structure and flowing water. The behavior of the fuel bundle in quiescent media is remarkably similar to dynamic response of a single fuel rod supported by spacer grids around the fundamental frequency.

The bundled structure reached damping increases in the nonlinear regime similar to those of the single rod supported by spacer grids. However, much higher harmonic forces were required to develop similar vibration amplitudes. Vibration components orthogonal to the excitation are negligible with respect to the flexural vibration parallel to the excitation. Moreover, the periodicity of the structure and the presence of intermediate supports and hydrodynamic coupling between the fuel rods causes the presence of scattered modes characterized by different combinations of the motion of single rods. This effect is particularly important for even modes, which present a node at the intermediate (central) spacer grid.

As observed for a single fuel rod supported by spacer grids, the bundle has a an initial (for relatively small vibration amplitudes) very strong softening nonlinear behavior that cannot be modeled by the modified Duffing oscillator developed in (Delannoy *et al.*, 2015). This initial strong softening behavior seems caused by the nonlinear boundary conditions due to the springs installed on the spacer grids. Therefore, the system cannot be described only by quadratic and cubic stiffness in the modified Duffing oscillator. In the future, dedicated experiments will be performed to characterize the interaction between spacer grids and fuel rods. It is also planned to add higher-order stiffness terms to the Duffing oscillator in order to reproduce the strongly softening behavior initially observed in the experiments.

The setup was installed in a water tunnel capable of fluid flows comparable to those existing in PWRs. A key factor was the presence of a stiff frame supporting the spacer grids without exerting large forces on them. The frame was also engineered to have minimal unwanted resistance to flow. Laser Doppler vibrometry was successfully used to measure vibrations without contact through water and acrylic walls. Since relatively large forces are required to excite large amplitude vibrations, a rubber-membrane was placed to prevent leak at the location of the stinger, which is used to excite the fuel assembly immersed in flowing water by means of an electrodynamic shaker.

The water flow is given as the nominal mean flow traversing the tunnel. However, in the future dedicated studies by means of Pitot tubes and/or Particle Image Velocimetry are planned to estimate the local flow values around and among the fuel rods. In fact, the close spacing of fuel rods and the mixing effect of spacer grids might alter substantially the local flow.

The presence of water flow does not have an important effect on natural frequencies for the specific boundary conditions constituted by spacer grids. As expected, no instabilities were detected in operative conditions, since axial flow values are too low to generate phenomena such as divergence or flutter. However, the strongly turbulent flow resulted in random noise superimposed onto the system vibration response. The damping ratio of the fundamental mode increases with flow. Therefore, water flow causes random vibrations, but dampens externally excited vibrations. Interestingly, while in quiescent water the damping value increased six times for the force range under exam, it increased much less, approximately two times, for tests in water flow. Therefore, damping ratio is higher for water flow, but the equivalent damping in the nonlinear regime increases less in case of large amplitude vibrations because of flow.

In conclusion, at the highest flow rate, the equivalent damping for large-amplitude vibrations is similar to the value obtained in the water tunnel with still water, while the damping ratio for small-amplitude vibrations is twice higher; the associated softening frequency shift is unchanged, as well as the peak vibration amplitude obtained with the same harmonic force is very similar. Therefore, it can be concluded that overall, in the flow and forcing ranges under exam, coolant flow does not change significantly the severity of forced vibrations in nonlinear (large-amplitude) regime while it reduces vibration in linear (small-amplitude) regime.

Acknowledgements

The authors would like to thank the NSERC CRD Grant Program (project 490978-15) for its financial support. The authors would also like to thank Framatome Canada Ltd. for their support.

References

- Adhikari, S., Woodhouse, J. (2001a). Identification of damping: Part 1, viscous damping. Journal of Sound and Vibration, 243, 43-61.
- Adhikari, S., Woodhouse, J. (2001b). Identification of damping: Part 2, non-viscous damping. Journal of Sound and Vibration, 243, 63-88.
- Alijani, F., Amabili, M., Balasubramanian, P., Carra, S., Ferrari, G., Garziera, R. (2016). Damping for large-amplitude vibrations of plates and curved panels, part 1: modelling and experiments. International Journal of Non-linear Mechanics, 85, 23-40.
- Amabili M. (2008). Nonlinear vibrations and stability of shells and plates. Cambridge University Press, New York, USA.
- Amabili M. (2018a). Nonlinear mechanics of shells and plates: composite, soft and biological materials. Cambridge University Press, New York, USA.
- Amabili, M. (2018b). Derivation of nonlinear damping from viscoelasticity in case of nonlinear vibrations. Nonlinear Dynamics, 1-13.
- Amabili, M. (2018c). Nonlinear damping in large-amplitude vibrations: modelling and experiments. Nonlinear Dynamics, 93(1), 5-18.
- Amabili, M. (2018d). Nonlinear damping in nonlinear vibrations of rectangular plates: derivation from viscoelasticity and experimental validation. Journal of the Mechanics and Physics of Solids, 118, 275-292.
- Amabili, M., Alijani, F., Delannoy, J. (2016). Damping for large-amplitude vibrations of plates and curved panels, part 2: Identification and comparisons. International Journal of Non-Linear Mechanics, 85, 226–240.
- Amabili, M., Carra, S. (2012). Experiments and simulations for large-amplitude vibrations of rectangular plates carrying concentrated masses. Journal of Sound and Vibration, 331, 155–166.
- Balasubramanian, P., Ferrari, G., Amabili, M. (2018). Identification and comparison of various damping models during large amplitude vibrations. Mechanicals Systems and Signal Processing 111, 376-398.
- Balasubramanian, P., Ferrari, G., Amabili, M., del Prado, Z.J.G.N. (2017). Experimental and theoretical study on large amplitude vibrations of clamped rubber plates. International Journal of Non-Linear Mechanics, 94, 36-45.
- Bennet, G., Antunes, J., Mendes, J., Piteau, Ph. (1997). Some issues on the identification of experimental fluid-elastic forces. In: Transactions of the 14th International Conference on structural Mechanics in Reactor Technology (SMiRT 14), Lyon, France, August 17-22.
- Bhattacharya, A. (2013). Investigations on Flow and Flow-Induced Vibration of CANDU Fuel Bundles. Thesis. Ryerson University, Toronto, Ontario, Canada.
- Brenneman, B., Shah, S.J. (2000). Damping in fuel assemblies for axial flow. In: PVP-Vol.414-1, Emerging Technologies in Fluids, Structures, and Fluid/Structure Interactions Volume 1, Seattle, Washington.
- Brockmeyer, L., Merzari, E., Solberg, J.M., Karazis, K., Hassan, Y. (2019). High Fidelity Simulation and Validation of Crossflow through a Tube Bundle and the Onset of Vibration. Lawrence Livermore National Lab. LLNL-TR-772580.
- Burgreen, D., Byrnes, J.J., Benforado, D.M. (1958). Vibration of rods induced by water in parallel flow. Transactions ASME80, 991-1003.
- Chang, D., Tavoularis, S. (2007). Numerical simulation of turbulent flow in a 37-rod bundle, Nuclear Engineering and Design, 237:6, 575-590.

- Chen, S.S. (1975a). Dynamic responses of two parallel circular cylinders in a liquid. ASME Journal of Pressure Vessel Technology 97, 78-83.
- Chen, S.S. (1975b). Vibrations of a row of circular cylinders in a liquid. ASME Journal of Engineering for Industry 97, 1212-1218.
- Chen, S.S. (1975c). Vibration of nuclear fuel bundles. Nuclear Engineering and Design 35, 399-422.
- Chen, S.S., Jendrzejczyk, J.A. (1978). Experiments on fluidelastic vibration of cantilevered tube bundles. ASME Journal of Mechanical Design 100, 540-548.
- Chen, S.S., Wambsganss, M.W. (1972). Parallel-flow induced vibration of fuel rods. Nuclear Engineering and Design 18, 253-278.
- Chung, H., Chen, S.S. (1977). Vibration of a group of circular cylinders in confined fluid. Journal of Applied Mechanics 44, 213-217.
- Collard, B., Pisapia, S., Bellizzi, S., Broc, D. (2004). Flow induced damping of a PWR fuel assembly. In: Transactions of 8th International Conference on Flow-Induced Vibration, FIV2004, Paris, France.
- Connors, H.J., Savorelli, S.J., Kramer, F.A. (1982). Hydrodynamic damping of rod bundles in axial flow. Pressure Vessel and Piping, 63, 109-124
- Dalton, C. (1980). Inertia coefficients for riser configurations. ASME Journal of Energy Resources Technology 102, 197-202.
- De Pauw, B., Weijtjens, W., Vanlanduit, S., Van Tichelen, K., Berghmans, F. (2015). Operational modal analysis of flow-induced vibration of nuclear fuel rods in a turbulent axial flow. Nuclear Engineering and Design, 284, 19-26.
- De Santis, D., Shams, A. (2017). Numerical modeling of flow induced vibration of nuclear fuel rods. Nuclear Engineering and Design, 320, 44-56.
- Delannoy J., Amabili M., Matthews B., Painter B., Karazis K. (2015). Non-linear damping identification in nuclear systems under external excitation, ASME 2015 International Mechanical Engineering Congress and Exposition. Houston, Texas, USA, IMECE2015-52874.
- Delannoy J., Amabili M., Matthews B., Painter B., Karazis K. (2016) Identification of Non-Linear Damping of Nuclear Reactor Components in Case of One-to-One Internal Resonance, ASME 2016 International Mechanical Engineering Congress and Exposition, Phoenix, Arizona, USA, IMECE2016-66311.
- Dragunov, Yu.G., Solonin, V.I., Perevezentsev, V.V., Petrov, I.V. (2013). Vibrations of fuel-element bundles in VVER fuel assemblies excited by turbulent coolant flow. Atomic Energy, 113, 153-162.
- Eichler, A., Moser, J., Chaste, J., Zdrojek, M., Wilson-Rae, I., Bachtold, A. (2011). Nonlinear damping in mechanical resonators made from carbon nanotubes and graphene. Nature nanotechnology, 6(6), 339.
- Eifler, W., Nijsing, R. (1967). Experimental investigation of velocity distribution and flow resistance in a triangular array of parallel rods. Nuclear Engineering and Design 5, 22-42.
- Fardeau, P., Barbier, D., de Langre, E., Rigaudeau, J. (1997). Damping from axial coolant flow in the response of PWR fuel assemblies to horizontal seismic loads. In: Transactions of the 14th International Conference on Structural Mechanics in Reactor Technology (SMiRT 14), Lyon, France.

- Ferrari, G., Balasubramanian, P., Le Guisquet, S., Piccagli, L., Karazis, K., Painter, B., Amabili, M. (2018). Non-linear vibrations of nuclear fuel rods. Nuclear Engineering and Design, 338, 269-283.
- Ferrari, G., Franchini, G., Balasubramanian, P., Giovanniello, F., Le Guisquet, S., Karazis, K., Amabili, M. (2019, submitted). Nonlinear vibrations of a nuclear fuel rod supported by spacer grids. Nuclear Engineering and Design.
- Hassan, M.A., Rogers, R.J., Gerber, A.G. (2011). Damping-controlled fluidelastic instability forces in multi-span tubes with loose supports. Nuclear Engineering and Design, 241, 2666-2673.
- Hofstede, E.ter, Kottapalli, S., Shams, A. (2017). Numerical prediction of flow induced vibrations in nuclear reactor applications. Nuclear Engineering and Design, 319, 81-90.
- Hooper, J.D., Rehme, K. (1984). Large-scale structural effects in developed turbulent flow through closely-spaced rod arrays. Journal of Fluid Mechanics 145, 305-337.
- Jeong, B., Cho, H., Yu, M. F., Vakakis, A. F., McFarland, D. M., Bergman, L. A. (2013). Modeling and measurement of geometrically nonlinear damping in a microcantilever–nanotube system. ACS nano, 7(10), 8547-8553.
- Kang H., Song K., Kim H.-K., Yoon K., Jung Y. H. (2001). Verification Test and Model Updating for a Nuclear Fuel Rod with Its Supporting Structure, Nuclear Engineering and Technology, 33(1), 73-82.
- Khan, M. O., S. Hussain, M. Rafique, A. Ahmad, W. Akhtar. (2013). CFD study of single phase flow in a PWR spacer grid. *Proceedings of 2013 10th International Bhurban Conference on Applied Sciences & Technology (IBCAST)*, Islamabad, pp. 243-248.
- Kim, H.K., Kim, M.S. (2005). Vibration analysis of PER fuel rod. Journal of Sound and Vibration, 282, 553-572.
- Le Guisquet, S., Amabili, M. (2019, submitted). Identification by means of a genetic algorithm of nonlinear damping and stiffness of slender and thin-walled structures subjected to large-amplitude vibrations. Part I: single-degree-of-freedom responses. Mechanical Systems and Signal Processing.
- Lin, H.C., Chen, S.S. (1977). Acoustically induced vibrations of circular cylindrical rods. Journal of Sound and Vibration 51, 89-96.
- Lin, W.H., Raptis, A.C. (1986). Acoustic resonances in cylinder bundles oscillating in a compressible fluid. ASME Journal of Pressure Vessel Technology 108, 197-201.
- Liu, C.C., Ferng, Y.M., Shih, C.K. (2012). CFD evaluation of turbulence models for flow simulation of the fuel bundle with a spacer assembly. Applied Thermal Engineering, 40, 389-396.
- Liu, H., Chen, D., Hu, L., Yuan, D., Gao, H. (2017). Numerical investigations on flow-induced vibration of fuel rods with spacer grids subjected to turbulent flow. Nuclear Engineering and Design, 325, 68-77.
- Lu, Z. Q., Hu, G. S., Ding, H., Chen, L. Q. (2019). Jump-based estimation for nonlinear stiffness and damping parameters. Journal of Vibration and Control, 25(2), 325-335.
- Moretti, P.M., Lowery, R.L. (1976). Hydrodynamic inertia coefficients for a tube surrounded by rigid tubes. ASME Journal of Pressure Vessel Technology 98, 190-194.
- Païdoussis, M.P. (1965a). Pressure waves in horizontal liquid-filled flexible tubes. IMechE Journal of Mechanical Engineering Science 7, 380-390.
- Païdoussis, M.P. (1965b). The amplitude of fluid-induced vibration of cylinders in axial flow. Atomic Energy of Canada Report AECL-2225.

- Païdoussis, M.P. (1965c). The stability of towed flexible cylinders in axial flow. Unpublished report, CRNL, Atomic Energy of Canada Ltd., Chalk River, Ontario, Canada.
- Païdoussis, M.P. (1966a). Dynamics of flexible slender cylinders in axial flow. Part 2: experiments. Journal of Fluid Mechanics 26, 737-751.
- Païdoussis, M.P. (1966b). Vibration of cylinders with supported ends, induced by axial flow. Proceedings of the Institution of Mechanical Engineers 180, 268-278.
- Païdoussis, M.P. (1979). The dynamics of clusters of flexible cylinders in axial flow: Theory and experiments. Journal of Sound and Vibration 65, 391-417.
- Païdoussis, M.P. (2004). Fluid-structure interactions: Slender structures and axial flow. Elsevier Academic Press.
- Païdoussis, M.P. Besançon, P. (1981). Dynamics of arrays of cylinders with internal and external axial flow. Journal of Sound and Vibration 76, 361-380.
- Païdoussis, M.P., Chaubernard, J.-P., Genadry, M.R., El Barbir, K.N. (1983a). Dynamics of a cluster of flexibly interconnected cylinders. Part 2. In axial flow. Journal of Applied Mechanics 50, 429-435.
- Païdoussis, M.P., Curling, LL.R. (1985). An analytical model for vibration of clusters of flexible cylinders in turbulent axial flow. Journal of Sound and Vibration, 98, 493-517.
- Païdoussis, M.P., Curling, Ll.R., Gagnon, J.O. (1982). Experiments on fluidelastic instability of cylinder clusters in axial flow. Journal of Fluids Engineering 104, 342-347.
- Païdoussis, M.P., El Barbir, K.N., Genadry, M.R., Chaubernard, J.-P. (1983b). Dynamics of a cluster of flexibly interconnected cylinders. Part 1: In vacuum. Journal of Applied Mechanics 50, 421-428.
- Païdoussis, M.P., Suss, S. (1977). Stability of a cluster of flexible cylinders in bounded flow. Journal of Applied Mechanics 44, 401-408. Discussion 1978, 45, 455 and 703.
- Païdoussis, M.P., Suss, S., Pustejovsky, M. (1977). Free vibration of clusters of cylinders in liquid-filled channels. Journal of Sound and Vibration 95, 443-459.
- Pavlica, R.T., Marshall, R.C. (1966). An experimental study of fuel assembly vibrations induced by coolant flow. Nuclear Engineering and Design 4, 54-60.
- Peeters, B., Lowet, G., Van der Auweraer, H. and Leuridan, J. (2004). A new procedure for modal parameter estimation. Sound and Vibration, 38(1), 24-29.
- Quinn, E.P. (1962). Vibration of fuel rods in parallel flow. U.S. Atomic Energy Commission Report GEAP-4059.
- Quinn, E.P. (1965). Vibration of SEFOR fuel rods in parallel flow. U.S. Atomic Energy Commission Report GEAP-4966.
- Rehme, K., Trippe, G. (1980). Pressure drop and velocity distribution in rod bundles with spacer grids. Nuclear Engineering and Design, 62:1–3, 349-359.
- Ricciardi, G. (2016). Fluid-structure interaction modelling of a PWR fuel assembly subjected to axial flow. Journal of Fluids and Structures, 62: 156-171.
- Roström, K.G. (1964). Seven-rod fuel element Vibration test. Ab. Atomenergi (Stockholm), Arbetsrapport RRL-726.
- Roström, K.G., Andersson, N. (1964a). Boiler element for Marviken. Vibration tests with one rod. Ab. Atomenergi (Stockholm), Arbetsrapport RRL-724.
- Roström, K.G., Andersson, N. (1964b). Superheater element for Marviken. Vibration tests with one rod. Ab. Atomenergi (Stockholm), Arbetsrapport RRL-725.
- Shields, C.M. (1960). N.S. Savannah fuel design and development program Fuel rod vibration. U.S. Atomic Energy Commission Report GEAP-3583.

- SOGREAH. (1962). Study if vibrations and load losses in tubular clusters. Societé Grenobloise d'etudes et applications hydrauliques, Special Report no. 3, EURAEC-288.
- Vandiver, J.K. (2012). Damping parameters for flow-induced vibration. Journal of Fluids and Structures, 35, 105-119.
- Viallet, E., Kestens, T. (2003). Prediction of flow induced damping of a PWR fuel assembly in case of seismic and LOCA load case. In: Transactions of the 17th International Conference on Structural Mechanics in Reactor Technology (SMiRT 17), Prague, Czech Republic.
- Weppelink, H. (1979). Free vibrations of finite circular cylindrical shells and tubes with and without a surrounding fluid. M.Sc. Thesis. Technische Hogeschool Twente, Enschede, The Netherlands.
- Yamamoto, T. (1976). Hydrodynamic forces on multiple circular cylinders. ASCE Journal of the Hydraulics Division 102, 1193-1210.
- Yeh, Y.S., Chen, S.S. (1990). Flow-induced vibration of component cooling water heat exchangers. In Flow-Induced Vibration 1990 (eds S.S. Chen, K. Fujita & M.K. Au-Yang), PVP–Vol. 189, pp. 153-163. New York: ASME.

Chapter 4

Nonlinear Vibrations of Beams with Bilinear Hysteresis at Supports: Interpretation of Experimental Results

Prabakaran Balasubramanian (1), Giulio Franchini (1), Giovanni Ferrari (1), Kostas Karazis (2), Marco Amabili (1, 3),

- (1) Department of Mechanical Engineering, McGill University 817 Sherbrooke Street West, Montreal, Canada H3A 0C3
- (2) Framatome Inc., 3315 Old Forest Rd., Lynchburg, 24501 VA, USA
- (3) University of Parma, Dipartimento di Ingegneria and Architettura, Parco Area delle Scienze 181/A, 43124 Parma, Italy

Running headline: Nonlinear vibrations of beams with bilinear stiffness at supports

Keywords: Beams; nonlinear vibrations; nonlinear boundary conditions; bilinear hysteresis; bilinear stiffness

Abstract

Experimental vibration responses of beams with nonlinear boundary conditions were interpreted using a bilinear spring model. Two systems of beams were considered: one is a single rod and the second one is a cluster of parallel beams. The boundary conditions at the beam ends, for both systems, were given by spacer grids, which are specific supports used in nuclear industry. The

experiments were conducted with the beams immersed in still water. The spacer grids imposed nonlinear boundary conditions to the beams. A bilinear stiffness model with viscous damping was used to interpret the experimental results. A dynamic characterization of the nonlinear boundary conditions was carried out. The boundary conditions change from being linear at low vibration amplitudes to being bilinear with hysteresis at higher vibration amplitudes. The stiffness of the supports decreases with increasing vibration amplitude. In addition, the equivalent viscous damping of the system grows with the vibration amplitude. Very good agreement between numerical and experimental results were obtained for both the beam systems studied.

Introduction

Many physical systems present some form of hysteresis during vibrations and there are numerous studies on hysteresis in the literature [1, 2]. The hysteresis could take many different forms [3] and bilinear hysteresis is one among them. The bilinear hysteresis is mainly associated to intermittent contacts or elasto-plasticity. It could also be due to riveted, bolted or clamped connections combined with friction and elastic forces. The systems presenting bilinear hysteresis are not only abundant in mechanical, civil, aerospace and nuclear engineering but in other disciplines as well.

There are various studies about systems with bilinear hysteresis. First and foremost is the study by Caughey [4], in which he used the method of slowly varying parameters to study a single-degree-of-freedom system with bilinear hysteresis and obtained the frequency response curves. In the next paper, Caughey investigated the response of bilinear hysteresis system to a random excitation [5]. Subsequently, Iwan [6] studied the response of two-degrees-of-freedom system using a similar procedure. Many other scholars analyzed the same system by considering an equivalent linear model [7-9]. There are serval approaches available for the description of the hysteresis. Models were developed by Preisach [10], Bouc and Wen [11] and Prandtl [3]. Bilinear hysteresis models consist of piecewise linear equations. Even though the responses can be found analytically around the individual linear areas, the overall response of the system is complicated. The method of slowly varying parameters used by Caughey [4] is particularly suitable for bilinear systems with hysteresis. The method averages the response of the system during one whole cycle, thus eliminating the complexity to deal with nonlinearity. Pratap and co-workers [12] studied the bilinear hysteretic oscillator utilizing the piecewise linear nature of the system to find the analytical

solutions for each linear domain and them patched the solutions to arrive at the total solution. Kalmár-Nagy and Shekhawat [13] studied the stability and bifurcations of bilinear hysteresis system with hybrid systems framework. Recently many studies have been conducted to understand the complex response of bilinear systems using modern tools, such as harmonic balance [14], Poincare maps [15] and non-smooth temporal transformation [16].

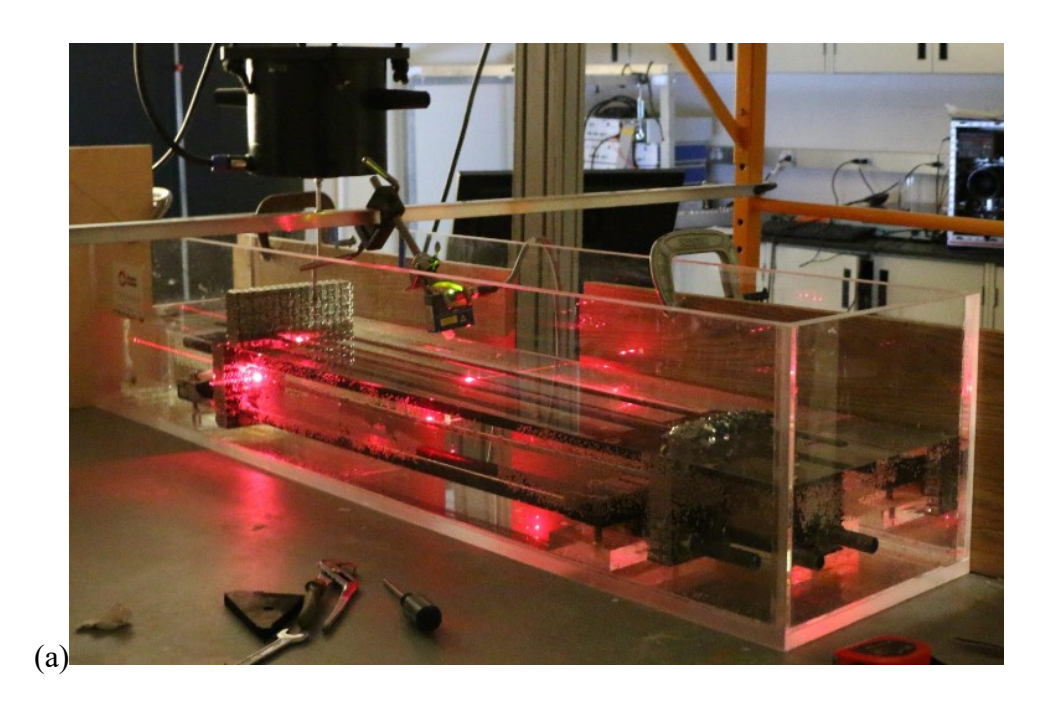
There are numerous numerical and analytical studies on the bilinear hysteresis systems. However, experimental results of such systems are little, and interpretation of the results using the bilinear model is scarce. Many mechanical systems present bilinear hysteresis and the ability to characterize their behavior helps to understand and design them effectively. The two beam systems with nonlinear boundary conditions under study here exhibited softening type behavior during their large-amplitude vibrations. Their nonlinear dynamic responses to harmonic excitation were interpreted using a single-degree-of-freedom model with bilinear stiffness and viscous damping.

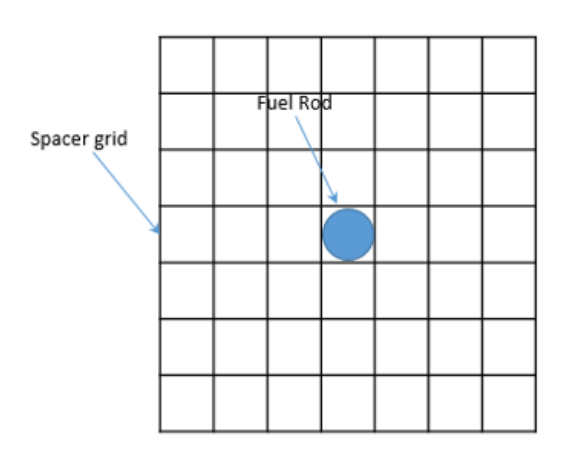
2. Nonlinear response of beams systems

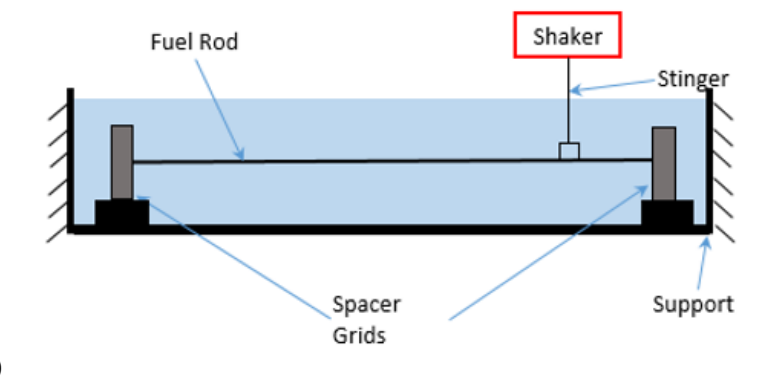
Nonlinear response of beams in two different configurations were measured. The beams tested here are Zirconium alloy tubes used as nuclear fuel rods in Pressurized Water Reactors (PWR). Each beam has a length of 900 mm, a diameter of 9.51 mm and a thickness of 0.3 mm. The first system consists of a single beam supported at both ends by spacer grids, as shown in Figures 1(a,b). Spacer grids are rectangular grid like structures which supports nuclear fuel rods in the nuclear fuel assembly. There are 17×17 cells in each spacer grid and each cell is used to house either a fuel rod, a control rod or a guide tube.

The second system is shown in Figures 1(c,d) and is composed by 9 beams in 3×3 matrix configuration supported at both ends by spacer grids; the beams are linked together by a spacer grid placed at mid-length. Both systems were tested immersed in water to simulate the surrounding cooling liquid of the PWR. Experimental modal analysis was carried out and subsequently nonlinear (i.e. large-amplitude) vibration experiments around the fundamental mode of the structure were performed. An electrodynamic shaker was used to give the punctual harmonic excitation in the frequency neighborhood of the fundamental mode of the structure. The nonlinear response of the beam systems was measured at the middle of the beam (or cluster of beams) using

a laser Doppler vibrometer and an established stepped sine test procedure. More information on both of the beam systems and respective experimental setups can be found in references [17, 18].







(b)



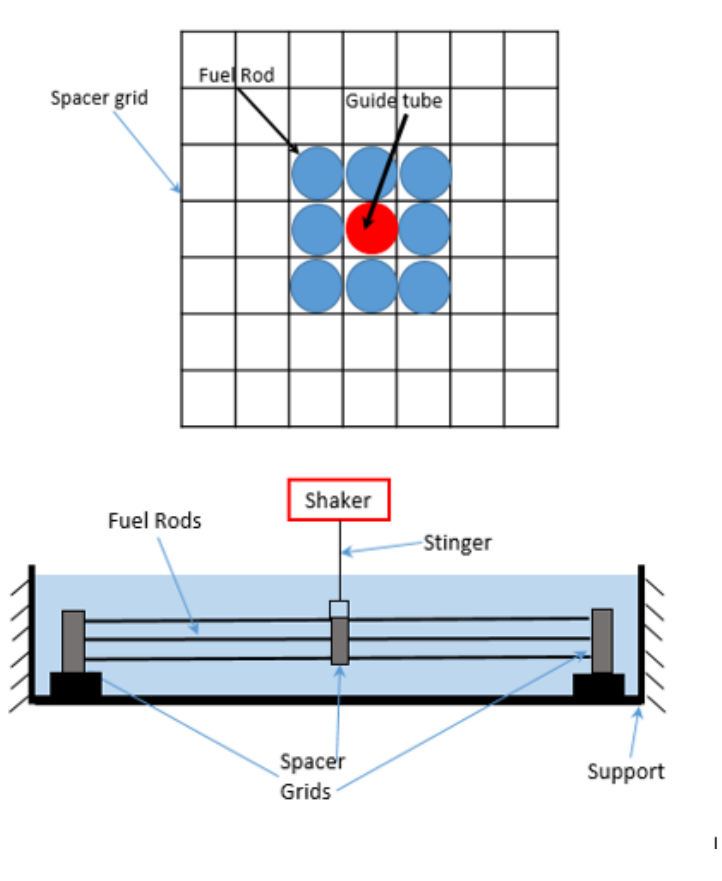
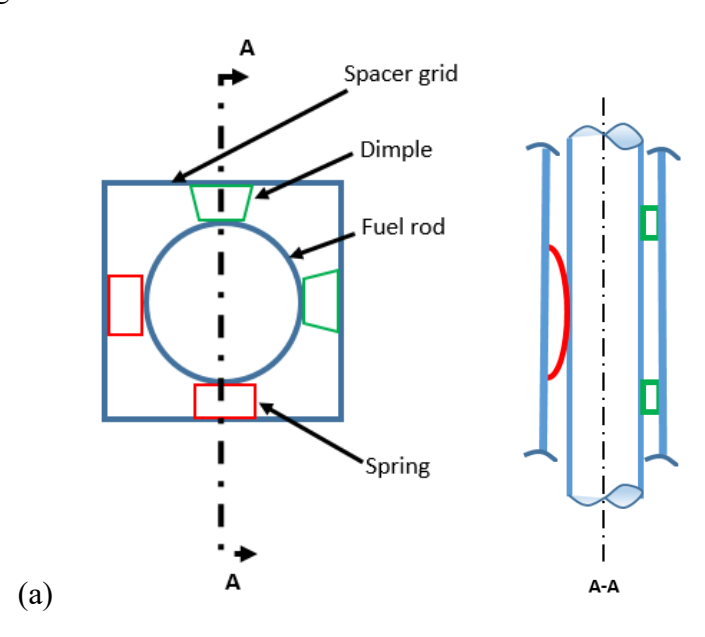


Figure 1. Experimental setup of the beams in two different configurations: (a) single beam supported by spacer grids at both ends, (b) sketch of the single beam supported by spacer grids (c) cluster of beams (3×3) supported by spacer grids, (d) sketch of the cluster of beam (3x3) supported by spacer grids

(d)

3. Dynamic characterization of boundary conditions

The spacer grids apply nonlinear boundary conditions to the beam systems under test. The mode shape of the beams shows that they are neither simply supported nor clamped at both ends by the spacer grids. The complex boundary condition given by the spacer grid is due to the nature of its design to increase the efficiency of the nuclear fuel assembly. The spacer grid is a grid like structure with 17×17 cells arranged in a square pattern. The whole structure is made of thin Zirconium alloy sheets. Each cell has dimples and springs for supporting the respective beams. The dimples are rigid support points with very high stiffness. Whereas, the springs are compliant and nonlinear. The dimples and springs are arranged in the cell as per Figure 2(a). There are four dimples and two springs supporting each beam. Among these six points of contacts, some might lose connection during the vibration of the fuel rods giving rise to intermittent contacts. There is also friction between the beam and the points of contacts, thus making the boundary condition given by the spacer grid nonlinear.



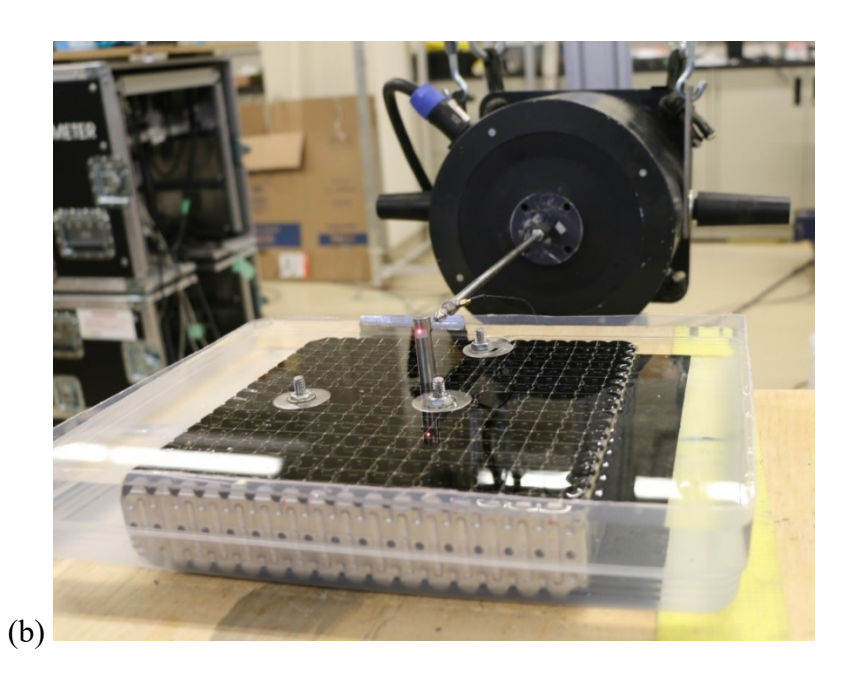


Figure 2. Geometry of the spacer grid. (a) Diagram of a single cell of the spacer grid and its cross-sectional view (A-A); (b) experimental setup for characterizing the nonlinear dynamic behavior of the spacer grid.

The nature of the nonlinear boundary condition enforced by the spacer grid was quantified using an experimental setup as shown in Figure 2(b). For this purpose, a spacer grid was fixed flat firmly and a rigid rod with the same dimension of the fuel rod was inserted in to one single cell. The whole setup was immersed in water to simulate the condition of the two systems studied here. The rigid rod was connected to an electrodynamic shaker via a miniaturized force transducer by B&K (model 8203). Harmonic excitation was given from 5 Hz to 50 Hz in steps of 5 Hz to the rigid rod. The displacement was controlled, and the corresponding force was measured for five displacements levels (0.01, 0.05, 0.1, 0.15 and 0.2 mm). The force-displacement loop for the displacement level 0.15 mm at 15 Hz is given in Figure 3(a). It clearly shows the bilinear hysteresis behavior of the spacer grid boundary condition. The slope of the loop decreases from its initial value due to possible intermittent contacts and friction. The force-displacement of all five levels of vibration amplitude at 15 Hz are presented in Figure 3(b). The first two levels (0.01 mm and 0.05 mm) are characteristics of a simple linear system. Thus, the loops take the shape of an ellipse. However, from displacement level 0.1 mm, the system becomes bilinear and presents hysteresis. Observing Figure 3(b), it is also clear that the loops rotate clockwise with the increase of the

excitation level (i.e. increase in size of the loop). Therefore, both stiffnesses of the bi-linear system decrease with the increase of the vibration amplitude.

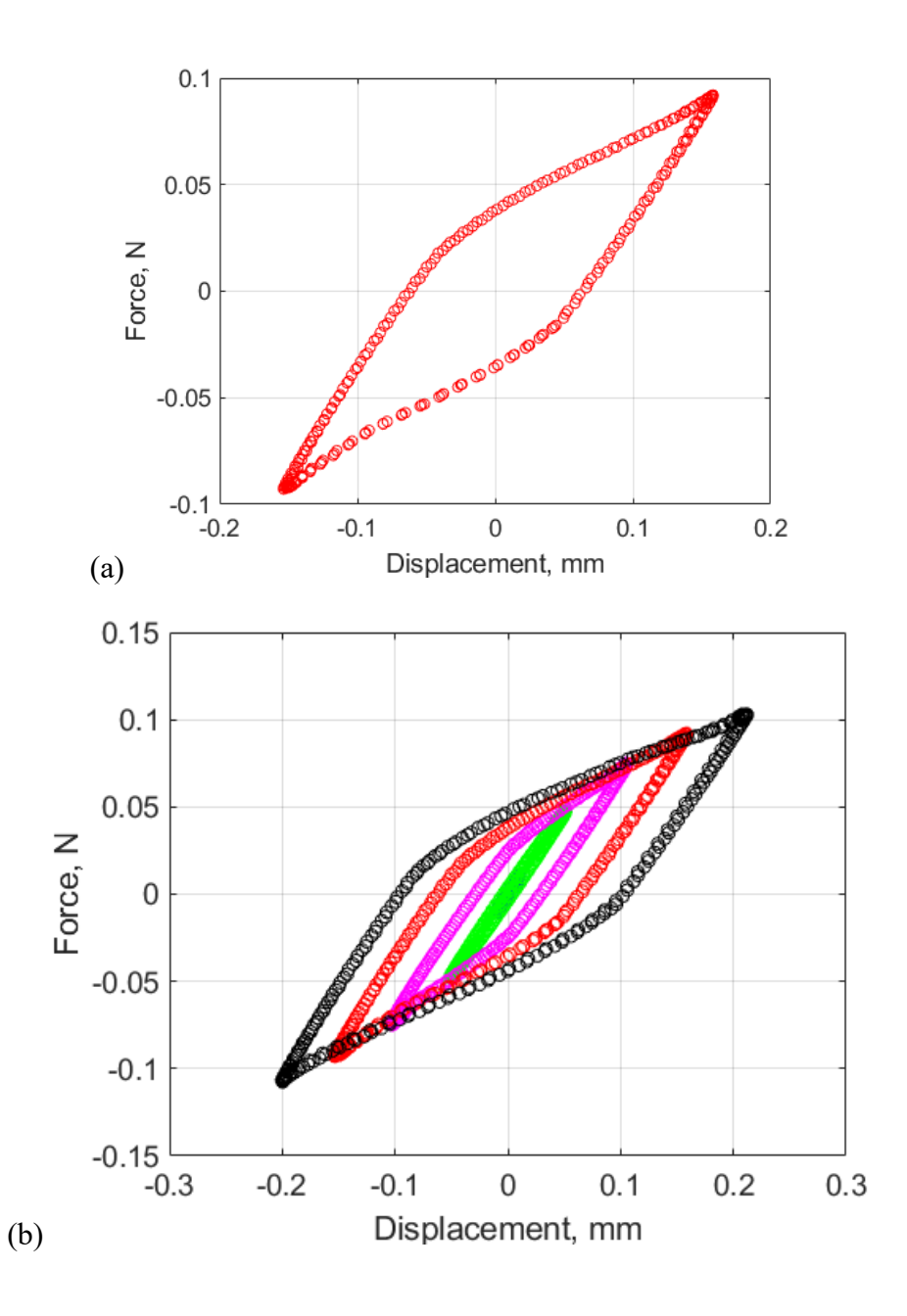


Figure 3. The bilinear response of spacer grids for harmonic excitation at frequency. (a) Single loop at a displacement level of 0.15 mm, excitation frequency 15 Hz; (b) the five loops at different levels of vibration amplitude, excitation frequency 15 Hz.

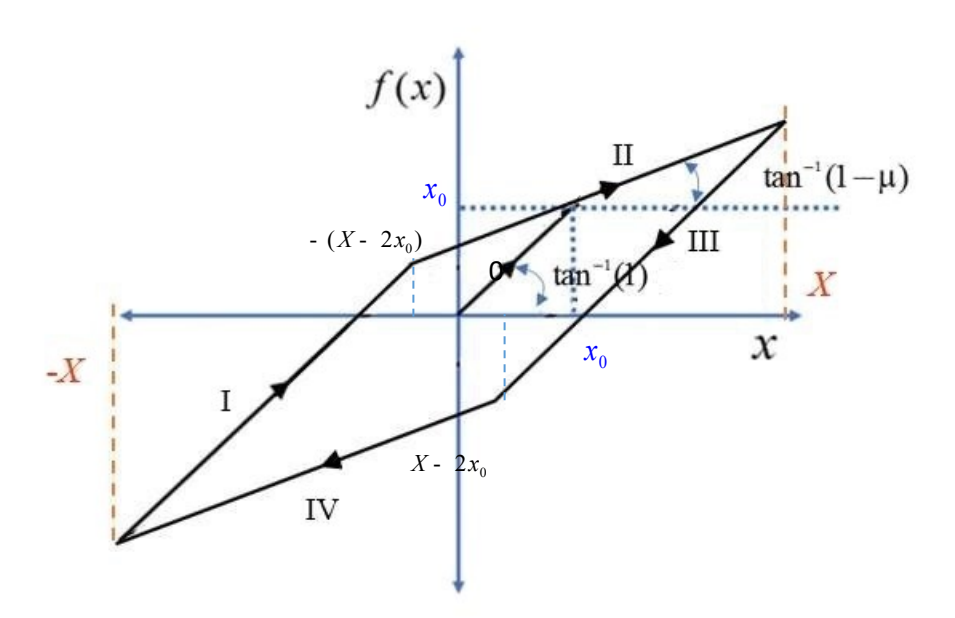


Figure 4. Force-displacement response of a bilinear hysteresis system.

The bilinear hysteresis model introduced by Caughey [4] can be used to fit the force-displacement loops measured on the spacer grids. The force-displacement hysteresis loop of the Caughey model is shown in Figure 4. Assuming an input harmonic displacement of frequency ω given by $x = X \cos \omega t$ where t is the time and X is the vibration amplitude, the steady-state response of the bilinear hysteresis model is given by

$$f(x) = \mu(X - x_0) + x$$
, if $-X \le x \le -(X - 2x_0)$, segment I,
 $f(x) = \mu x_0 + (1 - \mu)x$, if $-(X - 2x_0) \le x \le X$, segment II, (1)

for the loading curve; and

$$f(x) = -\mu(X - x_0) + x$$
, if $X - 2x_0 \le x \le X$, segment III,
 $f(x) = -\mu x_0 + (1 - \mu)x$, if $-X \le x \le X - 2x_0$, segment IV, (2)

and for the unloading curve, where x_0 is the displacement at which the spring initially (line "0" in Figure 4, starting from the equilibrium point at the origin) switches from the initial unitary slope to a reduced slope and μ is defined in Figure 4. In particular, the slope of the segments I and III is one, while the slope of the segments II and IV is 1- μ . Therefore, μ represents the reduction in slope of the bilinear system. The parameter μ takes values from 0 to 1. There is also the condition that $X - 2x_0 > 0$.

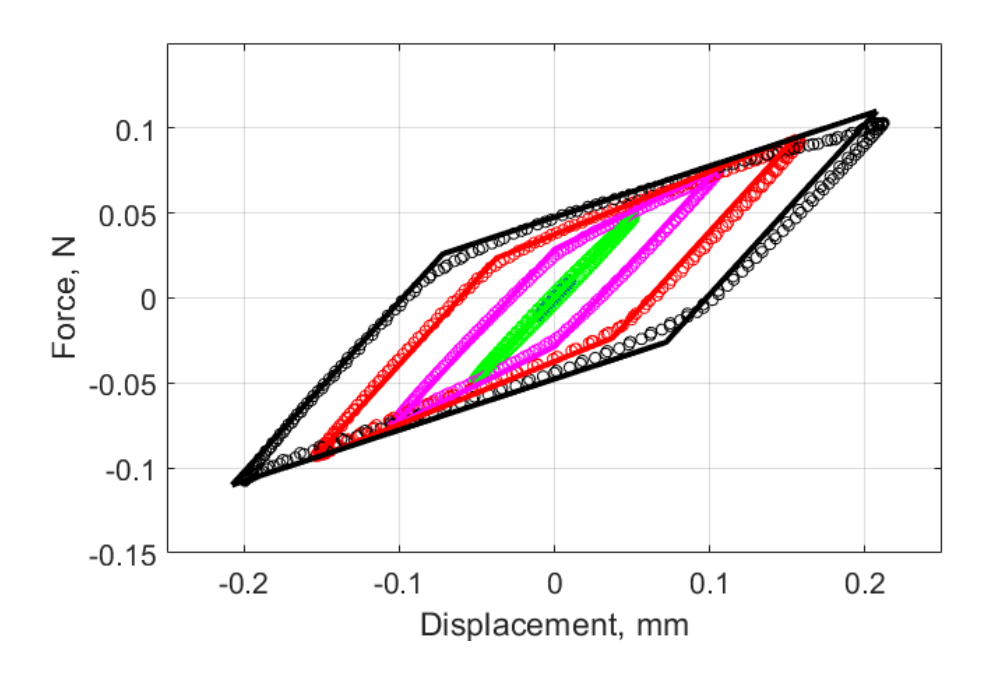


Figure 5. Comparison of the identified models and experimental loops for the dynamic responses of the spacer grid. Excitation frequency 15 Hz.

The force-displacement loops measured from spacer grids were fitted with the bilinear hysteresis model and the comparisons are shown in Figure 5. The identified parameters are given in Table 1. The first two loops are essentially those of a linear system. From the third level onwards, the bilinear switch distance x_0 increases and the bilinear parameter $(1 - \mu)$ decreases with the increasing displacement levels. Excellent agreement between experimental and numerical results are obtained. Thus, justifying the use of a bilinear stiffness model in the following section.

Table 1. Extracted parameters from the force-displacement loops measured on the spacer grid.

Displacement	Bilinear switch	Bilinear parameter,
level, mm	distance, x_0	$(1-\mu)$
0.01	0.0000	1.00
0.05	0.0000	1.00
0.10	0.0520	0.45
0.15	0.0593	0.37
0.20	0.0680	0.30

4. Bilinear spring with viscous damping model

A bilinear stiffness model can be considered for the interpretation of the experimental results of the above-mentioned configurations. This is justified by the fact that spacer grids introduce bilinear stiffness at the supports in both systems as shown in the previous Section. Instead of representing dissipation by the hysteresis model described by equations (1, 2), viscous damping is introduced. In fact, the beam systems have a more complex dissipation mechanism than the single spacer grid excited by a rigid rod. The equation of motion of such a single-degree-of-freedom model with bilinear stiffness and viscous damping is given by

$$m\ddot{x}(t) + c\dot{x}(t) + kf(x) = F\cos(\omega t), \tag{3}$$

where, f(x) is the displacement-dependent bilinear stiffness function, F is the harmonic force excitation, m, c and k are the mass, damping and stiffness parameters of the system. For computational convenience, equation (1) was made non-dimensional

$$\ddot{x}(\tau) + 2\zeta\dot{x}(\tau) + f(x) = \lambda \sin(\Omega \tau),\tag{4}$$

where, $\lambda = F/m\omega^2$, $\Omega = \omega/\omega_n$, $\tau = t\omega_n$, ω_n is the natural frequency and ζ is the damping ratio. The bilinear function f(x) considered here is plotted against the displacement x in Figure 6. There are three (I, II and III) line segments shown in Figure 6. The line segments are defined as follows

I:
$$f(x) = x$$
, $|x| \le x_0$, (5)

II:
$$f(x) = (1 - \mu)x + \mu x_0, \qquad x > x_0,$$
 (6)

III:
$$f(x) = (1 - \mu)x - \mu x_0, \qquad x < -x_0.$$
 (7)

The second-order ordinary differential equation (4) can be rewritten in the state space form and solved numerically for getting the frequency response using e.g. the Adams-Gear backward integration method. A continuation method based on pseudo-arclength and collocation method

implemented in the software AUTO [19] was used for obtaining frequency responses for both the beam systems studied here.

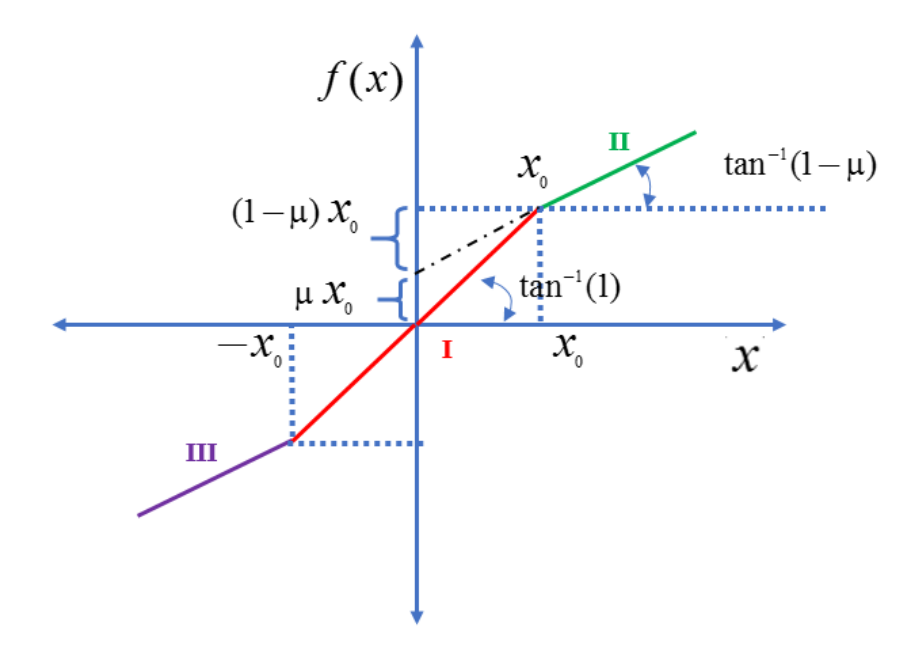


Figure 6. Bilinear stiffness model

5. Interpretation of the experimental results

The experimental responses (linear and nonlinear) of both beam systems were used to identify the model parameters in equation (4). For each response curve, the unknown parameters $(x_0, \mu, \lambda, \zeta)$ were obtained minimizing the weighted distance between the experimental points and the model.

The experimental and numerical results of the first beam system (rod supported by spacer grids, fully immersed in water) are compared in Figure 7. The values of the unknown parameters used in the model to get the numerical responses are given in Table 2.

Table 2. Extracted parameters of the configuration with single beam supported by spacer grids.

	Force	Bilinear switch	Bilinear parameter,	Damping
	level, N	distance, x_0	$(1-\mu)$	ratio, ζ
l		,	, ,	ŕ
	0.1	0.02	0.95	0.015

0.5	0.05	0.84	0.025
0.7	0.05	0.82	0.027
1.0	0.05	0.81	0.028
1.5	0.05	0.80	0.032

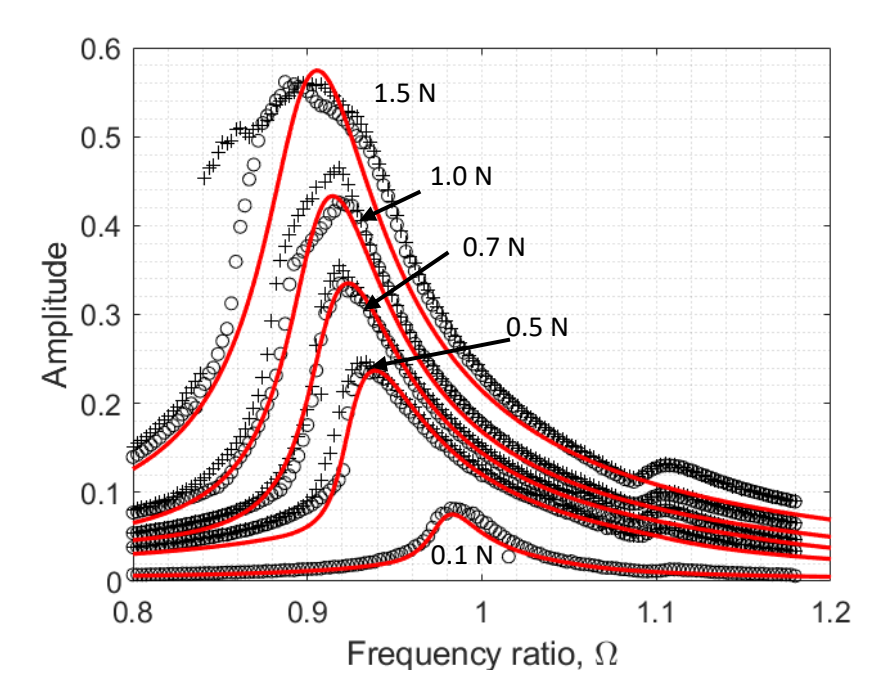


Figure 7. The numerical and experimental results comparison of the single rod supported by spacer grids: 'o' experimental results (sweep up), '+' experimental results (sweep down), '-' numerical results.

There are five force levels in which the experimental and numerical responses were compared. Very good agreement was found between the experimental and numerical results for the first four levels, while the largest level has a slightly lower agreement. In particular, the numerical model captured the softening response around the resonance very well, which is typical of a bilinear system [4]. The first level itself presents a nonlinear response as it is not symmetric around the resonance; the identified parameters reflect this behavior. The force-displacement hysteresis loops of experimental and numerical results at three different frequencies are compared for the force level 1 N in Figure 8.

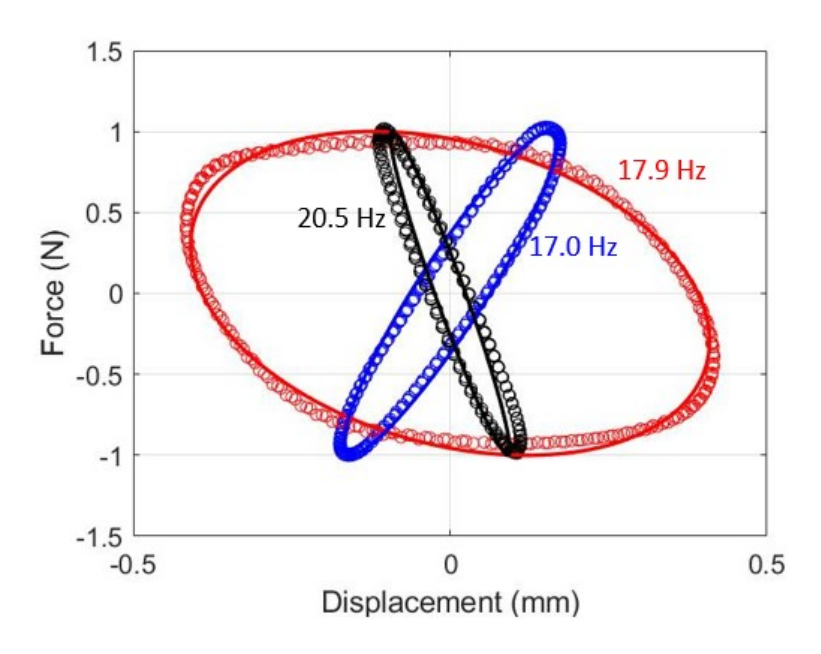


Figure 8. Comparison of force-displacement hysteresis loops of the single rod supported by spacer grids (force level 1 N): 'o' experiemental results, '-' numerical results.

The three frequencies are 17, 17.85 and 20.5 Hz (corresponding to non-dimensional frequencies 0.8713, 0.9154 and 1.051) and they are before, at and after the resonance, respectively. The very good agreement between numerical and experimental force-displacement loops confirms that the numerical model chosen not only captures with accuracy the amplitude of the frequency response but also the phase and dissipation of the system. This confirm that the choice of the bilinear stiffness and viscous damping is particularly effective to describe the nonlinear dynamics of the system.

Table 3. Extracted parameters of the configuration with cluster of beams supported by spacer grids.

Force level, N	Bilinear switch distance, x_0	Bilinear parameter, $(1 - \mu)$	Damping ratio, ζ
0.10	0.00	1.00	0.012
0.30	0.02	0.94	0.016
1.00	0.04	0.88	0.024

2.00	0.09	0.81	0.034
4.00	0.13	0.70	0.042
7.00	0.16	0.63	0.046
10.00	0.18	0.58	0.046
12.00	0.20	0.57	0.048

The comparison between experimental and numerical responses of the second beam system (cluster of beams supported by spacer grids and immersed in water) are shown in Figure 9. The corresponding values of the model parameters are presented in Table 3. An excellent agreement between numerical and experimental results is observed. The numerical responses clearly capture the amplitude of the experimental frequency responses at all the seven force levels. It is quite interesting to observe that the nonlinear response in the frequency neighborhood of the fundamental mode of a relatively complex system can be described with high accuracy by the introduced single-degree-of-freedom model with properly identified system parameters. Results show that the system behaves as linear for the first force level and then the response becomes bilinear for larger force excitations. The force-displacement hysteresis loops of experimental and numerical results for excitation of 12 N are compared in Figure 10 for three different frequencies. Again, there is a very good agreement between experiments and numerical results. The bilinear parameter $(1-\mu)$ obtained from the system identification is plotted against the maximum vibration amplitude in Figure 11(a). The graph displays that the bilinear parameter decreases with the vibration amplitude. This result is in agreement with the parameter identified from the characterization of the spacer grid (see Table 1). The identified bilinear parameters are comparable between the two beam systems with the same vibration amplitude. This suggests that the bilinear behavior of (i) one cell and (ii) nine cells combined, is comparable at the same vibration amplitude. The damping ratios of both systems are plotted against the maximum vibration amplitude in Figure 11(b). The damping ratios increase with the amplitude: about two times the initial value for the single rod and four times for the cluster of rods.

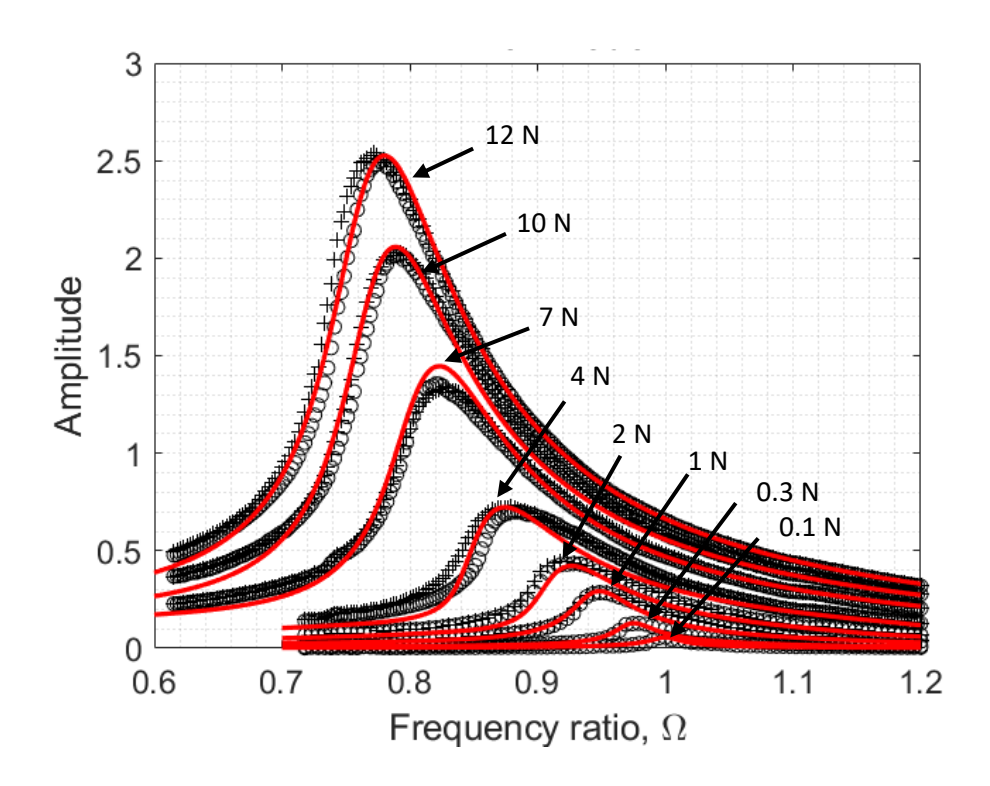


Figure 9. The numerical and experimental results comparison of the cluster of rods supported by spacer grids: 'o' experimental results (sweep up), '+' experimental results (sweep down), '-' numerical results.

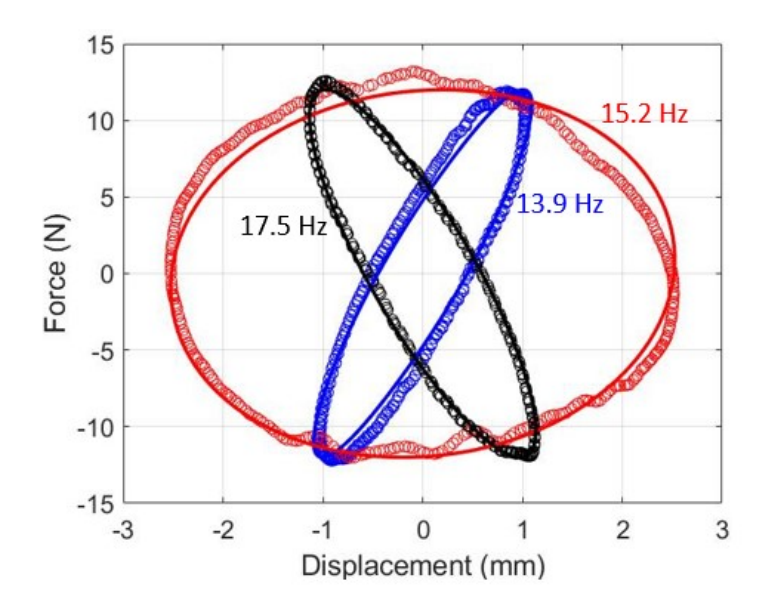


Figure 10. Comparison of force-displacement hysteresis loops of cluster of rods supported by spacer grids (12 N level): 'o' experiemental results, '-' numerical results.

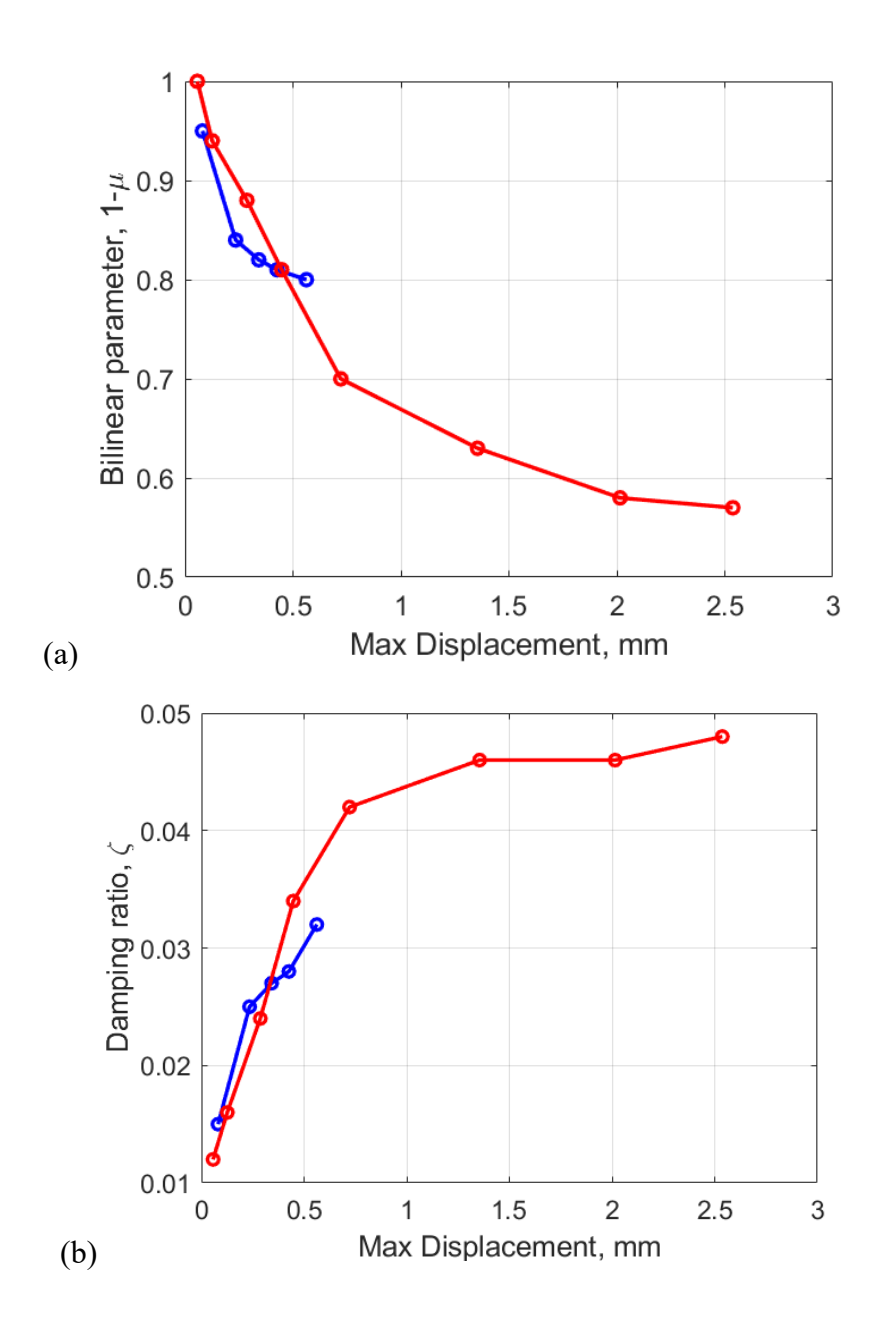


Figure 11. (a) Bilinear parameter $(1 - \mu)$, which is the slope of the reduced-stiffness spring, versus vibration amplitude; (b) viscous damping versus vibration amplitude. Blue line, single rod supported by spacer grids; red line, cluster of rods supported by spacer grids.

6. Conclusions

Nonlinear vibration responses of two different beam systems were interpreted using a model

based on bilinear stiffness and viscous damping. The beams studied were supported by spacer

grids at both ends, which imposed nonlinear boundary conditions with bilinear hysteresis. The

nonlinear response of both beam systems showed softening nonlinear behavior, where the

resonance frequency decreases with the vibration amplitude. The force-displacement hysteresis

loops of the spacer grids alone were measured, and the loops an almost perfect bilinear hysteresis

behavior. The bilinear hysteresis model introduced by Caughey [4] was used to fit these loops. A

single-degree-of-freedom model with bilinear stiffness and viscous damping was used to interpret

the experimental nonlinear response of the two systems of beams. The identified parameters show

that the stiffness of the boundary conditions reduces with amplitude. Moreover, the equivalent

damping of system increases rapidly, and stabilizes later, with the vibration amplitude. This paves

the way to a future study that introduces nonlinear damping, as observed in different systems [20-

23]. The model accurately captures the behavior of both systems, leading to an excellent agreement

between numerical and experimental results.

Acknowledgments

The authors acknowledge the financial support of the NSERC CRD Grant and the Framatome.

Conflict of Interest: The authors declare that they have no conflict of interest.

References

[1] G. Bertotti, Hysteresis in magnetism: for physicists, materials scientists, and engineers,

Academic press, 1998.

[2] D. Hughes, J.T. Wen, Preisach modeling of piezoceramic and shape memory alloy hysteresis,

Smart materials and structures, 6 (1997) 287.

- [3] M.A. Krasnosel'skii, A.V. Pokrovskii, Systems with hysteresis, Springer Science & Business Media, 2012.
- [4] T.K. Caughey, Sinusoidal excitation of a system with bilinear hysteresis, Journal of Applied Mechanics, 27 (1960) 640-643.
- [5] T.K. Caughey, Random excitation of a system with bilinear hysteresis, Journal of Applied Mechanics, 27 (1960) 649-652.
- [6] W.D. Iwan, The Steady-state response of a two-degree-of-freedom bilinear hysteretic system, Journal of Applied Mechanics, 32 (1965) 151-156.
- [7] P.C. Jennings, Equivalent viscous damping for yielding structures, Journal of the Engineering Mechanics Division, 94 (1968) 103-116.
- [8] W.D. Iwan, N.C. Gates, Estimating earthquake response of simple hysteretic structures, Journal of the Engineering Mechanics Division, 105 (1979) 391-405.
- [9] P.D. Spanos, A. Giaralis, Third-order statistical linearization-based approach to derive equivalent linear properties of bilinear hysteretic systems for seismic response spectrum analysis, Structural safety, 44 (2013) 59-69.
- [10] F. Preisach, On the magnetic aftereffect, IEEE Transactions on Magnetics, 53 (2017) 1-11.
- [11] Y.-K. Wen, Method for random vibration of hysteretic systems, Journal of the engineering mechanics division, 102 (1976) 249-263.
- [12] R. Pratap, S. Mukherjee, F. Moon, Dynamic behavior of a bilinear hysteretic elasto-plastic oscillator. Part 1: Free oscillations, Journal of Sound Vibration, 172 (1994) 321-337.
- [13] T. Kalmar-Nagy, A. Shekhawat, Nonlinear dynamics of oscillators with bilinear hysteresis and sinusoidal excitation, Physica D: Nonlinear Phenomena, 238 (2009) 1768-1786.
- [14] D. Capecchi, Accurate solutions and stability criterion for periodic oscillations in hysteretic systems, Meccanica, 25 (1990) 159-167.
- [15] W. Lacarbonara, F. Vestroni, Nonclassical responses of oscillators with hysteresis, Nonlinear Dynamics, 32 (2003) 235-258.
- [16] V.N. Pilipchuk, A.F. Vakakis, M. Azeez, Study of a class of subharmonic motions using a non-smooth temporal transformation (NSTT), Physica D: Nonlinear Phenomena, 100 (1997) 145-164.
- [17] G. Ferrari, G. Franchini, P. Balasubramanian, F. Giovanniello, S. Le Guisquet, K. Karazis, M. Amabili, Nonlinear vibrations of a nuclear fuel rod supported by spacer grids, Nuclear Engineering and Design, (2020) 110503.

- [18] G. Ferrari, G. Franchini, P. Balasubramanian, F. Giovanniello, S. Le Guisquet, K. Karazis, M. Amabili, Nonlinear vibrations of a nuclear fuel bundle supported by spacer grids, Nuclear Engineering and Design, (submitted 2020).
- [19] E.J. Doedel, A.R. Champneys, T.F. Fairgrieve, Y.A. Kuznetsov, B. Sandstede, X. Wang, Continuation and bifurcation software for ordinary differential equations (with HomCont), AUTO97, Concordia University, Canada, (1997).
- [20] M. Amabili, Nonlinear damping in large-amplitude vibrations: modelling and experiments, Nonlinear Dynamics, 93 (2018) 5-18.
- [21] P. Balasubramanian, G. Ferrari, M. Amabili, Identification of the viscoelastic response and nonlinear damping of a rubber plate in nonlinear vibration regime, Mechanical Systems and Signal Processing, 111 (2018) 376-398.
- [22] M. Amabili, Nonlinear damping in nonlinear vibrations of rectangular plates: derivation from viscoelasticity and experimental validation, Journal of the Mechanics and Physics of Solids, 118 (2018) 275-292.
- [23] M. Amabili, Derivation of nonlinear damping from viscoelasticity in case of nonlinear vibrations, Nonlinear Dynamics, 97 (2019) 1785-1797.

Chapter 5 Conclusions

Conclusions of this path can be divided into three distinct sets of results.

The results of the first article (one single rod) are the following:

- The trend of nonlinear vibration is always strongly softening. This is an important difference with respect to what happened in case of fixed-fixed boundary conditions (Ferrari *et. al.*, 2018). The presence of nuclear fuel pellets is the main factor influencing the vibration in the linear field by means of added mass and stiffness.
- The hysteresis here is negligible, most likely because of damping phenomena and similarly, nonlinear jumps are not found.
- Although axial symmetry is broken and damping increases, the presence of spacer grids does not inhibit the appearance of vibrations perpendicular to the direction of the excitation (companion mode), along with vibrations parallel to the excitation (driven mode). The composition of driven and companion mode for axisymmetric structures is explained in detail in Ferrari *et al.* (2018).
- Since spacer grids allow axial displacements, opposed by dry friction only, the axial vibration at the constraints was measured. As expected, the measured axial displacements were several times smaller in amplitude than those of the driven and companion modes. While the driven and the companion modes appear at different frequencies and interact in a complex manner (influenced, perhaps, by the vibration of the nuclear fuel pellets as well), the axial vibration occurs always at the same frequencies corresponding to the two main vibration modes. This seems to suggest that no specific vibration mode is present in the axial direction.
- Highly damped curves without nonlinear jumps and such a softening behavior, unfortunately, were not described successfully by the one DOF model based on a modified Duffing oscillator developed by this research group, forcing us to follow a new path for our future studies
- Given the moderate difference between free and fixed pellets conditions, the former may not be taken into account in future studies. During the operation of nuclear reactors, pellets

are in fact packed axially. However, the presence of pellets is the primary cause of large softening frequency decreases, which indicates the utility of taking pellets into account by the inclusion of additional degrees of freedom into future models and simulations.

With the development of the second article we enter the field of fluid iteration structure, studying the structure of the 3x3 bundle in the axial flow water tunnel.

- The behavior of the fuel bundle in quiescent media is remarkably similar to dynamic response of a single fuel rod supported by spacer grids around the fundamental frequency. The bundle has a an initial (for relatively small vibration amplitudes) very strong softening nonlinear behavior that cannot be modeled by the modified Duffing oscillator developed in (Delannoy *et al.*, 2015). This initial strong softening behavior seems caused by the nonlinear boundary conditions due to the springs installed on the spacer grids. Therefore, the system cannot be described only by quadratic and cubic stiffness in the modified Duffing oscillator.
- The setup was installed in a water tunnel capable of fluid flows comparable to those existing in PWRs. A key factor was the presence of a stiff frame supporting the spacer grids without exerting large forces on them. The frame was also engineered to have minimal unwanted resistance to flow.
- The presence of water flow does not have an important effect on natural frequencies for the specific boundary conditions constituted by spacer grids. As expected, no instabilities were detected in operative conditions, since axial flow values are too low to generate phenomena such as divergence or flutter. However, the strongly turbulent flow resulted in random noise superimposed onto the system vibration response.
- The damping ratio of the fundamental mode increases with flow. Therefore, water flow causes random vibrations, but dampens externally excited vibrations. Interestingly, while in quiescent water the damping value increased six times for the force range under exam, it increased much less, approximately two times, for tests in water flow. Therefore, damping ratio is higher for water flow, but the equivalent damping in the nonlinear regime increases less in case of large amplitude vibrations because of flow.

• Therefore, in the flow and forcing ranges under exam, coolant flow does not change significantly the severity of forced vibrations in nonlinear (large-amplitude) regime while it reduces vibration in linear (small-amplitude) regime.

The third and final article instead focuses attention on the boundary conditions of our problem: the spacer grids. After our investigation we can say that:

- The nonlinear response of both beam systems showed softening nonlinear behavior, where the resonance frequency decreases with the vibration amplitude.
- The force-displacement hysteresis loops of the spacer grids alone were measured, and the loops show an almost perfect bilinear hysteresis behavior. The bilinear hysteresis model introduced by Caughey was used to fit these loops.
- A single-degree-of-freedom model with bilinear stiffness and viscous damping was used
 to interpret the experimental nonlinear response of the two systems of beams. The
 identified parameters show that the stiffness of the boundary conditions reduces with
 amplitude. Moreover, the equivalent damping of system increases rapidly, and stabilizes
 later, with the vibration amplitude.

By analyzing the response of fuel rods and rod-cluster to harmonic excitation we can conclude that the behavior is certainly nonlinear and of the softening type. That is, we have a decrease in the first fundamental frequency by increasing the amplitude of oscillation; this behavior is due to the presence of spacer grids. These components allow to obtain an increase in the damping of the system producing a real advantage in terms of safety both in operating conditions and in exceptional conditions such as earthquakes. The damping values were identified by applying a bilinear stiffness model with viscous damping proving to be highly effective for describing the nonlinear response of the system.

References

Ferrari, G., Balasubramanian, P., Le Guisquet, S., Piccagli, L., Karazis, K., Painter, B., Amabili, M. (2018). Non-linear vibrations of nuclear fuel rods. Nuclear Engineering and Design, 338, 269-283.

Delannoy J., Amabili M., Matthews B., Painter B., Karazis K. (2015). Non-linear damping identification in nuclear systems under external excitation, ASME 2015 International Mechanical Engineering Congress and Exposition. Houston, Texas, USA, IMECE2015-52874.